

Estimating river surface velocity in Rönne Å from UASborne Doppler radar and PIV

Emilie Ahrnkiel Jørgensen s204350 Laura Riis-Klinkvort s204319

> 24th November 2023 DTU Sustain



Summary

River surface velocity is traditionally measured with in-situ methods, such as the electromagnetic velocity probe OTT MF Pro. Recent advances in remote sensing have made it possible to estimate surface velocity from Unmanned Aerial Systems (UAS). UAS-deployed remote sensing methods include Particle Image Velocimetry (PIV) and Doppler radar velocimetry. Deploying a Doppler radar from UAS is one of the more recent advancements. It is therefore necessary to investigate raw UAS-borne Doppler radar data, how it should be interpreted, and what the algorithm for picking the correct surface velocity should be. The aim of this study was thus to contribute valuable insights to what the algorithm for picking surface velocity should be, when the Doppler radar is UAS-borne rather than stationary.

This study compares Doppler radar, OTT MFpro and PIV velocimetry of five cross-sections located on a 10 km stretch of Rönne Å in Sweden. The Doppler radar was flown in altitudes of 2, 4 and 6 meters above the water surface of each cross-section. The three altitudes lead to three different footprint sizes. Every flight is therefore planned accordingly to cover the cross-section. The UAS must hover in place for 1 minute for each measurement. The OTT MF Pro measurements were done with a meter apart across each cross-section. PIV was also conducted in each cross-section. The raw Doppler radar data was filtered according to the received energy signal, flight altitude and hovering stabilization. The data collected at each waypoint was then fitted to a bimodal Gaussian distribution model, using non-linear least squares optimization. This model was chosen due to the appearance of two peaks in the Doppler velocity spectra. The hypothesis is that the two peaks in the data correspond to: one peak representing the river surface velocity and the other the sum of surface velocity and propeller-induced downwash. The algorithm assumes, that the surface velocity is the peak with the highest velocity. The Doppler estimated surface velocities were compared to the in-situ OTT MF Pro observations. From the comparison, mean biased errors (MBE) showed that the Doppler radar generally overestimates the in-situ observations, with MBE ranging from -1.63 cm/s to 27.17 cm/s across altitudes and cross-sections. Only XS1 showed a negative MBE. Root Mean Square Errors (RMSE) ranged from 4.84 cm/s to 32 cm/s across altitudes and cross-sections. Mean Absolute Errors (MAE) ranged from 4.35 cm/s to 27.17 cm/s. It was not possible to conclude on optimal flight altitude. The varying magnitudes of errors across all flight altitudes and cross-sections indicate that there are repeatability issues.

PIV results showed issues with low seeding density, leading to large gaps in results. It was attempted to explain the Doppler velocity spectra by utilizing PIV results for footprint analysis, i.e. inspecting PIV estimated velocities within the location of the Doppler radar footprint. It was possible to confirm the theory, that one of the peaks in the Doppler velocity spectra corresponds to the river surface velocity, and one to the sum of propeller-induced downwash and the surface velocity. Furthermore, it also showed, that the Doppler footprint sometimes registers several river surface velocities within the footprint. This makes estimation of one surface velocity particularly complex, especially when velocities fluctuate rapidly across the cross-section.

Sammenfatning

Strømningshastigheden i floder måles typisk med in-situ metoder, f.eks. magnetisk induktive flowmålere som OTT MF Pro. Nye metoder muliggør kontaktløse målinger fra droner. Particle Image Velocimetry (PIV) og Doppler radar er eksempler på nye dronebaserede metoder til estimering af strømningshastighed. Doppler radarer er før primært blevet benyttet stationært. Det er derfor nødvendigt, at analysere rå data fra den dronebårne Doppler radar, for at give indsigt i fortolkning af signalet, og hvorledes den korrekte strømningshastighed bestemmes i Doppler spektret. Formålet er, at afgøre med hvilken algoritme, strømningshastigheden af floden kan udvælges fra dataen.

Denne rapport sammenligner strømningshastigheder bestemt med OTT MF Pro, Doppler radar og PIV på fem tværsnit af Rönne Å i Sverige. Doppler radaren blev fløjet i 3 højder; 2m, 4m og 6m over vandoverfladen. De tre højder fører til tre forskellige footprint størrelser, som er arealet hvori radaren måler. Det fører derfor til forskellige antal målinger afhængig af flyvehøjde. Dronen skal svæve på stedet i 1 minut pr. måling. OTT MF Pro målinger blev foretaget hver meter på tværs. PIV video sekvenser blev også filmet ved hver lokation. Doppler dataen blev filtreret således at kun stabile målinger medtages, hvor dronen svæver korrekt, og hvor signalet er stærkt. Hver måling fittes derefter med en model baseret på en dobbelt normalfordeling ved brug af mindste kvadraters metode. Hypotesen er, at de to toppe i signalet repræsenter hhv. strømningshastigheden af floden og summen af flodens strømningshastighed, og strømningshastigheden skabt af dronens propeller. Den højeste af de to strømningshastigheder antages til at være flodens, og udvælges som Doppler radarens estimat. Estimaterne blev sammenlignet med målingerne fra OTT MF Pro, og Root Mean Square Error (RMSE), Mean Biased Error (MBE) og Mean Absolute Error (MAE) udregnes. Resultaterne af MBE viser, at Doppler radaren generelt overestimerer strømningshastigheden. De varierer mellem -1.63 cm/s til 27.17 cm/s, hvor kun en enkelt er negativ. RMSE varierer mellem 4.84 cm/s og 32 cm/s på tværs af flyvehøjder og lokationer. MAE varierer mellem 4.35 cm/s og 27.17 cm/s. Det er ikke entydigt hvilken flyvehøjde, der har estimeret strømningshastigheden bedst. Resultaterne varierer meget på tværs af flyvehøjder og lokationer, hvilket indikerer problemer med reproducerbarheden af resultaterne fra Doppler radaren.

PIV havde mangler i resultaterne, og gav enkelte steder underestimeringer af strømningshastigheden, på grund af lav seeding densitet, som er nødvendigt for succesfuld PIV. PIV blev brugt til at undersøge de footprints, hvori Doppler radaren måler, for at bekræfte hypotesen om de to toppe i Doppler spektrene. Det kunne bekræftes, at den ene top i Doppler spektret skyldes dronens propeller, da histogrammer af PIV hastighederne i footprintet kun har en top. Det viste også, at der kan registreres flere forskellige strømningshastigheder i samme footprint, hvilket besværliggør bestemmelse af strømningshastigheden med Doppler radaren. Dette gælder særligt, når strømningshastigheden ændrer sig hurtigt på tværs af floden.

Preface

This paper is authored by Environmental Engineering bachelor-students Laura Riis-Klinkvort (s204319) and Emilie Ahrnkiel Jørgensen (s204350). The project has been supervised by Peter Bauer-Gottwein. Data was obtained under validation survey of the project UAWOS in Rönne Å in Sweden.

Information about the project can be found here: https://uawos.dtu.dk/. All the data collected in Rönne Å is available on the data repository here: https://figshare.com/s/86d39f030f1a9a5d6c97.

This paper is focused on Doppler radar velocimetry, with the inclusion of Particle Image Velocimetry and in-situ velocimetry (OTT MF Pro).

We would like to acknowledge and thank all survey operators that were with us in the field: Monica Coppo Frias, Christine Lindenhoff, Sune Nielsen, Makar Lavish, Lars Yde, Alexander Rietz, Zhen Zhou, Daniel Olesen, Peter Bauer-Gottwein, Daniel Wennerberg, Viktor Fagerstroem, Jenny Axen, David Gustafsson. Thanks to Peter Bauer-Gottwein for supervision and guidance.

Jan Rallandrond

Both authors have contributed equally to all chapters of this paper, fieldwork and data treatment.

Signatures

Contents

1	roduction	6	
2	Met	${f thods}$	8
	2.1	Field site	8
	2.2	In-situ velocimetry	9
	2.3	Doppler Radar velocimetry	11
		2.3.1 UAS Platform and payload	11
		2.3.2 Velocity determination from the Doppler shift	12
		2.3.3 Doppler flight	13
		2.3.4 Doppler radar footprint	13
		2.3.5 Interpreting Doppler spectral data	15
		2.3.6 Modeling the Doppler signal	17
		2.3.7 Doppler data processing steps	17
	2.4	Positioning	19
	2.5	Particle Image Velocimetry	20
	2.6	Footprint analysis	22
3	Res	sults and analysis	25
	3.1	In-situ and Doppler radar velocimetry	26
		3.1.1 Error statistics	27
		3.1.2 XS1	28
		3.1.3 XS2	31
	3.2	PIV results	36
		3.2.1 XS1	36
		3.2.2 XS2	36
		3.2.3 PIV of XS3	39
		3.2.4 PIV of XS6	39
	3.3	Footprint analysis	40
		3.3.1 XS2	40
		3.3.2 XS3	43
4	Disc	cussion	46
	4.1	Discarded flights from XS5	46
	4.2	Decreasing hovering time	47
	4.3	Advantages and disadvantages of the three velocimetry methods	50
	1.0	4.3.1 PIV	50
		4.3.2 Doppler radar	50
		4.3.3 OTT MF Pro	51
	4.4	Pagelta of DIV	51

	4.5 Results of the Doppler radar	51
	4.6 Recommendations for future work	52
	4.7 Applications of the technologies	53
5	Conclusion	54
	References	56
A	Cross-sections from above	59
В	Boundaries and starting parameters for each flight	64
\mathbf{C}	Hovering positions	65
D	Argumentation for discarded waypoints	68
E	Basis for error statistics	80
F	Footprint analysis	87
\mathbf{G}	30 sec hovering results	88

1 Introduction

Measurements of surface velocity can be used for estimating discharge in rivers (Bandini et al., 2022). Discharge data is used for water resources planning and flood forecasting (Fulton et al., 2020). Traditionally, measurements of velocity are carried out in-situ by wading in shallow waters using velocity probes such as the electromagnetic probe OTT MF Pro, or with Acoustic Doppler Current Meter (ADCP) at larger depths (Fulton et al., 2020). Traditional methods, while reliable, often face limitations in terms of spatial coverage, cost, and operational efficiency. These methods are very time and man-power consuming. Furthermore, not all rivers and streams are equally accessible for the traditional methods, in remote and hard-to-reach areas even dangerous or impossible, especially during floods. Therefore many rivers and streams are currently unmonitored or little data is available. This study centers on Doppler radar technology as a primary tool for river surface velocity estimation. Doppler radar utilizes the principle of frequency shift caused by motion, allowing for non-intrusive and real-time measurement of surface water velocities. By mounting Doppler radar systems on Unmanned Aerial Systems (UAS), this technology can be applied in hard to reach areas (Bandini et al., 2022).

The UAS-borne Doppler radar is a recent advancement in contactless velocimetry. Previously, it has primarily been mounted on bridges or placed on the banks. Bandini et al. (2022) conducted surveys on 5 rivers in Denmark and Sweden, comparing UAS-borne Doppler radar with in-situ velocimetry and Particle Image Velocimetry (PIV). The Doppler radar used was a 24 GHz pulse radar. The paper emphasizes several challenges with UAS-deployment of a Doppler radar, such as "UAS vibrations, large instrument sampling footprint and large required sampling time" (Bandini et al., 2022). Overall, the UAS-borne radar didn't work very well on the Danish rivers examined, due to too low water surface roughness, a result of low flow, a soft bed material and not enough wind. While it worked better for the Swedish rivers with high flow and water surface roughness, it still showed poor repeatability. The errors may have been due to the filters applied to the data, that were intended for stationary use and thereby inability to correct and interpret data (Bandini et al., 2022).

Prior to this study, there has been a UAS-deployment of 24 GHz continuous wave (CW) Doppler radar measuring surface velocity in 5 rivers in North America by Fulton et al. (2020). They were able to validate the results using a handheld acoustic Doppler velocimeter and found a difference around -1 to 1%. However, the results only compare a single measurement of maximum surface velocity, not a full cross-sectional velocity profile. They found that Doppler velocimetry did not work well for surface velocities below 0.15 m/s. The flights were carried out at different altitudes, 8 m and 5 m are reported. Propwash, the surface waves generated by the UAS propellers were found to create a bias in the Doppler spectra that could influence results. They did not find propwash at altitudes greater than 5 m (Fulton et al., 2020).

Plant et al. (2005) performed various surveys with Doppler radar velocimetry; a CW radar of 24 GHz mounted from a bridge and a cableway, a pulsed Doppler radar from a riverbank, and attempts from both a helicopter and a plane. The stationary measurements from bridges, cableways and riverbank all showed accuracy within 10 cm/s, when compared to in-situ measurements. From the bridge, the radar was mounted at a height of 10 m above the water surface. Under low flow conditions, defined as less than 1 m/s, the sensors did not yield measurements unless wind speed was high or rain was falling. The Doppler radar deployed from a helicopter was a pulse radar with a transmitter and receiver on opposite sides, so that the received signal was not disturbed by

the transmitted pulse. The helicopter flights were most successful close to the water surface, where the helicopter generated downwash increased surface roughness. Airplane flights were less successful (Plant et al., 2005). Plant et al. (2005) has specified that the algorithm used for picking out the surface velocity from the Doppler spectra as being the midway frequency between Bragg lines.

Particle Image Velocimetry (PIV) is a well-studied optical method, that relies on tracking displacement of patterns of particles in consecutive image frames. PIV has shown good agreement with OTT MF Pro in the survey by Bandini et al. (2022), with errors of a few cm/s. Detert and Weitbrecht (2015) compared a low-cost PIV payload with ADCP measurements and found good agreement with mean standard deviations below 10%. The main challenges with regard to PIV is the sensitivity to seeding density (Saso et al., 2020). The result accuracy is also dependent on the ability to translate between pixel units and meters.

This paper will examine three different methods used for river velocimetry measurements, both in-situ with wading instrument OTT MF Pro and contactless methods, UAS-deployed Doppler radar and Particle Image Velocimetry. The aim of this paper is to understand Doppler radar data and refine surface velocity estimates from the Doppler radar. Different model assumptions will be applied to the data, and footprint analysis is performed to consolidate interpretations of the spectral output. PIV will be presented as a standalone result, but the primary purpose is to utilize PIV to better understand Doppler data.

2 Methods

In the following, an introduction will be given to the field sites surveyed in Rönne Å in Sweden, the three velocimetry methods: in-situ using OTT MF Pro electromagnetic probe, UAS-deployed Doppler radar velocimetry and Particle Image Velocimetry (PIV). Positioning of the data will also be explained.

2.1 Field site

The table below shows an overview of field site locations, survey dates and surveys carried out. The surveys were conducted from 29th of August to 31st of August 2023. Results of surveys highlighted in **bold** will be presented in this paper. More velocimetry methods as well as bathymetry surveys were conducted, but will not be presented. All days except 31/08/2023 had mild weather with sun and light wind. 31/08/2023 saw strong rainfall. River water levels were high with some flooding at surrounding fields for some stretches after a longer wet period prior to the survey.

Table 1: Field sites overview. Coordinates in SWEREF99.

bank coords | Right bank coords | Survey date | Surveys | Depth | Wi

Site	Left bank coords	Right bank coords	Survey date	Surveys	Depth	Width	Remarks
	Easting, Northing	Easting, Northing					
XS1	377178.7262,	377202.9943,	29/08/2023	OTT	2.8 m	33.4 m	First 5-6 m from
	6227686.785	6227709.81		Doppler			each bank very
				PIV			densely vegetated
				Bathymetry			
XS2	381436.6493,	381449.8463,	30/08/2023	OTT	0.7 m	16.0 m	Flow much faster
	6222655.516	6222666.31		Doppler			than other XS
				PIV			Very rocky, some vegetation
				Bathymetry			Only wadable XS
XS3	381204.028,	381207.04,	30/08/2023	OTT	1.7 m	25.8 m	Densely vegetated
	6222774.967	6222800.617		Doppler			first 10 m from right bank
				PIV			
XS4	379743.613,	379754.399,	31/08/2023	Bathymetry	2.2 m	26.6 m	Similar conditions
	6226315.925	6226339.718					to XS5 and XS6
XS5	379629.036,	379618.483,	31/08/2023	OTT	2.5 m	27.8 m	Densely vegetated
	6226245.33	6226271.15		Doppler			on right bank
				PIV			
				Bathymetry			
XS6	379400.035,	379393.676,	31/08/2023	OTT	1.7 m	20.1 m	Densely vegetated
	6226227.146	6226246.231		Doppler			on right bank
				PIV			
				Bathymetry			

A map of the field locations can be seen below, with orthophotos by SMHI overlaid Google satellite image of the area. Absolute accuracy of the ortophotos is better than 50 cm, and distances are accurate down to the cm level (Bauer-Gottwein, 2023). The stretch of the river that is inspected (Survey Centerline) is approximately 10 km.

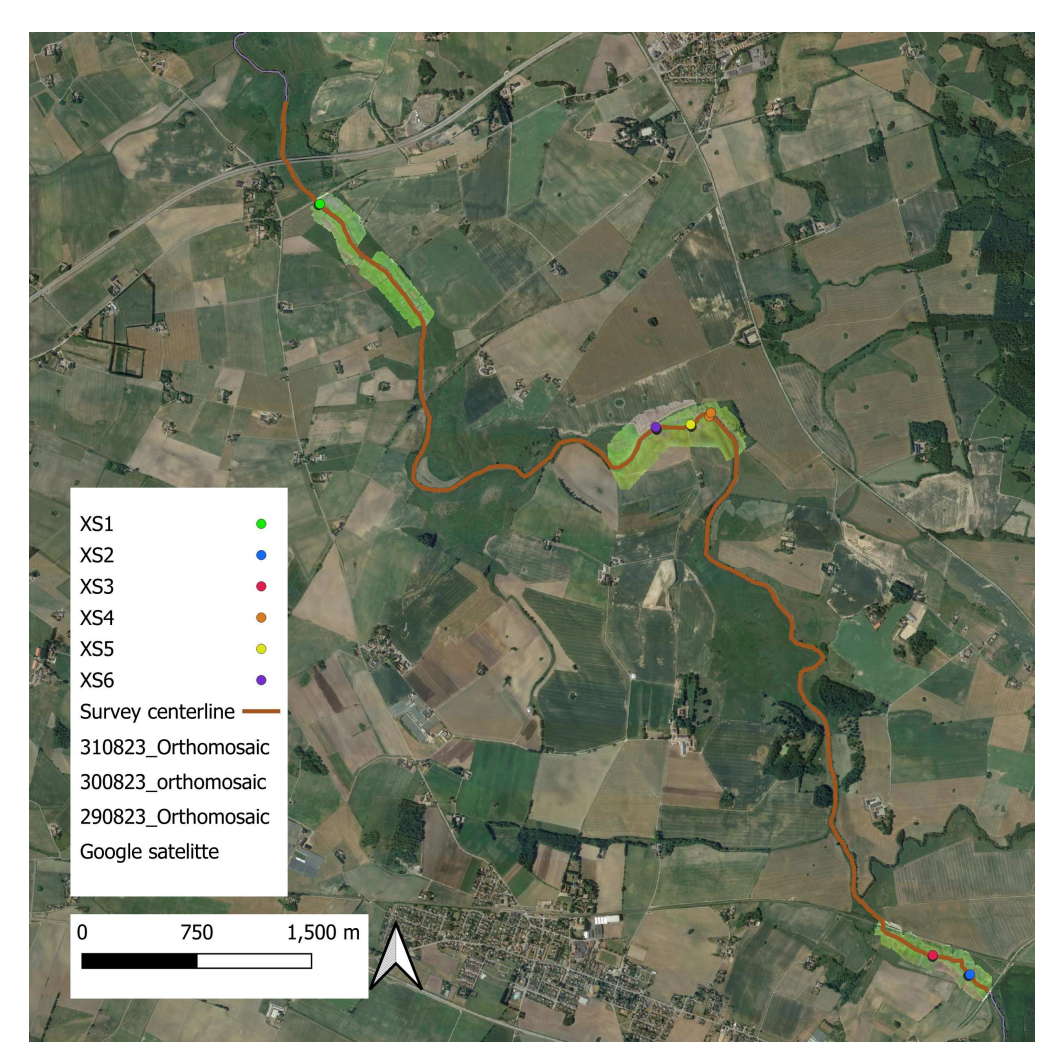


Figure 1: Map of the survey sites. Coordinate system SWEREF 99.

Aerial images of cross-sections 1,2,3,5 and 6 as retrieved by the Phantom 4 can be seen in Appendix A. Maps based on the ortophotos taken by SMHI can also be seen in Appendix A.

Prior to any other measurements, the cross-sections were first established with a tagline. The tagline was set up perpendicular to the flow direction. This was done by crossing the river by boat or wading, placing a pole at both sides and tying a rope and measuring tape between the poles. Right and left bank are determined by looking in the flow direction. In-situ velocimetry measurements were then carried out before UAS flights. Preparation of the tagline and in-situ velocimetry measurements took about 1 hour altogether for each cross-section. Both tagline pole coordinates are retrieved with Real Time Kinematics for georeferencing and flight planning. UAS flights were conducted hereafter.

2.2 In-situ velocimetry

The in-situ velocimetry measurements were carried out using an OTT MF Pro electromagnetic current meter. The OTT measurements are point measurements, meaning the measurements represent the velocity at that

specific point. The OTT MF Pro consists of an electromagnetic sensor, a wading rod and a meter display. Electromagnetic current meters are based on Faraday's principle (Fulford et al., ND). Faraday's principle states that a moving conductor in a magnetic field will generate a voltage proportional to the speed of the conductor (Fulford et al., ND). The sensor head on the OTT MF Pro generates a magnetic field, and water is a moving conductor. Thereby, a voltage is produced in the magnetic field when water flows through, and electrodes on the sensor head measure this voltage (OTT HydroMet, 2015). The sensor must be held straight against the flow direction. The figure below illustrates how the sensor on OTT MF Pro works:

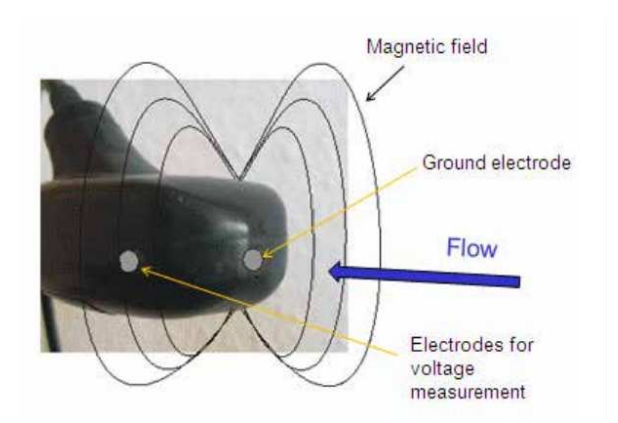


Figure 2: The magnetic field induced by the sensor and electrodes that measure the voltage upon water flowing through the field. Figure from OTT HydroMet (2015).

The OTT MF Pro can be used as a wading instrument, in rivers that can be waded through. Only one cross-section could be waded through, namely cross-section 2. All other cross-sections were crossed by boat, and the OTT measurements were done by submerging the current meter by hand from the side of the boat. The OTT MF Pro can be used to measure and calculate full discharge of a river (OTT HydroMet, 2015), however for this survey only the surface velocity was measured. This was done by keeping the sensor head fully submerged in the water at the very surface. The measurements were carried out every 1 m along the tagline. Every measurement is a Fixed Period Average velocity with the default period of 30 seconds (OTT HydroMet, 2015).

The OTT MF Pro has an accuracy of $\pm 2\%$ of measured value or 1.5 cm/s, depending on whichever value is larger (OTT HydroMet, ND). At cross-section 2 maximum velocities were around 136 cm/s, resulting in an accuracy of \pm 2.7 cm/s. For the other cross-sections the accuracy will not surpass \pm 1.5 cm/s. It bears mentioning that there is a trade-off between velocity errors and low-conductivity water, below 200 $\mu S/cm$. The magnitude of the error depending on the conductivity is described in OTT HydroMet (2015). The conductivities were measured in the field and are presented in table 2.

Table 2: Conductivities measured for the different cross-sections and dates.

Site	EC $\mu S/cm$	Date
XS1	150	Monday, August 28, 2023
XS2	199	Wednesday, August 30, 2023
XS2	216	Wednesday, August 30, 2023
XS3	200	Wednesday, August 30, 2023
XS5	161	Thursday, August 31, 2023
XS6	161	Thursday, August 31, 2023

The conductivities are adequate for electromagnetic probe measurements, so a larger error than reported is not expected.

2.3 Doppler Radar velocimetry

This chapter will describe the Doppler radar payload, the principles of how the Doppler radar measures velocimetry utilising the Doppler shift, as well as flight and measurement considerations. Furthermore, it will be explained how the data from the Doppler was interpreted and modelled for surface velocity determination.

2.3.1 UAS Platform and payload

The Doppler radar payload carries the Geolux RSS-2-300W Doppler radar onboard a DJI Matrice 300 (Geolux, ND). The DJI Matrice 300 is a quadcopter (DJI Enterprise, ND). It is reported to have a hovering accuracy of \pm 0.1 m horizontally and vertically when RTK is enabled (DJI Enterprise, ND). The UAS has an RTK antenna on the wings, that records positioning. The RTK positioning accuracy is reported to be 1 cm + 1 ppm horizontally and 1.5 cm + 1 ppm vertically (DJI Enterprise, ND). Additionally, an Emlid PPK antenna was mounted on the drone, that recorded RINEX positioning files, that were used for PPK post-processing of location, incase the RTK was temporarily offline (Bauer-Gottwein, 2023). The data was logged using the SkyHub onboard computer by SPH Engineering (SPH Engineering, 2023). The drone flight was fully automated using True Terrain Following technology based on the radar altimeter (SPH Engineering, 2021). The radar altimeter on the UAS was NRA24 by Hunan Nanoradar Science and Technology Co, a 24 GHz Altimeter Radar with a measuring accuracy of \pm 0.1 m (Nanoradar, ND).





Figure 3: Left: The DJI Matrice 300 up close with the Skyhub onboard computer. Right: Doppler radar payload inflight, the radar is the white square mounted below the main body of the drone.

The RSS-2-300W Doppler radar is a continuous wave (CW) radar, meaning it continuously emits electromagnetic radiation at a constant frequency. The frequency lies in the microwave spectrum, specifically in the K-band with a frequency between 24.075 to 24.175 GHz (Geolux, ND). The microwaves travel at the speed of light in air, resulting in a wavelength of 12.5 mm. Geolux reports that the radar works for river velocities between 0.02 m/s to 15 m/s. The velocity resolution is 7.3921 mm/s (Geolux, ND). Velocity resolution in a Doppler radar refers to the ability to distinguish between different velocities. The radar has a sampling rate of 10 sps (samples

per second) (Geolux, ND). Geolux reports an accuracy of $\pm 1\%$ (Geolux, ND).

2.3.2 Velocity determination from the Doppler shift

A continuous wave Doppler radar continuously emits a signal with a known frequency (Fulton and Ostrowski, 2008). The radiation emitted from the Doppler radar is reflected back by the surface it encounters. When the reflecting surface is moving, e.g. in a flowing river, the wavelength reflected back will be shortened or lengthened, depending on whether the object is moving towards or away from the radar (Fulton and Ostrowski, 2008). This change in wavelength and thereby also frequency is called the Doppler shift (MATLAB, 2022). The radar recorded the frequency shift of the backscattered signal. The frequency shift was translated into the radial velocity of the surface, meaning the line of sight velocity relative to the radar itself.

The observed shift in frequency, the Doppler shift, will depend on the radial velocity of the target as shown in equation 1. Note the multiplication by 2 since it is a two-way travel.

$$f\Delta = 2\frac{v_r}{c} \cdot f_0 \tag{1}$$

 $f\Delta$ is the Doppler shift (frequency shift), v_r is the velocity of the river relative to the velocity of the drone, c the velocity of the transmitted signal (speed of light) and f_0 the frequency of the transmitted signal. Only velocities in line-of-sight of the radar affect the Doppler shift. Considering the incidence angle of 45 degrees (as the tilt angle), the found velocities must be projected into the direction of the river to obtain the river flow velocity. Expanding on the equation 1 and rearranging for the velocity, the velocity is equal to:

$$v_r = \frac{f\Delta \cdot c}{2 \cdot f_0 \cdot \cos(45^\circ)} \tag{2}$$

The figure below shows a simplified overview of the Doppler shift.

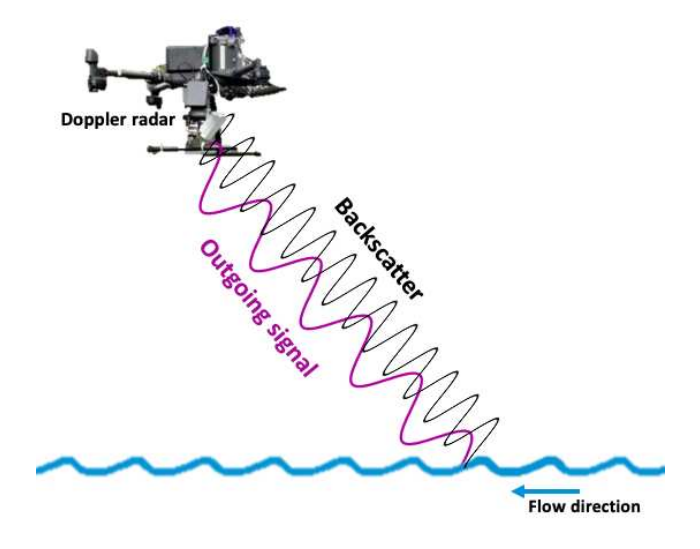


Figure 4: The figure shows how the wavelength of the backscattered signal is changed, when the surface is moving, thereby leading to a frequency shift known as the Doppler shift.

When the flow is oriented towards the radar as it was in these surveys, the frequency shift is negative.

2.3.3 Doppler flight

Doppler radars have more commonly been used stationarily e.g. mounted on a bridge (Bandini et al., 2022), as it measures relative velocity. When deploying the Doppler radar from the UAS, the drone therefore had to hover in place for a set amount of time, 1 minute at each hovering point as recommended by Lindenhoff (2023).

The Doppler was flown at several altitudes. The number of hovering points, called waypoints, depended on the altitude and the width of the cross-section. A chainage offset from the cross-section tagline was also planned, so that the radar footprint center would land on the tagline. The recommendations by Lindenhoff (2023) can be seen in the table 3 below. The altitude is kept steady by the altimeter, planned as +0.1m for the drone, to account for the Doppler radar mounted underneath. The total surveying time with the Doppler payload was 30-40 min. per cross-section.

Table 3: Flight plan for Doppler radar flights. Recommendations by Lindenhoff
--

Flight altitude	Chainage offset	Distance between hovering points
2 m (2.1 m)	2.2 m	1 m
4 m (4.1 m)	4.4 m	1.5 m
6 m (6.1 m)	6.6 m	2 m

From the two tagline pole coordinates, the Doppler flight was planned using UgCS software by SPH Engineering (SPH Engineering, ND). A pre-made template in UgCS of the number of waypoints and chainage offset based on 3 was fitted to the two pole coordinates (Nielsen, 2023). The figure below shows how the planned flight looks in UgCS software.



Figure 5: Example of flight plan in UgCS with the three different altitudes. Figure from (Nielsen, 2023).

2.3.4 Doppler radar footprint

The Doppler radar measures and averages the signal received over an area called the footprint, meaning the area on the ground that is covered by the radar beam. The footprint size depends on the flight altitude and tilt angle by which the sensor is mounted (Lindenhoff, 2023). Higher flight altitude or lower tilt angle results in a larger area of the footprint. The elliptical shape of the footprint is determined by the beam with an azimuth angle,

 θ_a , of 12 degrees and an elevation angle, θ_r , of 24 degrees (Geolux, ND). Geolux recommended a tilt angle of 45 degrees (Geolux, ND), causing the projected footprint to land infront of the UAS flight path. Figure 6, inspired by Lindenhoff (2023), shows the footprint and beam. The red ellipse depicts the footprint and the blue ellipse is the beam.

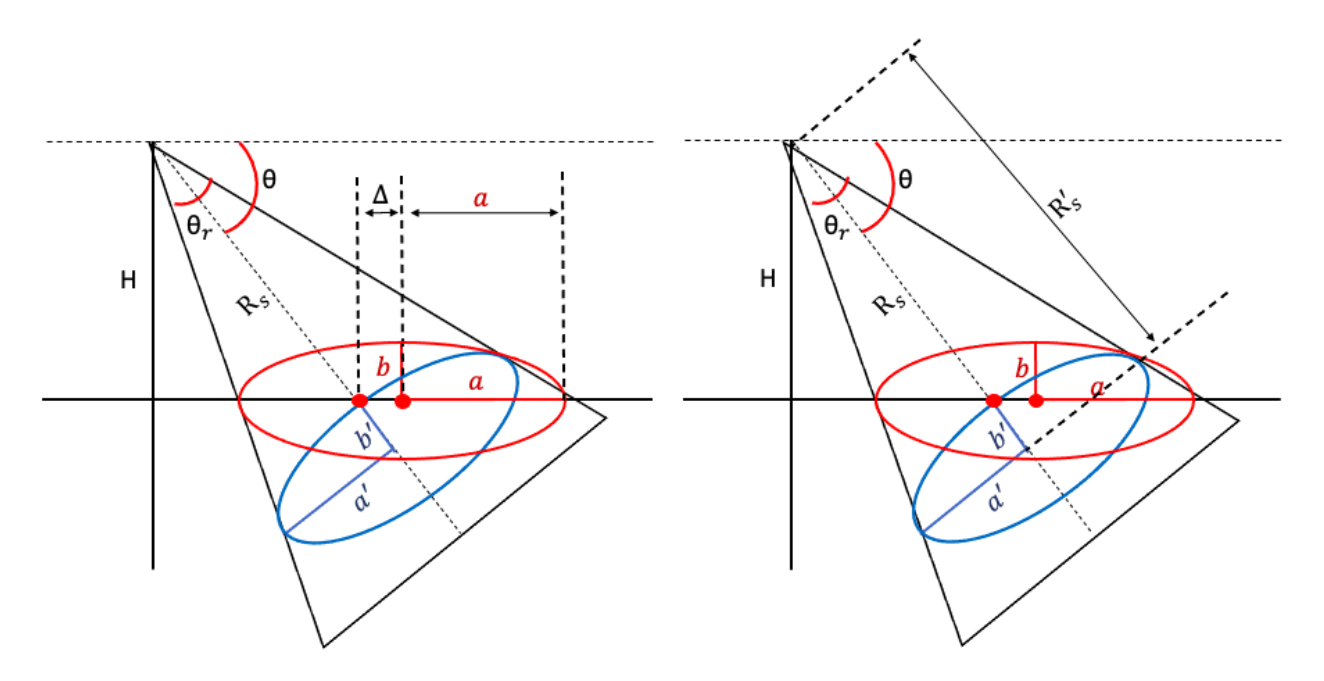


Figure 6: H denotes the flight altitude. θ is the tilt angle. θ_r is the elevation angle. a is the major axis of the footprint, and b the minor axis of the footprint. a' is the major axis of the beam, and b' the minor axis of the beam. Δ is the difference between the centerline intersection of the beam and the center of the footprint. R_s is the slant range from the drone to the centerline intersection of the beam and footprint center (Lindenhoff, 2023).

To determine the exact area of the footprint, it is necessary to determine the major and minor axis of the footprint. The major axis, a, is found by expression 3, described by Lindenhoff (2023).

$$a(\theta, H) = \frac{1}{2} \cdot (H \cdot \tan(\theta + \frac{\theta_r}{2}) - H \cdot \tan(\theta - \frac{\theta_r}{2})$$
(3)

The minor axis, b, is found from expression 4 described by Lindenhoff (2023).

$$b(\theta, H) = \frac{b'}{a'} \cdot \sqrt{(a')^2 + (\Delta \cdot \cos(\theta))^2}$$
(4)

Where Δ is the difference between the center of the footprint and the center line intersection of the beam. a' and b' are the major and minor axes of the beam (blue ellipse). Determination of these three variables is elaborated by Lindenhoff (2023).

Once the major and minor axis of the footprint is found, the distance from the drone to the center of the footprint can be determined. The distance is determined from Δ , the flight altitude and the tilt angle as

expressed in equation 5.

Distance drone to center of footprint =
$$\Delta + sin(\theta) \cdot \frac{H}{cos(\theta)}$$
 (5)

In the equation above, Δ is the distance illustrated in figure 4 found by Lindenhoff (2023) and H is the flight altitude. Each altitude leads to individual footprint sizes. The results in table 4 are based on equation 3, 4 and 5.

Table 4: Determined major and minor axis, and distance from drone to center of footprint according to flight altitude.

Altitude [m]	Major axis [m]	Minor axis [m]	Distance from drone to center of footprint [m]
2	0.890	0.304	2.189
4	1.781	0.608	4.379
5	2.226	0.761	5.473
6	2.671	0.913	6.568

2.3.5 Interpreting Doppler spectral data

The raw data was collected from the Doppler radar without the application of a filter or internal velocity calculation, to allow for spectral analysis and development of a new algorithm for picking the correct surface velocity. The data output was therefore Doppler spectra in a SEG-Y format, showing the returned energy per frequency shift. After translating the Doppler shift into velocity as in equation 2, finding the correct surface flow velocity is still not straight-forward. The received signal consists of composite surface scattering dominated by Bragg-resonant scattering (Bandini et al., 2022). Composite surface scattering refers to the complexity of the backscattered signal reflected by a rough surface, meaning there is a reflected signal from multiple scatterers. Bragg-resonance refers to the type of composite surface scattering, that occurs when the radar wavelength is comparable to the surface features causing the scattering. In velocimetry measurements, the surface features are short surface waves on the river with a magnitude of a few cm, that the beam impacted at an angle. The velocities of these features creates distinct peaks in the spectral data. It is therefore important, that the water surface has a certain roughness. Bandini et al. (2022) reports a surface roughness of at least 1 mm. The exact length of the waves causing Bragg-waves can be characterized by the formula for the Bragg resonance condition (Plant et al., 2005):

$$\lambda_b = \frac{\lambda}{2 \cdot \sin\theta} \tag{6}$$

Where λ is the wavelength that the Doppler radar emits, here 1.25 cm, θ the incidence angle of 45 degrees, resulting in a wavelength of the scatter-inducing waves of 0.88 cm (Fulton et al., 2020).

The Doppler spectra presented in this paper are an average of the samples recorded during the hovering period. Therefore, the velocity of the surface scatterers will primarily be caused by larger waves representing the river surface velocity, which can therefore be determined. By ensuring a long enough hovering period, other causes of movement such as rain drops or eddies will not give a distinct peak. Rivers primarily have a flow in one direction, wherefore the assumption would be that the Doppler spectra would have one peak representing the surface velocity.

When mounting the radar on the UAS, a second peak occurs due to the drone propellers causing propeller-

induced waves in the footprint, also called proposals. A second peak is visible in most of the recorded spectra, assumed to be the sum of the river surface velocity and proposals generated surface velocity. The equation below describes the two velocities received by the radar:

$$V_{Peak1} = -V_{\text{river}}$$

$$V_{Peak2} = V_{\text{propwash}} + (-V_{\text{river}})$$
(7)

The radar was placed against the flow direction and the river surface velocity recorded was therefore interpreted as negative (incoming). The proposal was generated against the flow direction and was a positive component, as presented in equation 7. When reporting the Doppler estimated surface velocity, it is the absolute velocity.

Looking at a waypoint velocity spectrum from XS1 in figure 7, the two peaks explained above are clear. The velocity axis is created from the velocity resolution divided by cosine to the tilt angle, as explained in equation 2. It is important to realise that velocities around 0 cm/s cannot be recorded, since there is no Doppler shift. Because of this, data is masked out from -15 cm/s to 15 cm/s (Bauer-Gottwein, 2023). The y-axis on the Doppler velocity spectra is returned energy. A taller peak therefore means a stronger returned signal. Figure 7 on the left demonstrates two peaks at -50 cm/s and -25 cm/s. Due to the orientation of the Doppler radar against the flow direction, it registers river surface velocities as negative. The absolute value is taken when reporting the surface velocity estimate. It is an average of the signal from all the traces recorded at the waypoint. Based on in-situ observations, the assumption is that the higher velocity of 50 cm/s corresponds to the river surface velocity. Note that it is the higher velocity, but not the taller peak in terms of returned energy. This shows that the proposal has a major impact on the signal recorded by the Doppler radar. Right plot shows the same data, but per trace instead of averaged, from here on called the full waveform plot. Traces are a collection of samples, since 10 samples are recorded per second. Returned energy is shown in the color instead of the y-axis, note that it is limited to a maximum of 500, but may be higher. A stable measurement will have a stable line of returned energy throughout all the traces. If this is not the case, it may mean the drone was unstable during the measurement.

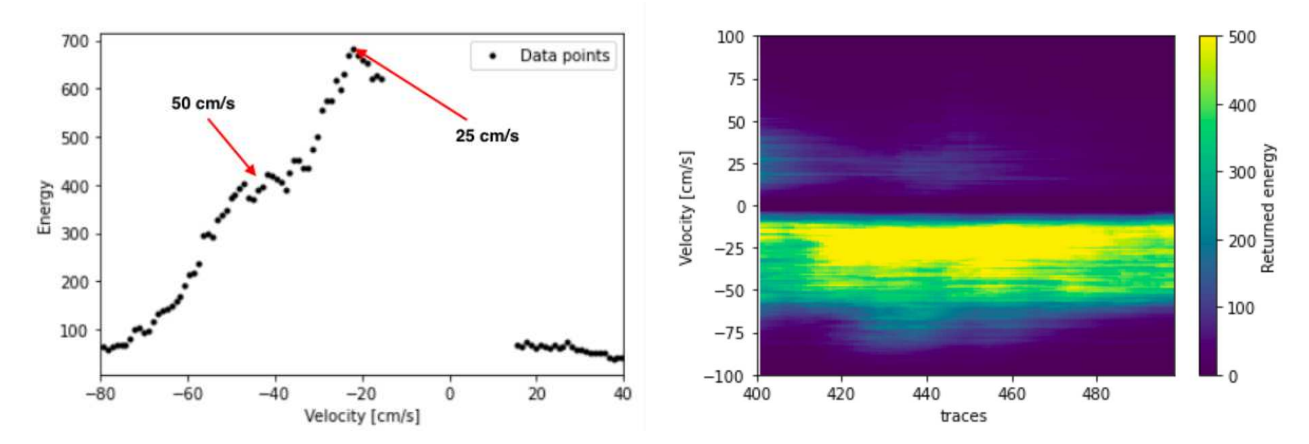


Figure 7: Left: Doppler spectrum averaged over traces collected at waypoint. Right: full waveform plot of signal for all the collected traces at the same waypoint.

2.3.6 Modeling the Doppler signal

To automate picking the correct river surface velocity in each waypoint, a model was built with two peaks. The velocity expectations were as shown in equation 7. The surface velocity of the river was assumed to be higher than the proposal velocity. The model was based upon a double peak Gaussian distribution. The Gaussian distribution, also known as a normal distribution, is a symmetrical bell curve distributed around a mean with a spread equal to the standard distribution (Athanasiou et al., 2017). The Gaussian distribution is by definition unimodal, meaning it only has one peak (Athanasiou et al., 2017). The model built for depicting the Doppler velocity therefore has the addition of another Gaussian peak, and becomes a bimodal model (Siegel and Wagner, 2022). The probability density function (PDF) is shown in equation 8, where the PDF of the individual Gaussian peaks were added together.

$$f(x) = f_1 \cdot \frac{1}{\sigma_1 \cdot \sqrt{2 \cdot \pi}} \cdot e^{\frac{(x - \mu_1)^2}{2 \cdot \sigma_1^2}} + f_2 \cdot \frac{1}{\sigma_2 \cdot \sqrt{2 \cdot \pi}} \cdot e^{\frac{(x - \mu_2)^2}{2 \cdot \sigma_2^2}}$$
(8)

Here μ_1 and μ_2 are the means of the peaks, σ_1 and σ_2 are the variances of the peaks, and f_1 and f_2 are the weight of each peak. The surface velocity of the river was assumed to be equal to one of the means, and the sum of proposals and river surface velocity was assumed equal to the other mean.

It was assumed that each peak could be approximated with a Gaussian distribution, based upon the look of the peaks, as shown in figure 8.

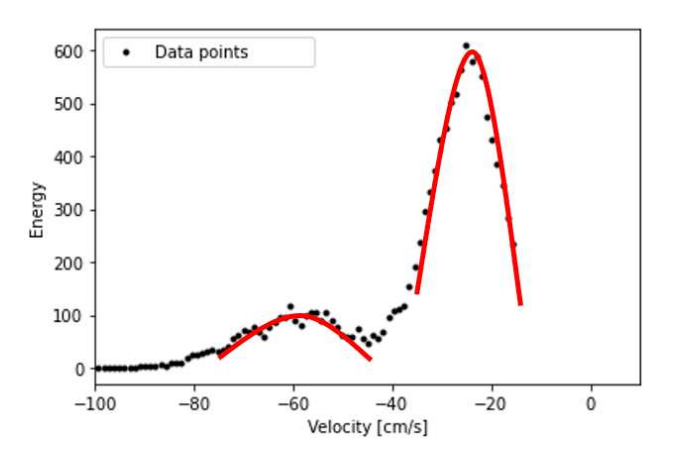


Figure 8: Double peak model of Doppler spectrum

When creating the double peak model, values were input for the mean, standard deviation and the weight of each peak. These inputs were found by approximation from the raw data. It was sufficient with an approximation, since the model afterwards was optimized to fit the data, as explained below.

2.3.7 Doppler data processing steps

The Doppler recorded the full flight, not just waypoints. To determine the waypoints in the data, it was assumed that the UAS distance along the tagline during hovering was constant. It was possible to distinguish only the hovering periods from the data, as the distance along the tagline could be seen as a horizontal straight line, when

plotting distance along the line against traces as in figure 9 to the right. Besides the distance to the tagline, the altitude should also be constant during hovering. The plot of these two variables against the traces of the full flight can be seen in figure 9. To define the waypoints in the data, the start and end trace, where the drone was hovering, were selected and saved. These are illustrated in figure 9.

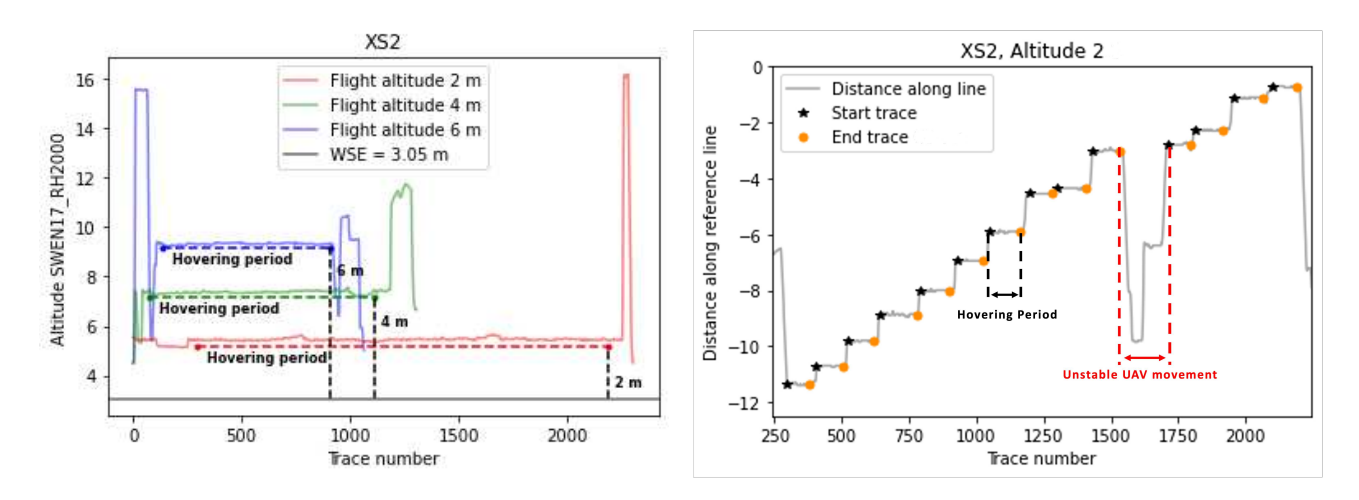


Figure 9: Left: Altitude vs. trace numbers. Right: Distance along tagline vs. trace numbers.

For each individual waypoint, the bimodal Gaussian distribution model was fitted with non-linear least squares optimization. The non-linear least squares method, is a method that aims to minimize the sum of the squared errors between a model and data points (The scipy community, ND). When trying to fit the model, a RUN-TIMERROR occasionally occurred and these waypoints were removed. From the optimization, the ideal parameters for the model were retrieved. The optimization was done either by providing a starting guess of the parameters, or by limiting the boundaries of the parameter estimation. When using starting parameters, these were manually determined from the shape of the velocity spectra for the individual flight. When using starting parameters, the boundaries where set to plus and minus infinity for each parameters, exect the weight which could only be positive. Limited boundaries for optimization was in some cross-sections set instead of starting parameters. The parameters or boundaries used for each flight can be seen in appendix B. The boundaries were also estimated manually, and the parameters were thus constrained to a region of values in the optimization. Starting parameters or boundaries were chosen, depending on what gave the best result for that particular flight.

As the ideal parameters were found for the bimodal Gaussian distribution model, the root mean square error (RMSE) between the data and the model was calculated. The root mean square error where found from equation 9 (M. Padhma, 2023).

$$RMSE = \sqrt{\frac{\sum_{i=1}^{N} (Predicted_i - Actual_i)^2}{N}}$$
(9)

A tolerance of RMSE = 50 was set for this analysis. The unit is returned energy, like the y-axis of the data points. The velocity where estimated from the two means in the optimized model, where it was assumed that the highest absolute mean of the two was equal to the river velocity, based on the assumption from section 2.3.5.

2.4 Positioning

When collecting and working with geospatial data, correlating the data with precise positioning is very important. For accurate positioning in the field, a real-time kinematic (RTK) rover, Emlid Reach RS+ (Emlid, NDd), was used to obtain coordinates. The rover was attached to a 2 m rod. The rover was controlled via a smartphone using the app Emlid Flow. With the rod, it took about 10-15 seconds to establish a fixed location for each measurement. The Doppler payload also carried an RTK antenna. Every trace recorded by the Doppler radar also had a location. RTK Global Navigation Satellite System (GNSS) technology is a GNSS technology, that improves GNSS positioning to cm accuracy for the rover, using a combination of satellite-emitted signals and a local base station with a known location (Odonohue, 2023). It differs from traditional GNSS systems, that are based only on satellite code signals and a single receiver, by incorporating the carrier phase measurement and the base station. Disturbances in the satellite signals such as atmospheric delays, clock errors and multipath errors cause traditional GNSS technology to have accuracy in the range of a few meters (Odonohue, 2023). By having a nearby stationary base station, the base station can transmit error corrections to the receiver in realtime, and the receiver's location is computed as relative to the base station. A base station was therefore set up in the field close to the surveying site, within a few kilometers at most of the surveying cross-section. RTK however require a stable connection between the rover and the base station which can be disturbed by trees at the site. The data from the UAS logs whether the RTK connection was on or off. Since it was often offline, it was necessary to do Post-Processed Kinematic (PPK) processing of the UAS position.

PPK are essentially the same technology as RTK, however in PPK the raw GNSS measurements are logged and no real-time correction is done while measuring (Emlid, NDb). Often PPK was used as a backup for RTK when the RTK went offline due to it's sensitivity to vegetation (Emlid, NDb). PPK processing was carried out using the software Emlid Studio (Emlid, NDe). RINEX (Receiver Indepedendant EXchange format) files from the rover and the base station were uploaded along with the precise coordinates of the base station. The coordinates of the base stations were found in the field by using RTK on most days of the fieldwork. In the few cases it had not been done, Precise Point Positioning (PPP) was used to establish it afterwards (Emlid, NDc). The raw RINEX files from the base station were uploaded to PPP service Canadian Spatial Reference System Precise Point Positioning (Emlid, NDa). PPP technology differs from RTK and PPK by not needing the distance between rover and base station to estimate position (Emlid, NDc). It instead refers to a global reference frame and precise ephemerides and clock error corrections are provided by the PPP service (Emlid, NDc).

RTK and PPK antennas onboard the UAS track position according to the WGS84 geodetic datum. Datum refers to a model with a specific ellipsoid that approximates the shape of the Earth and a specific fixing point for coordinate origin (Lantmäteriet, NDc). Geoid models that approximate Earth's mean sea level are the basis for fitting an ellipsoid to, essentially the geoid is Earth without surface topography, but due to different gravitational pulls the surface is still not a perfect ellipsoid. The WGS84 is the most common global-fit datum, fixed to the Earth's centre of mass (Lantmäteriet, NDc). Since the WGS84 is an ellipsoid, the drone's horizontal position is therefore logged in angular longitude latitude coordinates. The WGS84 also has a vertical datum (elevation), which gives the drone's altitude as the height above the ellipsoid. However, since the WGS84 is the best global fit, it may not be the best approximation for Sweden. Positions are therefore converted to the horizontal coordinate reference system (CRS) SWEREF 99 TM where coordinates will be given in Easting and Northings. SWEREF 99 coordinate system is based on ETRS89 datum, which is a European reference datum based on the GRS 1980 ellipsoid that is approximately equal to the WGS 84 ellipsoid except of a difference of

0.1 mm in half the minor axis (Lantmäteriet, NDb). The ETRS89 datum differs from the WGS84 datum in that it has it's fixed coordinate origin in Europe, so Europe's coordinates do not change due to continental drift, but the difference between the two is small. SWEREF 99 TM is a national realization of ETRS89, meaning specifically adjusted so that national Swedish coordinates do not change (Kempe et al., 2016). SWEREF 99 TM differs by 7-8 dm from WGS 84 (Lantmäteriet, NDb). The vertical datum, that drone altitude is transformed to, is SWEN17_RH200, a geoid model for Sweden, meaning locally the best possible approximation of mean sea level (Lantmäteriet, NDa). The altitude as given in SWEN17_RH200 is thereby the height above the geoid or mean sea level, instead of the height above the ellipsoid (Lantmäteriet, NDa).

As the exact coordinates of the radar were processed, the coordinates were compared to the coordinates of the tagline for the cross-section. The tagline coordinates were based on RTK coordinates of the right and left pole. A straight line between these two coordinates was then constructed. For plotting, data was plotted against its' distance along the tagline. Distance along the tagline was here measured from the river centerline. The 0 point was therefore approximately in the middle of the river, while negative values are moving to the left of the centerline and positive values are moving to the right.

2.5 Particle Image Velocimetry

Particle Image Velocimetry (PIV) is, like the Doppler radar method, a contactless method of river flow estimation (Bandini et al., 2021). It is an optical image cross-correlation technique. PIV tracks patterns on the surface to obtain the flow field using similarity and pattern recognition algorithms (Strelnikova et al., 2020). The method requires visible seeding on the surface, that may be recognised. This could be created by applying seeding in the form of woodchips, but often in this survey there was natural seeding such as bubbles or surface ripples present (Bandini et al., 2021). Videos of the flow at each cross-section were taken using a Phantom 4 Pro by DJI (Martin, 2017), shown in figure 10. The camera pointed nadir for minimal image distortion. The necessary flight time for taking a PIV video sequence was only a few minutes per cross-section, making it the fastest of the three methodologies in terms of surveying time per cross-section. Surveying time was longer when seeding had to be applied, and required several operators. It also required access to the riverbanks or somewhere where seeding could be applied from. Woodchips were applied in XS1 and XS6.



Figure 10: Phantom 4 by DJI. Image from Martin (2017).

The frame rate of the videos filmed by the Phantom 4 was 59.904 fps. The videos were trimmed to short clips of

1-2 seconds. The image resolution was 3840 x 2160 px with 0,0 at the top right corner. The table below shows which clips were used for PIV analysis, available on the data repository. It also shows determined meters per pixel unit for that particular cross-section. How this was determined will be elaborated in the following.

Field site	Video	Trim	Determined mpp
XS1	DJI_0006_XS1.MP4	30.983 to 36.034s	0.0086
XS2	DJI_0009_XS2.MP4	0 to 01.675 s	0.0088
XS3	DJI_0010_XS3.MP4	0 to 02.080 s	0.0067
XS6	DJI_0015_XS6.MP4	3 to 6 s	0.0073

Table 5: Video sequences extracted for PIV.

Prior to processing with PIVlab for Matlab, the clips were processed into individual frames using image segmentation, and stabilized using stable features on the image such as the banks. Image color masking was performed to transform the frames into binary images, meaning black and white, with white highlighting the tracers. One frame refers to one image pair, between which the movement of a pattern was analyzed. The frames were processed using PIVlab for Matlab (Thielicke, ND). The frames were masked to exclude non-river areas from the analysis. PIVlab then calculated vector fields for all pixels of the frame based on image pairs (Thielicke, ND). The default Fast Fourier Transformation (FFT) window deformation correlation algorithm was used with Gauss 2x3 point sub-pixel estimator. Four interrogation areas of sizes 256, 128, 64 and 32 were chosen for all PIV analyses based on recommendations by Bauer-Gottwein (2023). The PIVlab analysis settings and interrogation areas can be seen below in figure 11.

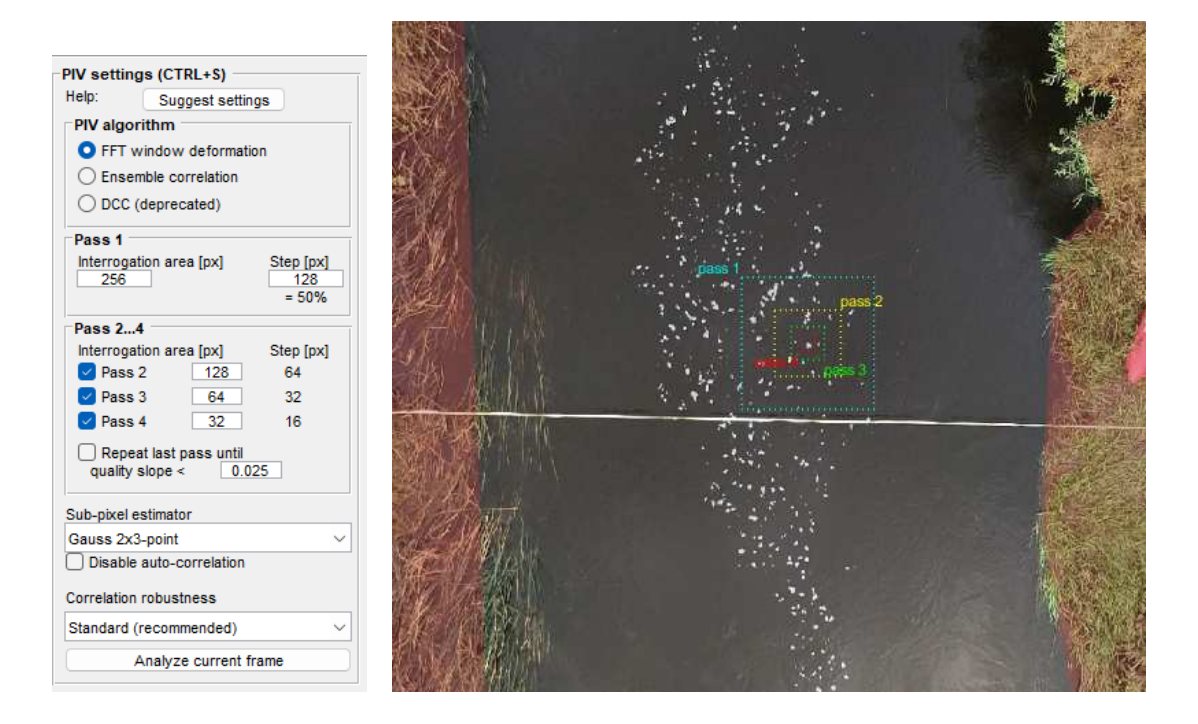


Figure 11: Left: PIV analysis settings. Right: Interrogation areas vizualised on a frame from XS3. Red areas on the borders indicate masked out areas on the banks. The bubbles on the surface are natural seeding.

Outliers were sorted out by taking out frames with irregularly large vectors, hinting at video instability, and by

looking at the kernel density plot of the vectors. The kernel density plot shows the distribution of the velocity vectors. Vectors that did not fall within the chosen range were then removed from the frames. The valid applied range was from 0 to 3 px/frame for the v vectors, knowing that only positive v vectors are in the flow direction. The u limit was lower since a lot of movement in the horizontal direction hints at video instability. The temporal mean across all frames was computed hereafter with no interpolation for missing values, and the result was horizontal velocity vectors u and vertical velocity vectors v in unit pixels/frame for every pixel of the image where a velocity was determined. The result was saved as a text file. Translating from pixels to meters requires two ground control points (GCPs) in the image with known real world coordinates. By obtaining their pixel-coordinates from the image, the real distance between GCPs can be divided by the pixel distance to obtain the meters per pixel. Frames were converted to seconds knowing the frame rate per second. The GCPs also allowed for georeferencing of the image, used for the footprint analysis where exact positions of the footprint on the flow images were analysed. This is explained in section 2.6.

When creating the velocity profiles for the cross-sections comparing PIV and in-situ, the cross-section was divided into sections of approximately every 5-10 cm. Velocity vectors from PIV that fell within 20-40 cm above or below the tagline were included in the sections and an average and standard deviation of the vertical velocity vector, v, was calculated within each section. The v vector was equal to the flow direction since all videos were aligned with the flow pointing straight down.

2.6 Footprint analysis

Footprint analysis was done for each of the cross-sections, to determine what and where the footprint of the Doppler radar was measuring. This analysis can explain some unrealistic Doppler velocity estimations, e.g. if the footprint encounters vegetation. In combination with PIV results, the PIV determined velocities contained in the footprints were analyzed. This was to confirm, whether the velocity peaks in the Doppler spectrum was as the assumption in section 2.3.5 states. To assess the velocities found in the footprints, the PIV results were overlaid with the footprints of the radar.

As described in 2.3.4, the size of the footprint increases with altitude. The distance from the UAS to the center of the footprint also increases with altitude. The flight was planned, so the center of the footprint always aimed on the tagline as described in section 2.3.4. When visualizing the footprints for each waypoint, an average of the UAS position during hovering was found. This made each footprint an approximation of the precise position during the hovering period of each waypoint. Each coordinate also had a standard deviation. The mean drone position was thus found in Easting, Northing (SWEREF99) coordinates with a standard deviation for each coordinate as shown in table 6. For the remaining flights the hovering positions can be found in appendix C.

Table 6: UAS position for each waypoint during hovering, with standard deviations noted for each average position for cross section 3 altitude 4.

XS	Altitude	Waypoint	Easting [m]	SD easting [m]	Northing [m]	SD northing [m]
	4	1	381200.264	0.03	6222781.677	0.02
		3	381200.855	0.02	6222783.754	0.01
3		4	381200.456	0.03	6222784.005	0.03
'		5	381201.143	0.01	6222786.124	0.02
		6	381201.019	0.01	6222787.196	0.02
		7	381201.052	0.01	6222787.633	0.02

To determine the velocities inside the footprint of the waypoint, the PIV data was overlaid the orthophotos of the cross section. This can be seen in figure 12 for XS3. By using the mean of the drone position for each hovering point, the elliptical footprint found in section 2.3.4, was drawn into the cross-section using the QGIS shape tool. The footprint was drawn with the center of the footprint at the distance to the drone calculated in table 4. Using the results from the PIV analysis, the text file velocity vectors v were loaded into QGIS as a heatmap. The heat map shows the lightest color, where the velocities were higher as shown in figure 12.

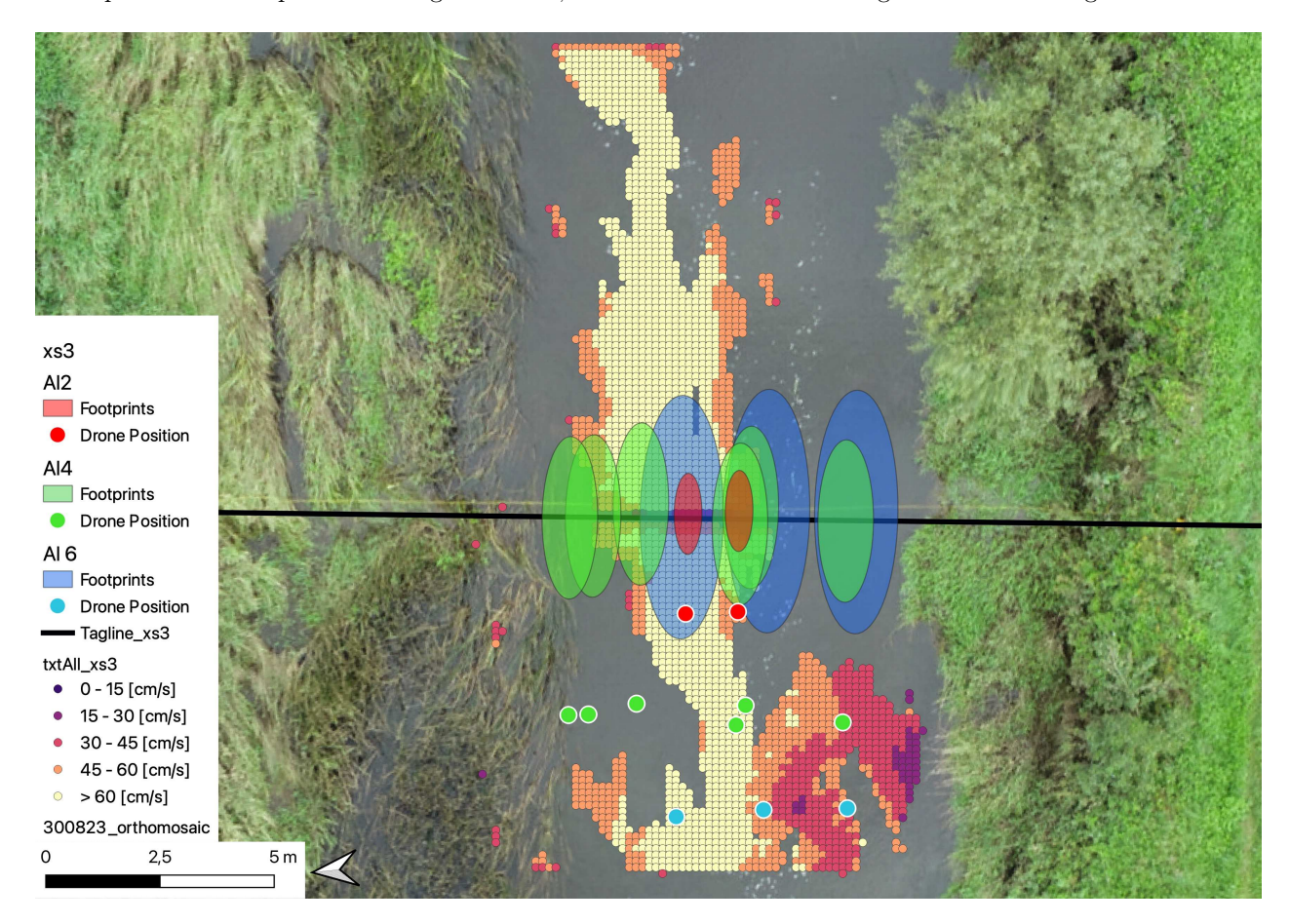


Figure 12: PIV results as a heatmap with Doppler radar measuring footprints relative to the drone position.

Based on the footprints and the heatmap, the velocities within each footprint were cut out using the cut vector based on masked layer tool in QGIS. This generated a cutout from the full text files only including the information

found inside the elliptical footprint as shown in figure 13.

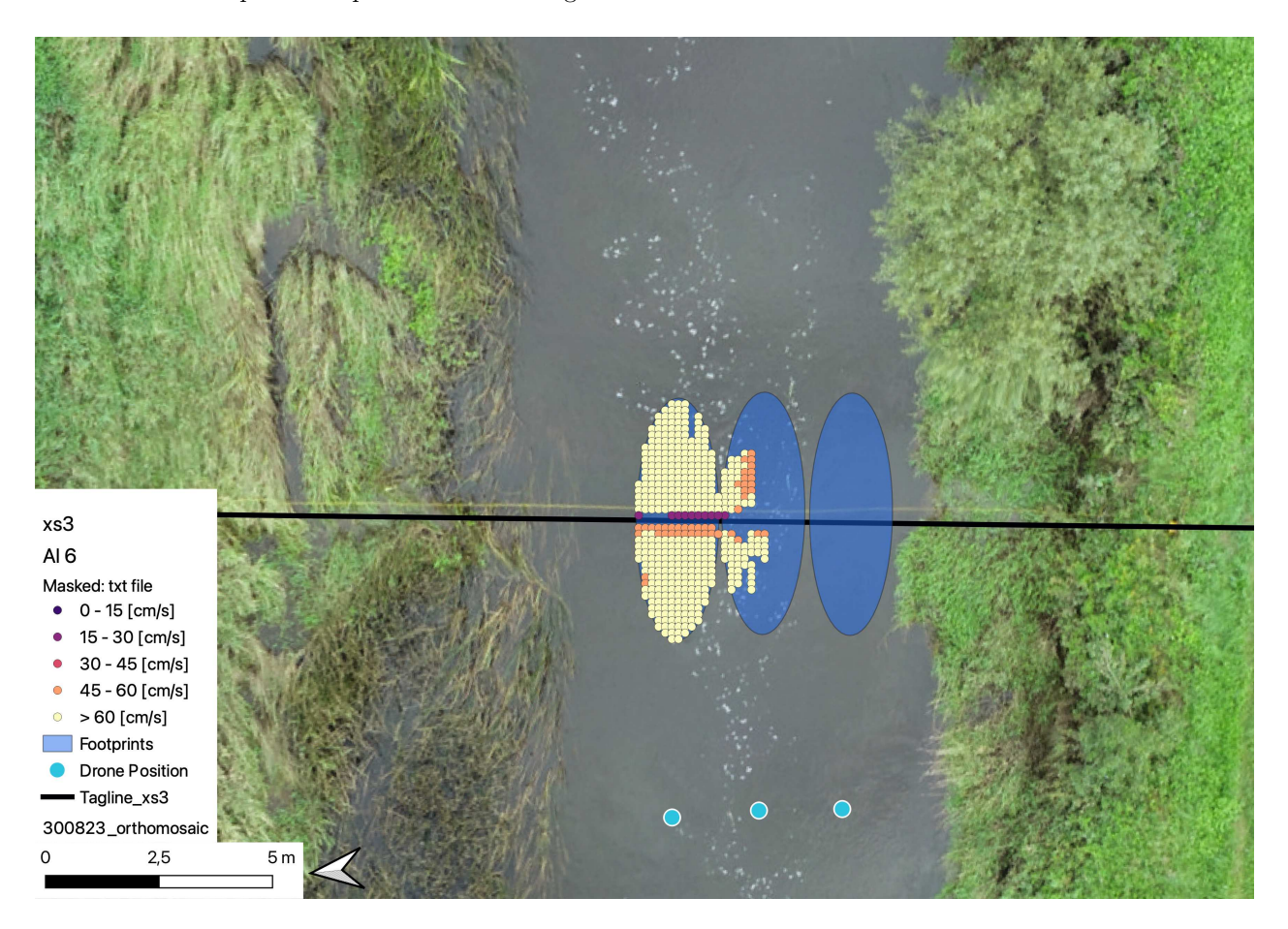


Figure 13: Extracted PIV results that are within the footprints from flight altitude 6.

Based on the masked out PIVlab text file, velocity histograms were generated for the size and frequency of the velocity vector v. The histogram illustrated the surface velocities found within the footprint of each waypoint. A comparison between the histogram and the velocity spectrum from the Doppler data, created insights into what velocities the Doppler radar was measuring. This was used to confirm or deny the assumption about the double peak model explained in equation 7 . In the histogram, it was assumed that only one velocity peak would be visible, a peak equal to the surface velocity, since the PIV payload was flown at an altitude that did not cause propwash.

3 Results and analysis

Before presenting the final results, some Doppler waypoints and flights were discarded on the basis of unstable measurements. In order to make sure the data retrieved from the Doppler raw data has a great quality the full waveform plot of the data was inspected. This was done to make sure the data only consisted of waypoints with stable measurements, i.e. no UAS drifting. An example of a waypoint inspection is presented below based on the full waveform plot of the waypoint. If it seemed like the measurement went wrong or was unstable, the waypoint was discarded. Filtering these out automatically could easily be implemented with a warning message in real-time if an ongoing measurement is not valid. It is important that the UAS is stable during hovering explained in section 2.3.7.

When inspecting the full waveform plot of waypoint 1 from XS1 altitude 5, it became clear that the measurement was unstable, as the signal fluctuates throughout the traces.

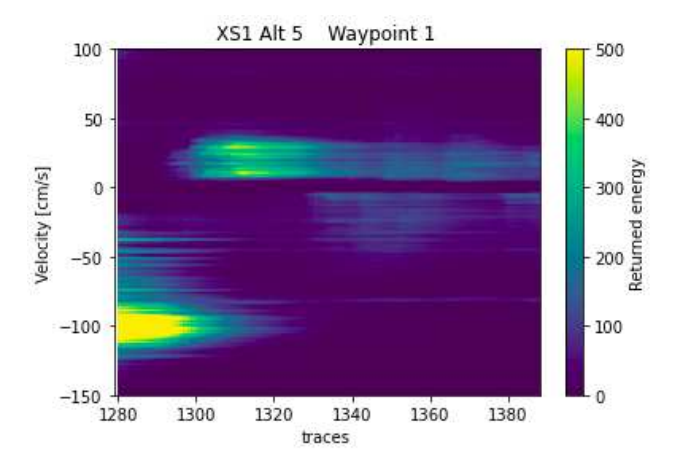


Figure 14: Full waveform plot of XS1, altitude 5 m, waypoint 1. The signal is clearly changing throughout the measurement period.

This waypoint was therefore discarded from the observations. The same procedure has been applied to inspect all waypoints and discard unstable measurements.

Table 7: Waypoints that can be discarded on the basis of a invalid measurement. The argumentation for discarding is shown in appendix D.

XS	Flight altitude	Flight id.	Discarded waypoint(s)	Reason
1	5.1	2023-08-29-14-27-35	1	Unstable measurement
1	10.1	2023-08-29-14-27-35	All	Large sd. and Low energy signal
3	4.1	2023-08-30-19-16-02	2	Unstable measurement
3	6.1	2023-08-30-19-27-42	1,5	Unstable measurement
5	2.1	2023-08-31-11-18-27	All	Not stable altitude, based on hovering plot
5	4.1	2023-08-31-11-42-32	All	Not stable altitude, based on hovering plot
5	6.1	2023-08-31-17-15-37	All	Low energy response, weak signal
5	6.1	2023-08-31-17-25-53	All	Only receiving positive velocities.
6	2.1	2023-08-31-17-42-02	1	To far from tagline
6	4.1	2023-08-31-18-00-19	4, 5	Unstable measurement/Low energy
6	6.1	2023-08-31-18-08-21	1	Unstable measurement/Low energy response

3.1 In-situ and Doppler radar velocimetry

The results of the remaining Doppler estimated velocities along with in-situ OTT MF Pro measurements can be seen in the figures below. Note that the Doppler radar was flown at altitudes 2 m and 5 m at XS1. For all other cross-sections the recommended altitudes of 2 m, 4 m and 6 m were flown.

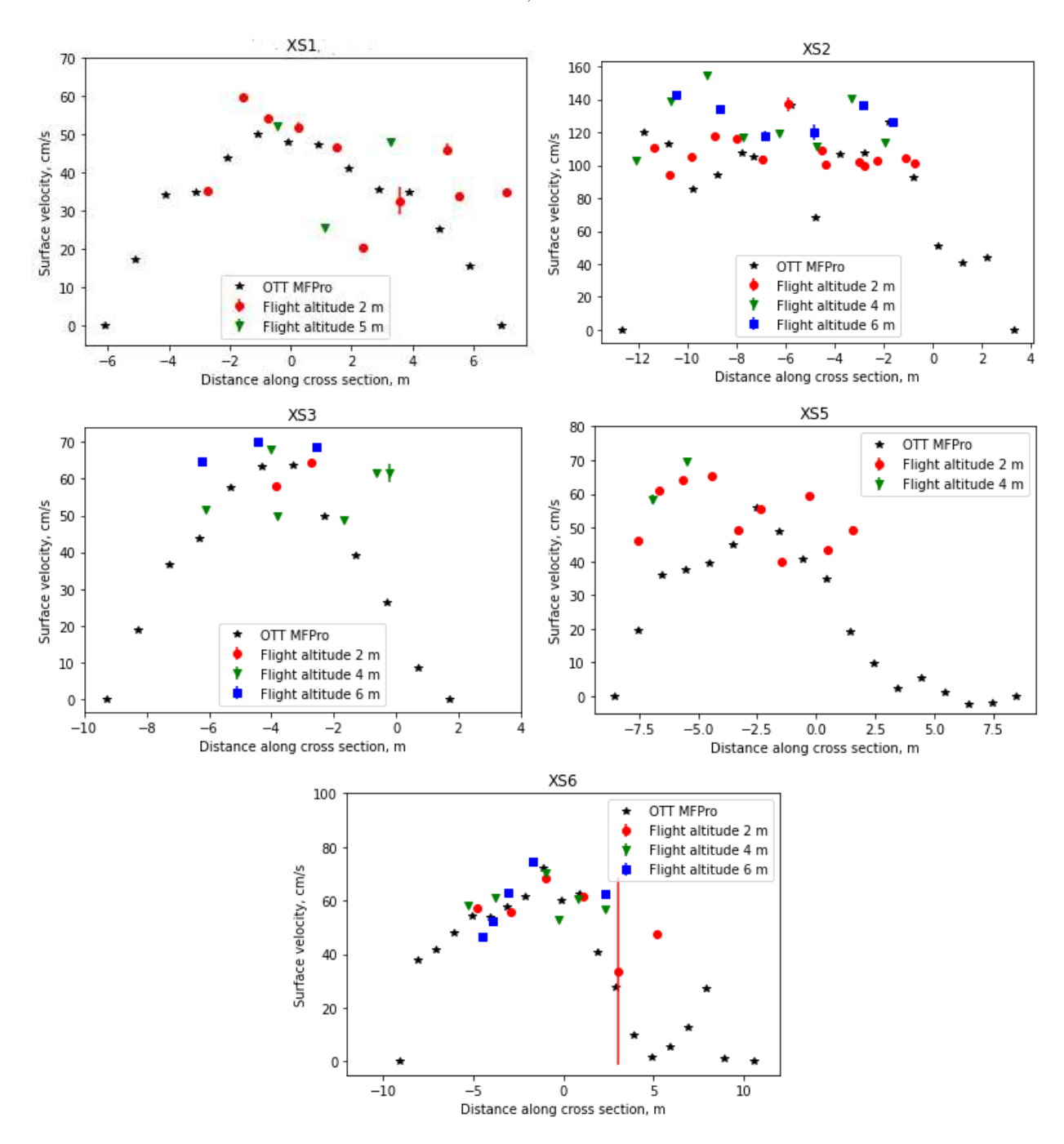


Figure 15: Results of Doppler flights at all flown altitudes for each cross-section.

In section 2.1 the different cross-sections were presented. Looking at the in-situ velocimetry of XS1, a clear shape

and tendency is visible. The surface velocity peaks in the center of the cross-section. The shape is a typical cross-section velocity profile without disturbances in flow, correlating with the observation of no or very little obstructions in the surface of the river. In XS2, a fluctuating surface velocity is measured. In XS2 disturbances were present on the riverbed and the cross-section had a much lower depth than the other cross-sections. In XS2 the velocity was also faster than in any of the other cross-sections, based on the figure 15. XS5 and XS6 show low velocities near the right bank, due to the vegetation described in section 2.1. The maximum and mean velocities measured by OTT MF Pro for each cross-section can be seen in the table below.

Table 8: Maximum and mean in-situ velocities per cross-section for reference.

Site	Surface velocity cm/s			
	Max	Mean		
XS1	50.21	30.63		
XS2	136.6	83.32		
XS3	63.85	34.00		
XS5	55.84	24.73		
XS6	72.19	33.81		

XS2 stands out with higher surface velocities while the remaining cross-sections have similar conditions.

As a result of the double peak model, described in section 2.3.6, one Doppler velocity is picked at each waypoint. The velocity is picked as the peak with the highest velocity, based on equation 7, and as mentioned in section 2.3.5. In figure 15, the Doppler estimated velocities can be seen along with the OTT measurements. The plots show the results of each flight and the standard deviation of each estimated velocity illustrated as errorbars. The general tendency is that the Doppler radar overestimates in-situ velocities. Especially large deviations can be seen near the fringes of the cross-sections, as visible in XS1, XS3, XS5 and XS6.

3.1.1 Error statistics

For comparing the Doppler results to OTT MF Pro measurements, three error statistics were calculated. Root Mean Squared Error (RMSE), Mean Absolute Error (MAE) and Mean Biased Error (MBE) (M. Padhma, 2023). All of the statistics were found by comparing each Doppler waypoint to the nearest OTT MF Pro measurement (nearest in distance along line). The statistics are shown in table 9. The figures showing the relation between the OTT MF Pro comparison points and the velocity estimates from the Doppler radar are found in appendix E.

Table 9: RMSE, MAE and MBE between velocities found from the Doppler using double peak model and their nearest OTT MF Pro measurement. Reported by cross section and flight altitude.4 (1) corresponds to flight 2023-08-31-17-55-38 from XS6 and 4 (2) is flight 2023-08-31-18-00-19 also from XS6. All errors are found in cm/s.

XS	Altitude [m]	RMSE [cm/s]	MAE [cm/s]	MBE [cm/s]	OTT MF Pro points for comparison
1	2	16.05	12.02	7.41	[4,6,6,7,9,9,11,12,13,14]
1	5	14.64	12.81	-1.63	[7,8,10]
	2	18.87	15.05	5.67	[2,3,4,5,6,7,8,9,9,11,11,12,13,13]
2	4	32.00	27.49	15.63	[2,3,5,6,8,9,10,12]
	6	32.04	27.29	27.15	[3,5,7,9,11,12]
	2	11.04	10.01	4.65	[6,8]
3	4	21.84	17.70	13.29	[4,6,6,9,10,10]
	6	16.75	15.54	15.54	[4,6,8]
5	2	17.93	14.86	12.62	[2,3,4,6,7,8,9,10]
"	4	27.57	27.17	27.17	[3,4]
	2	20.83	11.80	8.91	[7,9,11,13,15]
6	4, (1)	4.84	4.35	3.07	[5,6,9]
0	4, (2)	10.05	8.30	2.15	[10,11,12]
	6	12.47	10.57	7.62	[6,6,7,8,10,12]

Table 9 shows that the Doppler radar generally overestimates surface velocities, as is apparent by the Mean Biased Errors (MBE) which are all positive except for XS1, altitude 5 m. MAE are within a range of 4.35 - 27.49 cm/s. Errors of up to 32 cm/s are quite high relative to the velocities and indicate very different results. Other papers usually cite error statistics of 0.1 m/s or less to be in good agreement with in-situ results (Bandini et al., 2022). XS2 has the largest errors overall, where flight altitude 4 m had the absolute largest MAE and RMSE. XS2 was also the one with the most variation in in-situ velocities. The largest array of recorded Doppler results is from XS2 altitude 2 m, where 14 measurements were found. They are compared to 11 unique OTT MF Pro measurements. This array generally shows a close relation to the in-situ measurements keeping in mind that XS2 is the most fluctuating. For XS6 altitude 4 m (1), the errors are remarkably lower than the rest with a RMSE at 4.84 cm/s, MAE at 4.35 cm/S and MBE at 3.07 cm/s. The flight recorded only three waypoints points all with a close relation to the in-situ observations.

Selected results and outliers from the Doppler estimated velocities will be analyzed in depth for XS1 and XS2.

3.1.2 XS1

Figure 16 shows flight altitudes 2 m for XS1, with annotation of each waypoint. An inspection of the model fit is shown based on the individual velocity spectra of each waypoint.

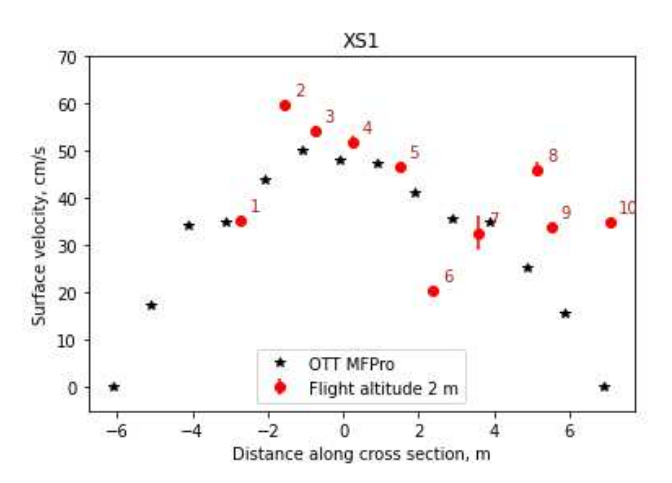


Figure 16: Velocity profile for XS1 as measured with the Doppler radar at 2 m and OTT MF Pro. Each waypoint is annotated for reference.

Waypoint 8, 9 and 10 from altitude 2 m are close to the edge of XS1. They show a large overestimation of the in-situ observations, probably due to the footprint also taking in higher surface velocities further from the edge. Figure 17 show the two velocity spectra of waypoint 8 and 10.

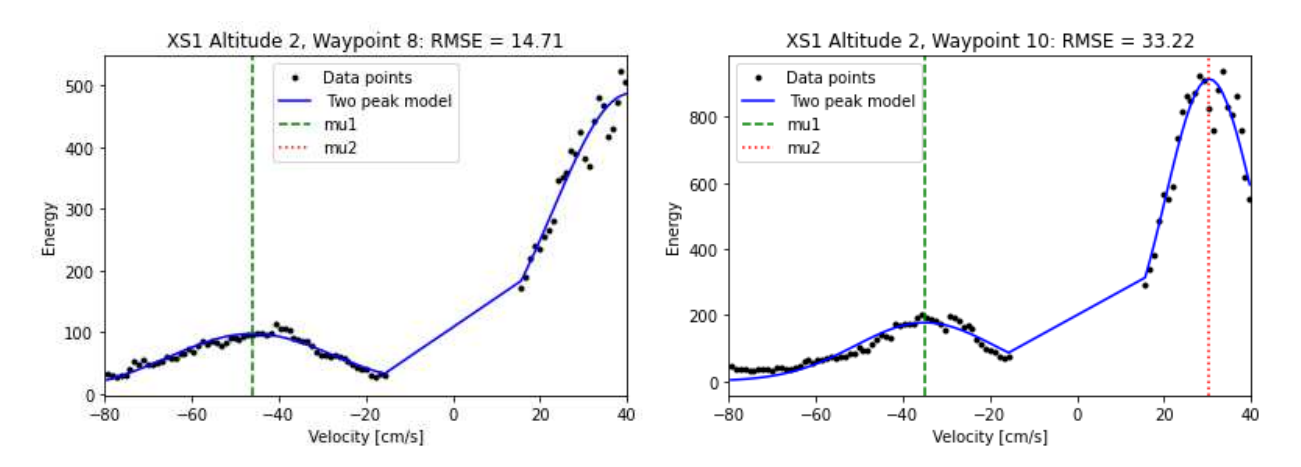


Figure 17: Waypoint 8 and 10, altitude 2 m, XS1

The energy received is very low for the left peak of waypoint 8 and 10, representing the surface velocity. The left peaks are all slightly widened and peaking at higher than 20 cm/s, it is possible that the Doppler radar is picking up higher surface velocities on the edge of it's footprint. This illustrates the issues with correctly estimating low surface velocities (20 cm/s and lower). As mentioned in section 2.3.5, velocities below 15 cm/s are masked out, making it impossible to see if the radar would have registered any lower velocities. The second peak of these waypoint also shows a positive velocity from the propwash, indicating that the propwash has a higher velocity than the surface velocity of the river.

Waypoint 2 and 6 from altitude 2 m also show a deviation from the in-situ observations. Inspecting each of these waypoints in figure 18, it is clear, that the model is not choosing the correct velocity.

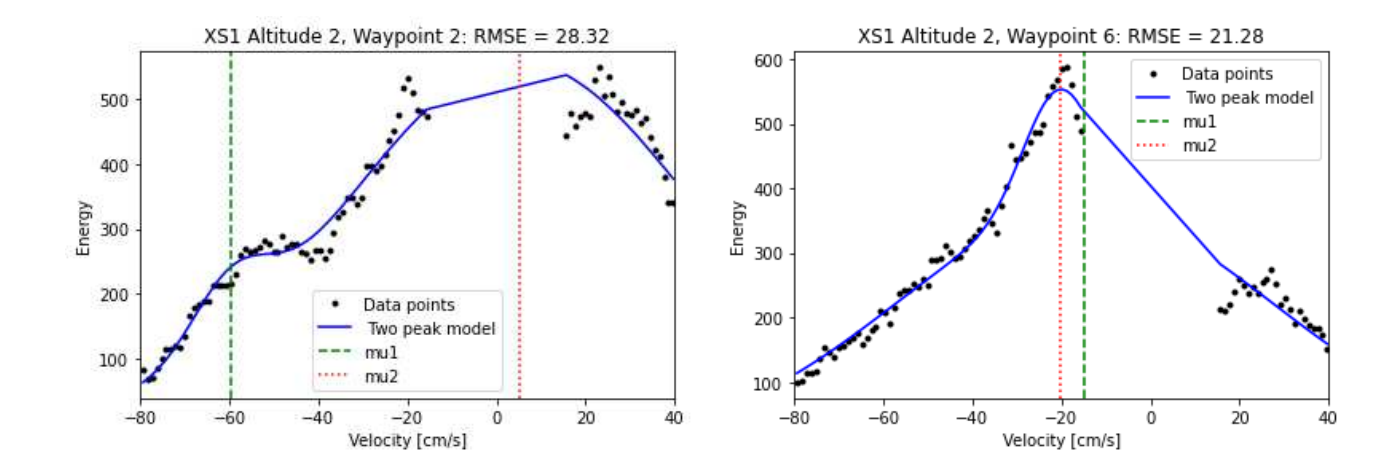


Figure 18: Waypoint 2 and 6 from XS1, altitude 2 m.

In figure 18, the two waypoints can be seen, along with the fit of the double peak model and the two means estimated by the model. For waypoint 2, two peaks are clearly visible. However the velocity is slightly overestimated from the model. The true velocity in this waypoint should be around 50 cm/s, based on the in-situ observations. The model has estimated mu1 at -60 cm/s. Visually, the left peak of the data points should be around -55 cm/s. For waypoint 6, the data points show a less clear double peak trend. The true peaks of this waypoint seem to be around -45 cm/s and -20 cm/s according to the data, however the model does not correctly fit to these peaks, and the velocity becomes underestimated.

For altitude 5 m from XS1 the annotated velocity profile is shown in figure 19.

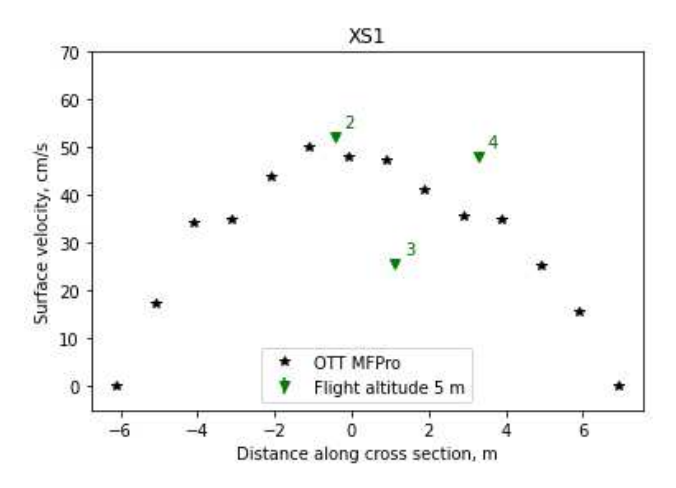


Figure 19: Velocity profile for XS1 as measured with the Doppler radar at 5 m altitude and OTT MF Pro. Each waypoint is annotated for reference.

At flight altitude 5, waypoint 3 underestimates the in-situ observations, leading to the MBE for this flight of -1.63 cm/s. This is the only flight that leads to a negative MBE. Figure 20 shows the Doppler velocity spectrum for this waypoint.

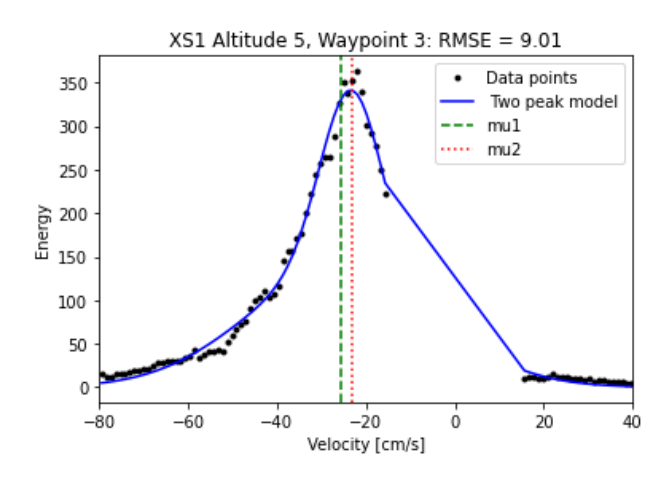


Figure 20: Waypoint 3, XS1, altitude 5 m.

The true velocity should be around 50 cm/s based on the in-situ observations. The waypoint 3 spectrum shows one clear peak around -23 cm/s, and one less clear peak around -45 cm/s. The model fit only recognizes the clear peak, and the true surface velocity of the river is not recognized.

3.1.3 XS2

Since XS2 stands out with the highest errors, the results at this cross-section will be inspected to see if other model assumptions could improve the velocity estimates. The figures below shows the results from XS2 using the double peak model for the three altitudes 2 m, 4 m and 6 m. Doppler waypoints are annotated for reference. As reported, the flow changed more across this profile, and surface velocity is generally higher than the other cross-sections, making this cross-section a special case. The results of the double peak model generally seem to overestimate the in-situ velocity based on the MBE.

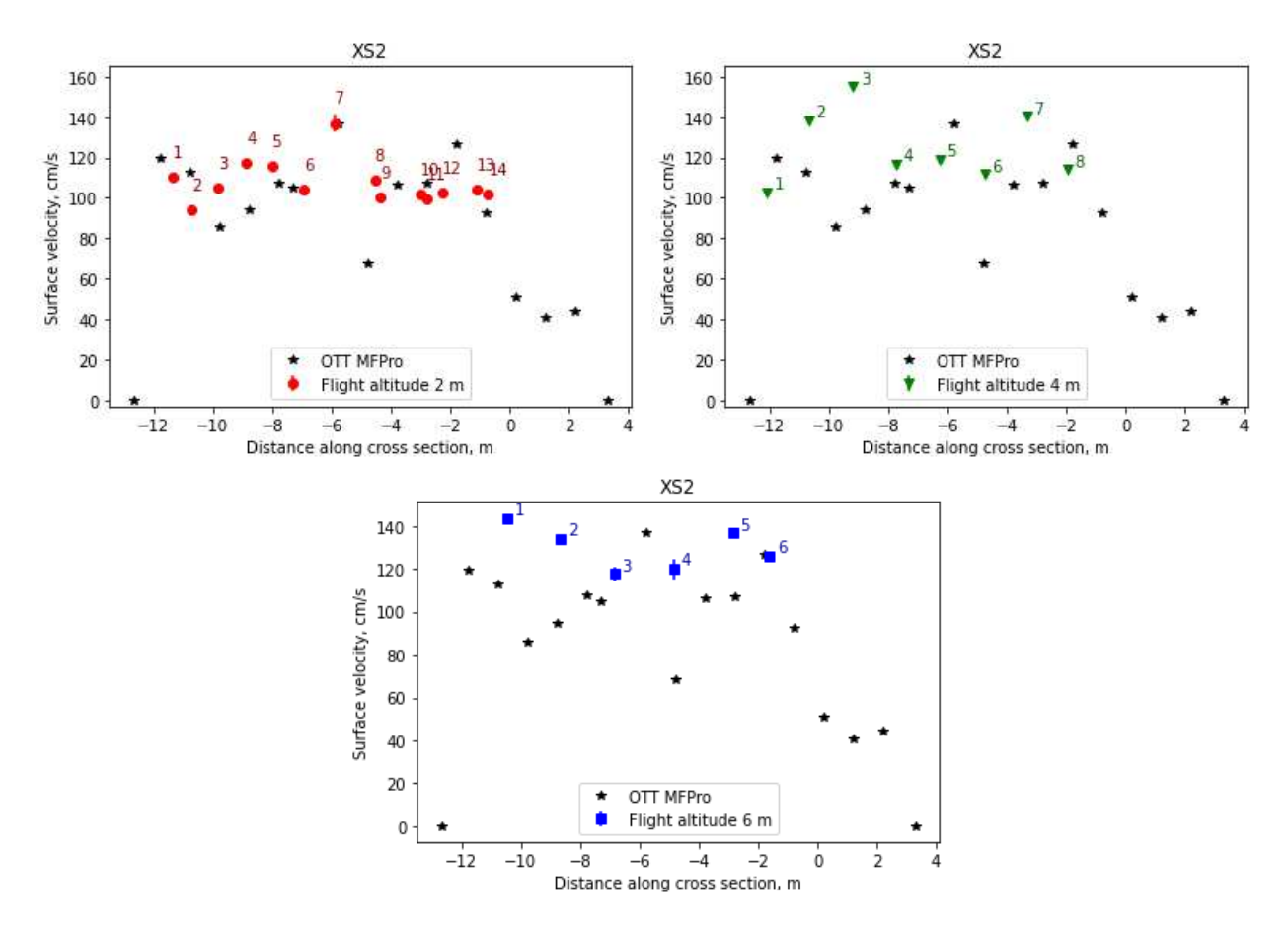


Figure 21: Results of XS2 altitudes 2 m, 4 m and 6 m using the double peak model.

Upon inspecting the outliers, the double peak model seems to not always be the best model assumption for picking the correct surface velocity for XS2. In XS2, the surface velocities were a lot higher than the other cross-sections. This caused some of the Doppler spectra to only have one peak and a stronger received signal from the surface velocity, than for the lower velocity cross-sections. This could be due to proposal having less influence, when surface velocity is higher. In other spectra, there still seems to be two peaks, but less discernible. The figures below show examples of the spectra of some of the outliers, namely flight altitude 2 m waypoint 3, flight altitude 4 m waypoint 3 and flight altitude 6 m waypoint 5.

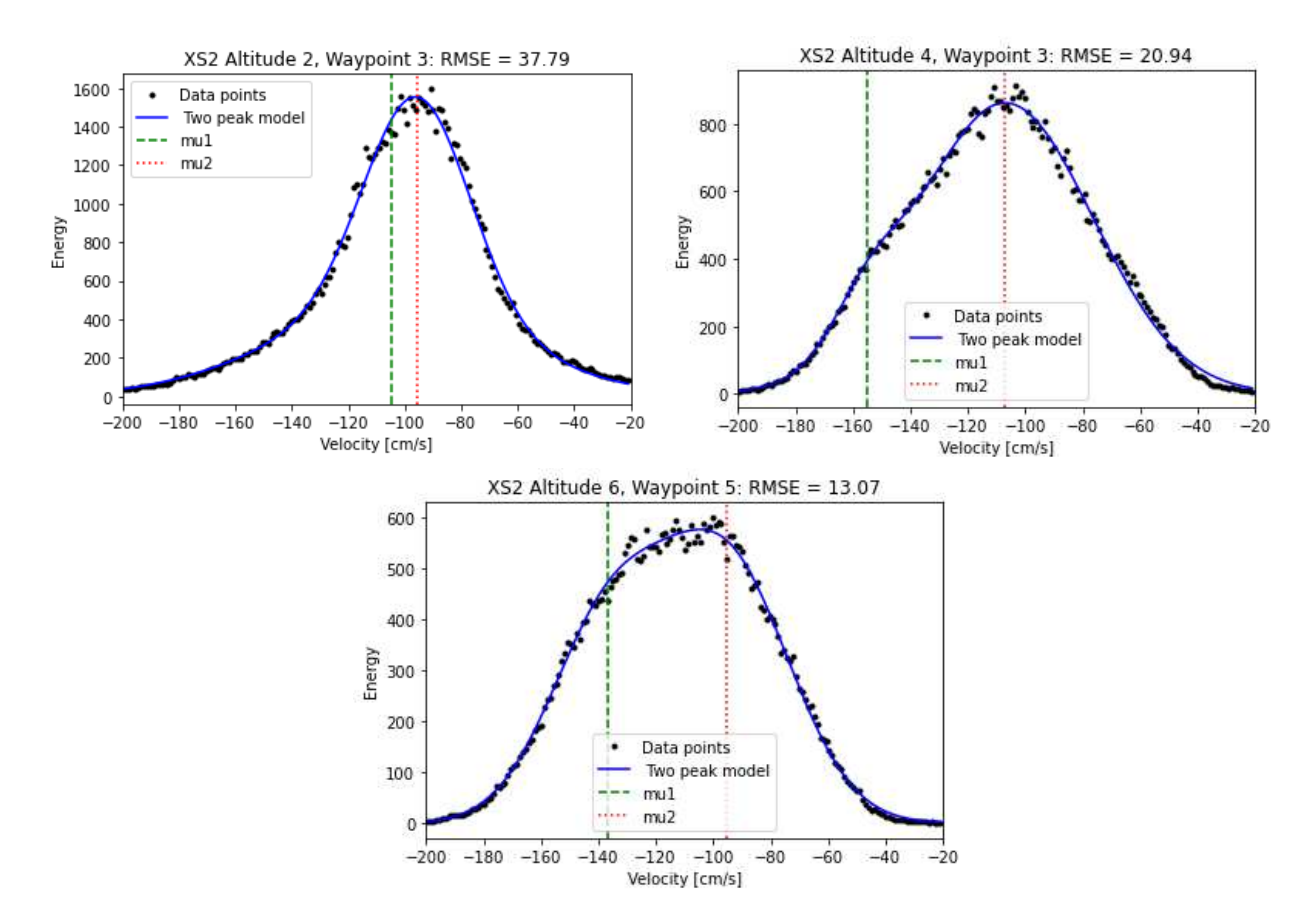


Figure 22: Doppler spectra of some outliers for XS2. For reference the closest OTT measurement to altitude 2 m waypoint 3 is 85.8 cm/s, the closest to altitude 4 m waypoint 3 is 94.4 cm/s, and the closest to altitude 6 m waypoint 5 is 107.2 cm/s.

As illustrated, some of the spectra seem to have just one peak, wherefore it is attempted to use a one peak model instead. For flight altitude 4 m two peaks seem to be present albeit not as distinct, but the correct velocity is not the higher velocity of 158 cm/s but the slower velocity of 110 cm/s (the highest peak in terms of energy). In flight altitude 6 m the tendency is more of one very broadened peak. Perhaps because of a larger footprint multiple velocities were picked up within the footprint, and it becomes hard to pick one. Two different model assumptions have therefore been tested on XS2: a one peak model fit and double peak but where the lower velocity is picked. The formula for the one-peak model is:

$$f(x) = \frac{1}{\sigma \cdot \sqrt{2 * \pi}} \frac{\frac{(x-\mu)^2}{2 \cdot \sigma^2}}{(10)}$$

The velocity would hence be μ . The figure below shows the velocities as estimated by the one-peak model. For previous model fits, the RMSE threshold was 50 for determining if the model fit was decent. To fit the one peak model, the threshold had to be raised to 100, already indicating that the one peak model is a worse fit for the data.

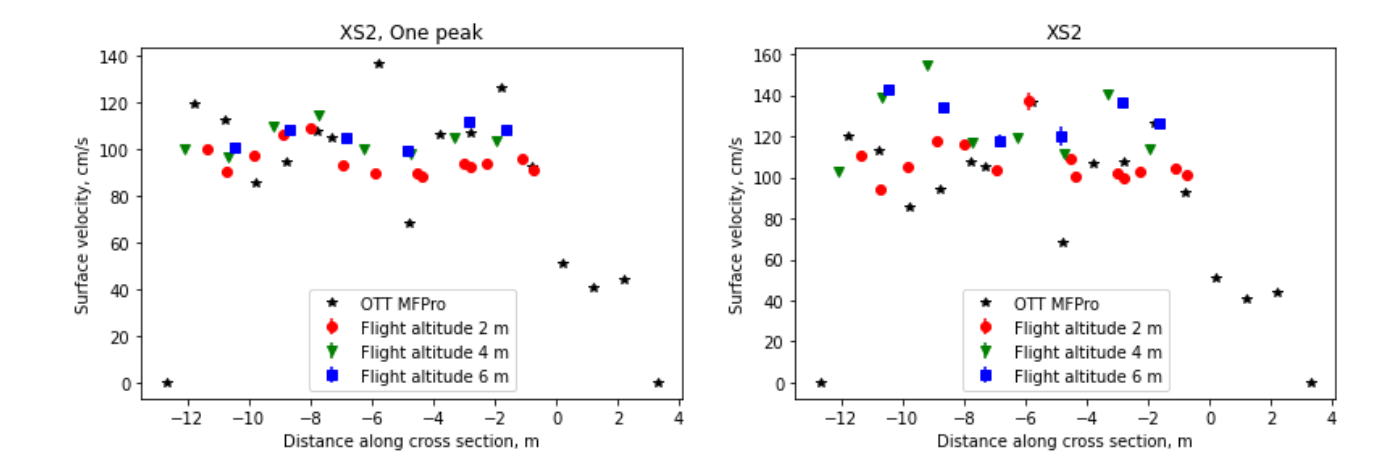


Figure 23: Left: Velocities picked by the one-peak model for the three different altitudes flown at XS2 along with OTT MF Pro velocities. Right: Velocities picked by the double peak model for the three different altitudes flow at XS2.

The one peak model leads to lower velocity estimates, seemingly they are closer to the in-situ observations and closer to the mean velocity for XS2 reported in table 8. Since even the OTT measurements have some outliers with the values of 136 cm/s and 68 cm/s in the middle of the cross-section that could be explained by local disturbances such as a rock, this might be a better estimate of the velocities. However, when inspecting the fit of the Doppler velocity spectra, as seen below in figure 24, the one peak model does not fit the spectra from especially altitude 2 m very well. This is evident from the high RMSE values. The fit of the one peak model gets better at the higher altitudes. This could be explained by propwash diminishing and the larger the footprint, the higher the chance of including several river surface velocities, causing the broadened one peak shape.

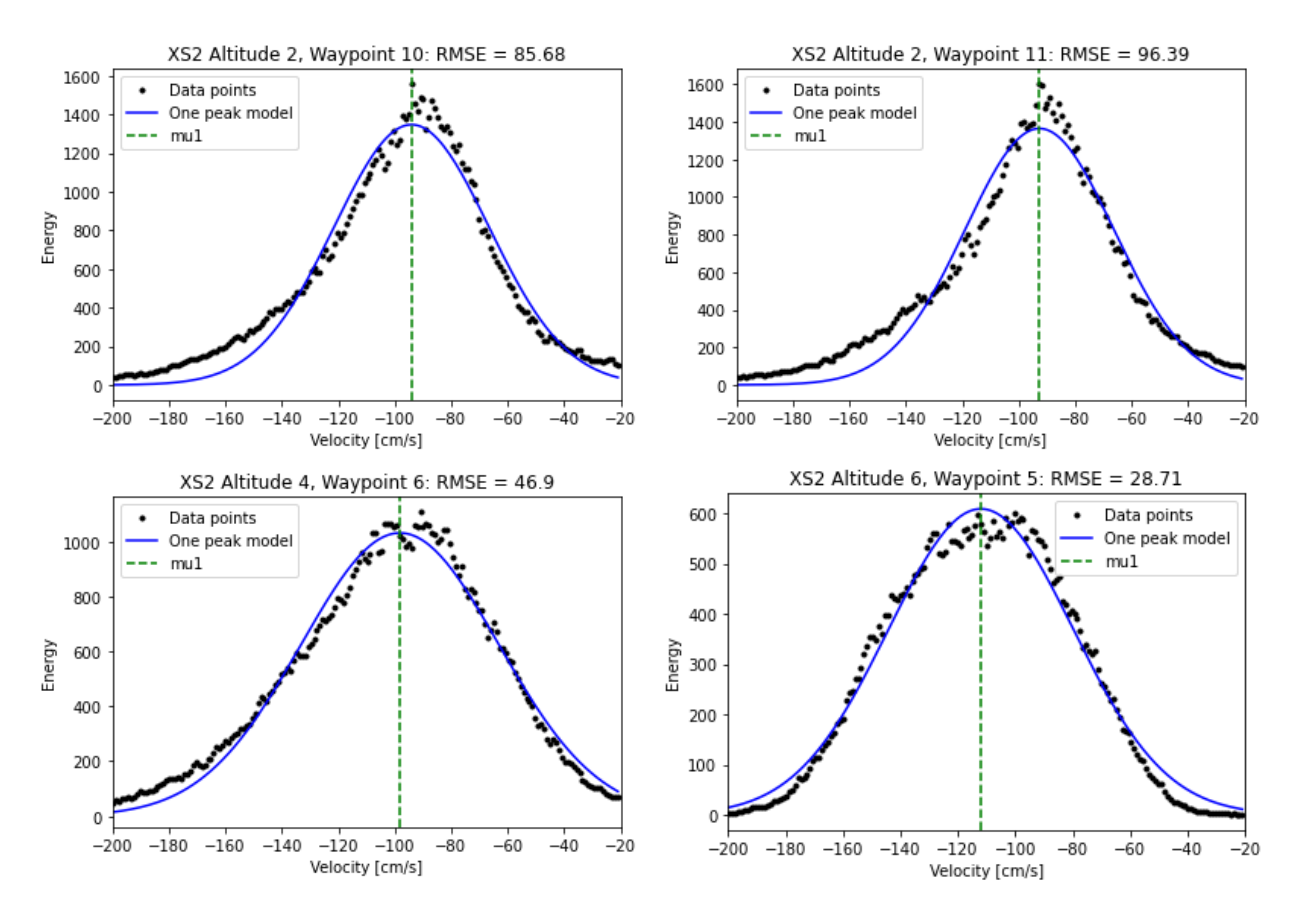


Figure 24: Waypoints from XS2 at three different altitudes with the one peak model fit. The high RMSE values from altitude 2 m show that the one peak model is not a good fit for the data.

It was also attempted with a two-peak model but the lower velocity pick. The results of this analysis can be seen below.

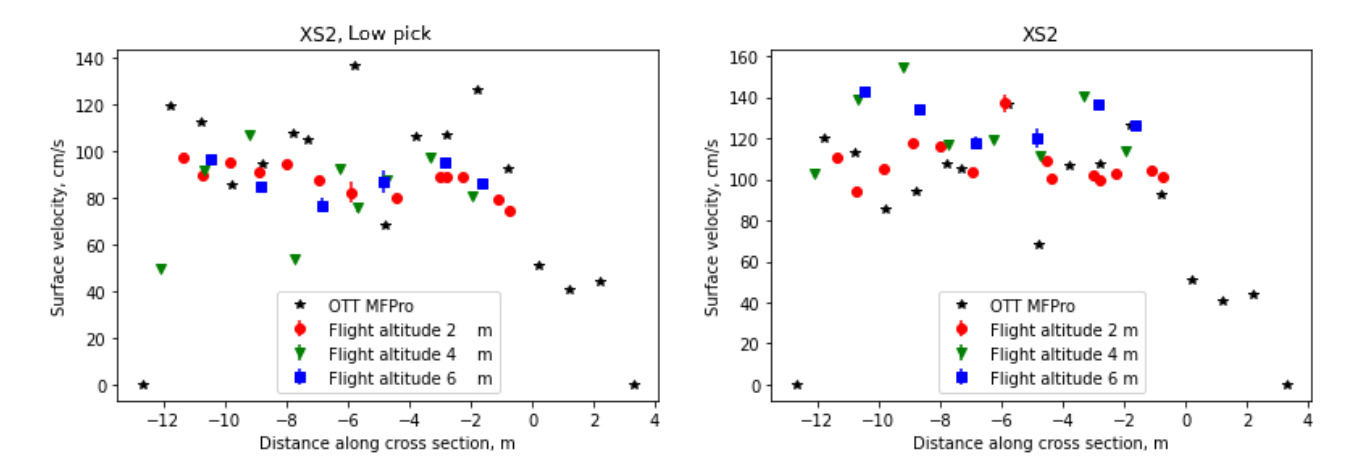


Figure 25: Left: Velocities picked with the double peak model but where the lowest μ is chosen as surface velocity for the three different altitudes. Right: Velocities picked by the double peak model for the three different altitudes flow at XS2.

The double peak model with low pick velocity shows a large underestimation rather than the overestimation from the double peak high velocity pick model. To conclude, the original double peak model picking the highest velocity will still be recommended going forward.

3.2 PIV results

Video sequences of XS1, XS2, XS3 and XS6 were analyzed with PIVlab as described in section 2.5. Results and analysis of each cross-section follow hereafter. XS5 was not analyzed as little to no seeding was present in the videos.

3.2.1 XS1

XS1 was split into 300 sections with 40 cm on each side of the tagline. The resulting mean velocities and their standard deviations can be seen in figure 26. It shows good agreement with OTT data for -5 m to -3 m mark. From -3 m to -1 m mark, it seems to underestimate surface velocities. For the remainder of the cross-section, no results are found by PIV. The issues are due to low seeding density in the remaining part of the cross-section.

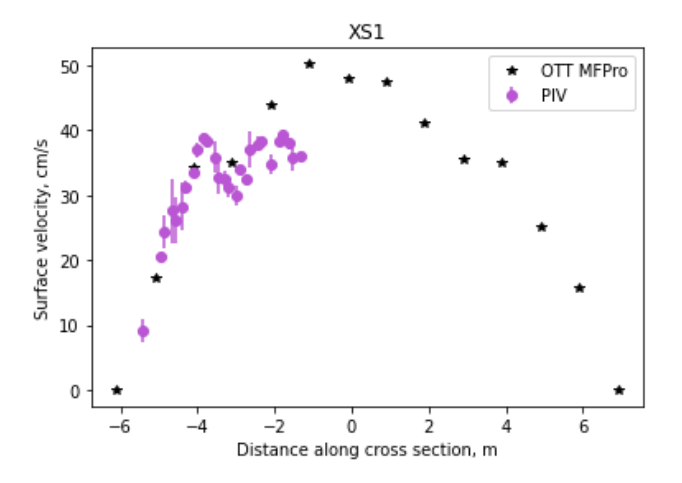


Figure 26: PIV and in-situ velocimetry for XS1.

3.2.2 XS2

XS2 was split into 400 portions with 30 cm on each side of the tagline. A mean of the velocity vectors in those portions and standard deviation was calculated. Not all portions had measurements from PIV due to lack of seeding. The results of PIV analysis of XS2 show a large deviation from in-situ results in most parts of the cross-section. The maximum velocity found by PIV analysis is 108.6 cm/s, far from the maximum with OTT MF Pro at 136 cm/s. Good agreement can be seen near the -3 m to 0 m mark. The largest deviations can be seen in the -7 m to -5 m mark. The standard deviations range from 0.223 cm/s to 26.447 cm/s, indicating some very uncertain results. Some velocities have no standard deviations, if the mean of the portion is based on a single value only.

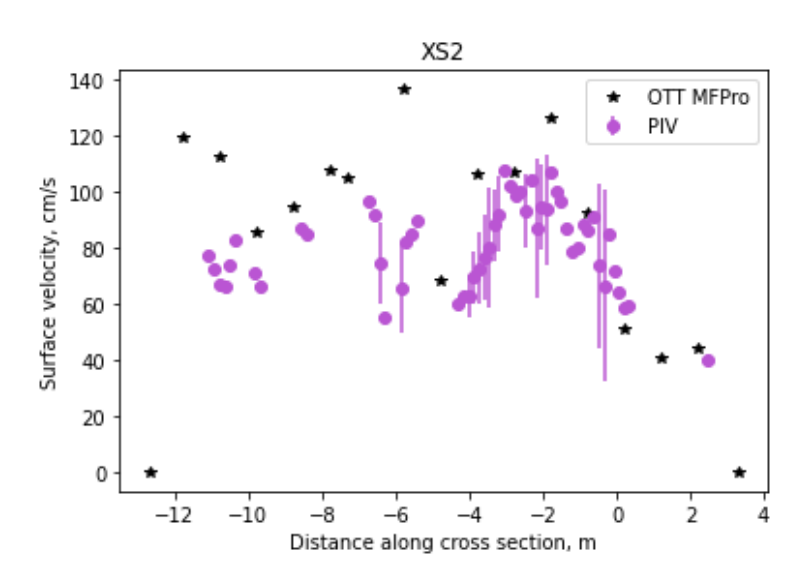


Figure 27: PIV with standard deviation and in-situ velocimetry for XS2.

When inspecting the images on which it was based, the deviations can be explained by the presence of a sunglint on top of ripples that were caused by stones. When binarizing the image, this glint is highlighted as white, along with the particles that PIV should track. The PIV technique inaccurately assesses this glint as a pattern to track, but since this glint remains in place, the determined velocity becomes too low. The in-situ maximum velocity was also found at this place, the high value can be explained by it being placed on top of a large rock resulting in shallow water with fast flow passing over the rock. Due to the large amount of obstacles at this cross-section causing the very varied flow field, this is not an optimal location for PIV velocimetry, and the survey could have been moved slightly down the river for a better location. The issues with PIV for XS2 are summarized in figure 28, that shows the binarized image.

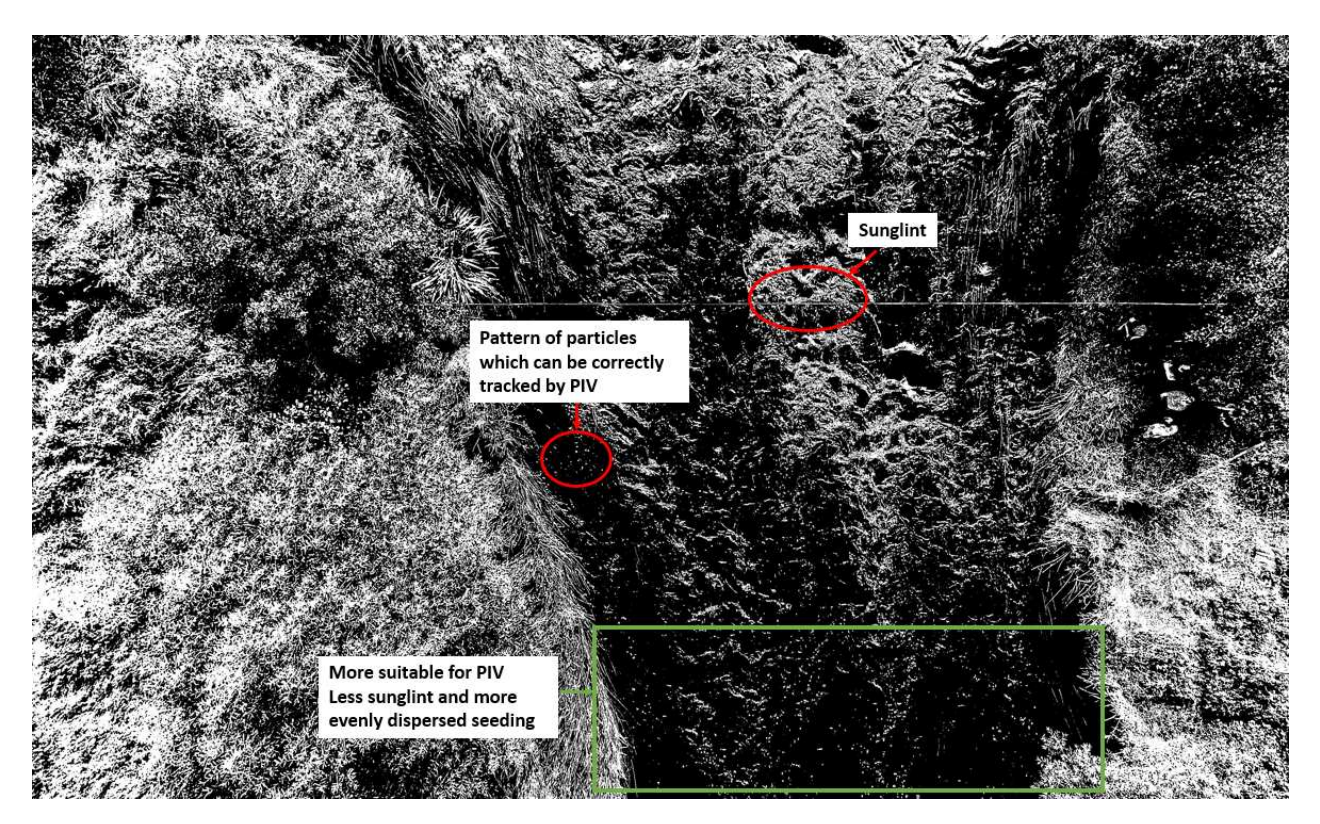


Figure 28: The figure shows the sunglints, that cause problems for the PIV analysis, along with correct seeding pattern that should be tracked.

The results can also be explained by the heatmap in figure 29. The heatmap shows all vectors that were captured in the mean of all frames. Axis units are pixel units of the image. For XS2 the meter per pixel ratio is estimated at 0.0088 m/px. Knowing this, it is clearly visible that the gap of no found vectors to the left of tagline 0, is the same area as the large underestimation in figure 27 at the -7 m to -5 m mark.

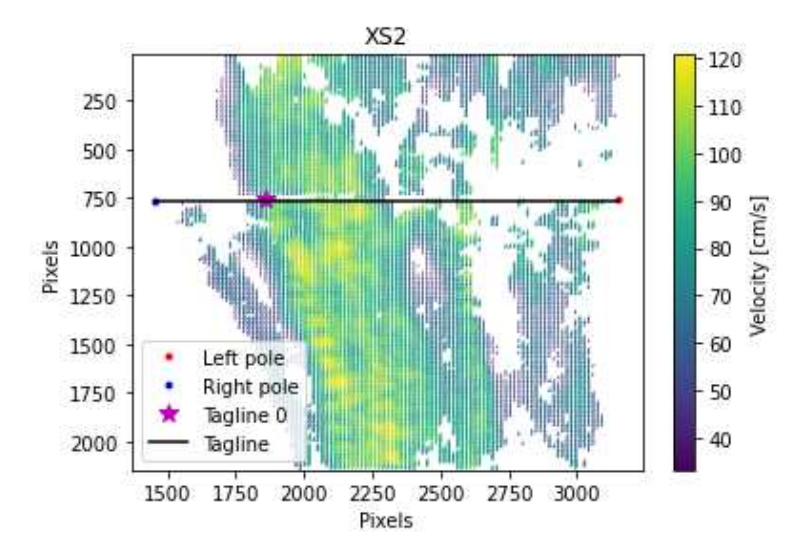


Figure 29: Heatmap of the mean vectors of full video sequence from XS2. The map shows left and right pole and tagline 0. Note x and y axis units of pixels while velocity has been calculated into cm/s.

3.2.3 PIV of XS3

XS3 was split into 300 sections, including 20 cm on each side of the tagline. For XS3, PIV shows good agreement with in-situ velocimetry, however only a small portion in the middle of the cross-section had sufficient seeding. The results can be seen below. The middle is at -4 m since the centerline 0 point is offset to the right at this cross-section.

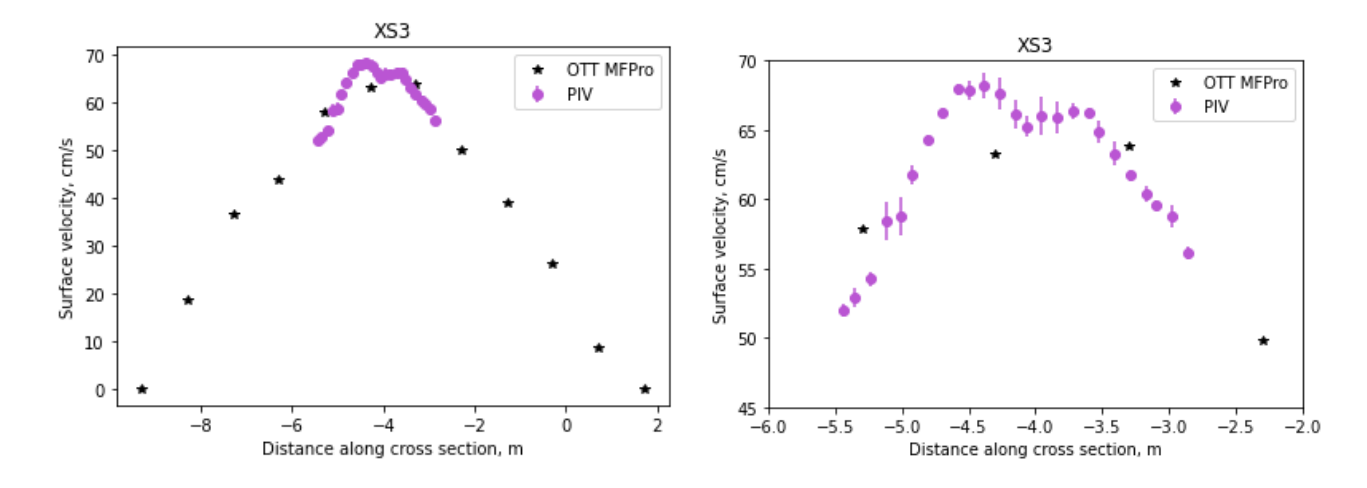


Figure 30: Left: PIV and in-situ velocimetry for XS3. Right: Zoomed in on PIV results.

The standard deviations range from 0.267 cm/s to 1.374 cm/s. The heatmap of XS3 below shows why velocities could only be found for a small portion of the cross-section. For XS3, the meter per pixel ratio is estimated at 0.0067 m/px.

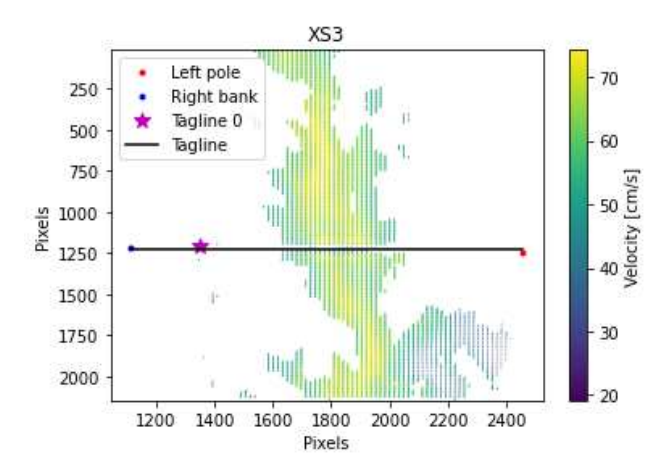


Figure 31: Heatmap of XS3. The map shows left and right pole and tagline 0. Note x and y axis units of pixels while velocity has been calculated into cm/s.

3.2.4 PIV of XS6

XS6 was split into 400 sections with 20 cm on each side of the tagline. Like XS3, it shows fairly good agreement with OTT MF Pro but only has results for a very small portion of the cross-section, because seeding density

was only sufficient in the middle.

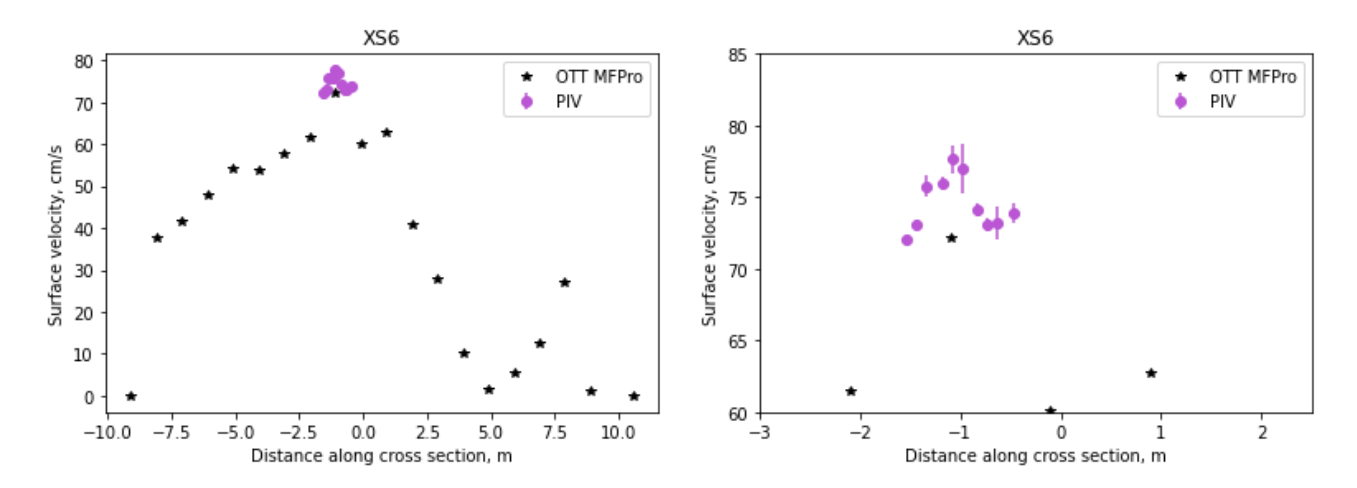


Figure 32: Left: PIV and in-situ velocimetry for XS6. Right: Zoomed in on PIV results.

3.3 Footprint analysis

The footprint analysis was performed for XS2 and XS3 since these had more dense PIV data available within the location of the footprints.

3.3.1 XS2

In XS2, the most rapid and fluctuating flow was found. It is therefore essential to do the footprint analysis for this cross-section. It is suspected that the double peaks found at XS2 are both surface velocities, rather than one being the result of propwash. The broadened one peak shape of some spectra could also be due to multiple surface velocities recorded with equally strong signal. In appendix F the footprints for each flight altitude is shown with the PIV data on the map for XS2. The figure below shows the footprints from altitude 4 m with the PIV data contained in the footprints.

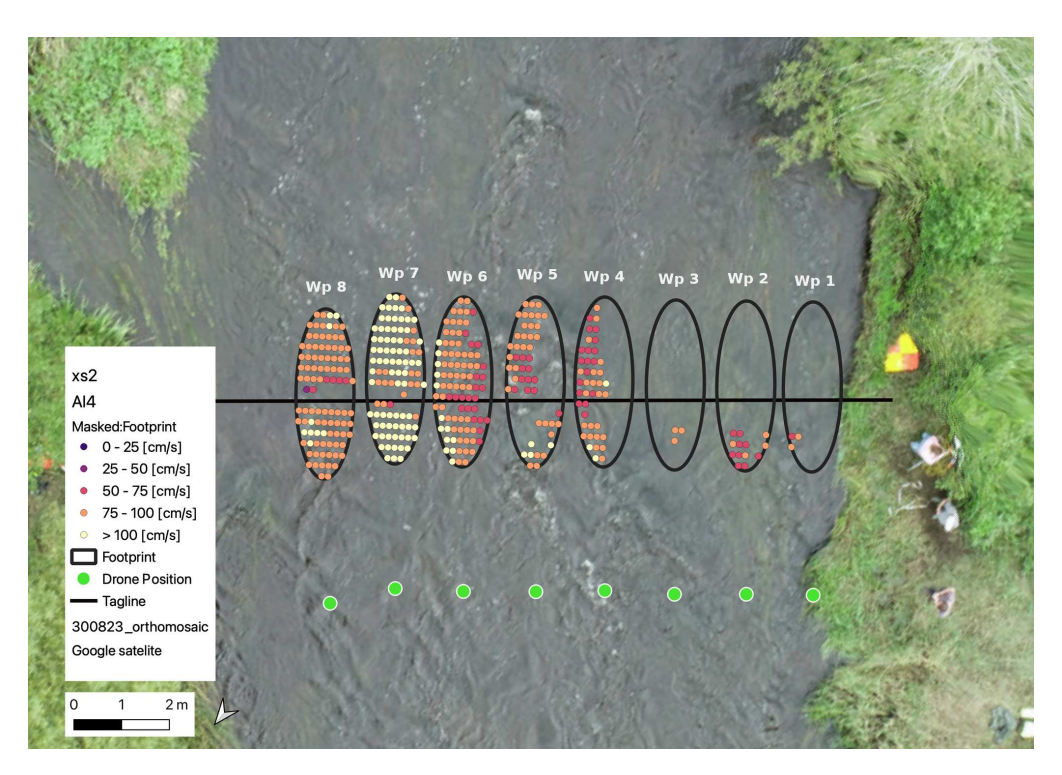


Figure 33: Footprints for annotated waypoints from 4 m altitude, XS2.

Waypoint 7 and 8 from altitude 4 m has sufficient PIV data. Figure 34 shows the Doppler spectra of these two waypoints, with the corresponding PIV velocity histograms in the same plot.

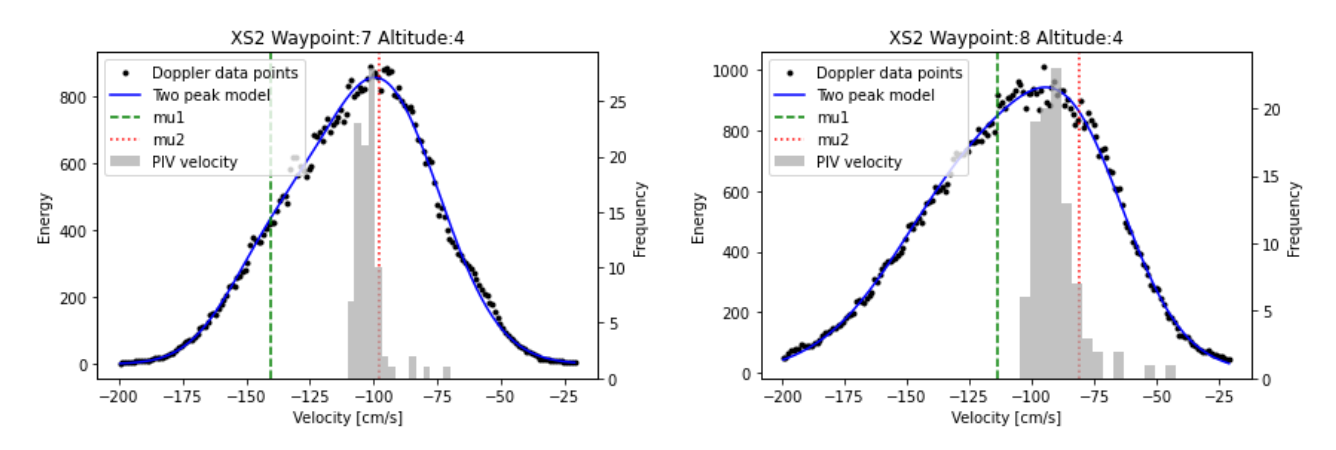


Figure 34: Left: Histogram of PIV estimated velocities in the footprint of waypoint 7 altitude 4 m. Right: Histogram of PIV estimated velocities in the footprint of waypoint 8 altitude 4 m.

The histogram for waypoint 7 shows most frequent velocities in a range between 95 cm/s and 110 cm/s, where the double peak model picks a surface velocity around 140 cm/s. As touched upon in section 3.1.3, it seems that the lowest mean of the two means is a more accurate surface velocity for this footprint, when compared to the result from PIV. Likewise, waypoint 8 from altitude 4 m shows a wide peak with a less distinguished second peak. Here, the histogram shows velocities between 75 cm/s to 100 cm/s. The double peak model indicated that the

surface velocity is around 118 cm/s. The Doppler velocity spectrum is a very wide peak. Both the histogram and the spectrum indicates that multiple velocities are indeed measured in this footprint. This is supported by the PIV histogram since the peak of velocities measured is wider with a range of velocities at almost equal frequencies.

The figure below shows the annotated footprints from altitude 6 m, XS2 and the PIV data contained in them.

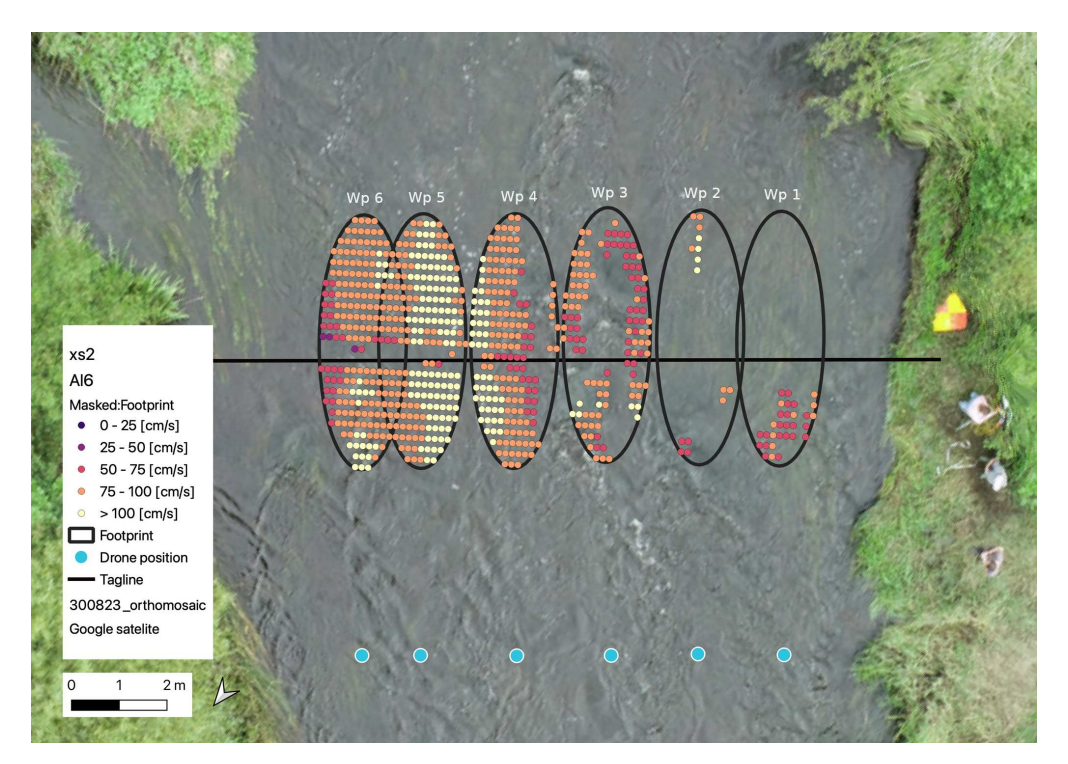


Figure 35: Footprints for annotated waypoints from 6 m altitude, XS2.

From altitude 6 m, waypoint 4, 5 and 6 have sufficient PIV data for histogram analysis. Figure 36, again support the assumption about XS2 having broadened peaks due to many surface velocities present in the footprint, as especially the histogram from waypoint 4 is very wide.

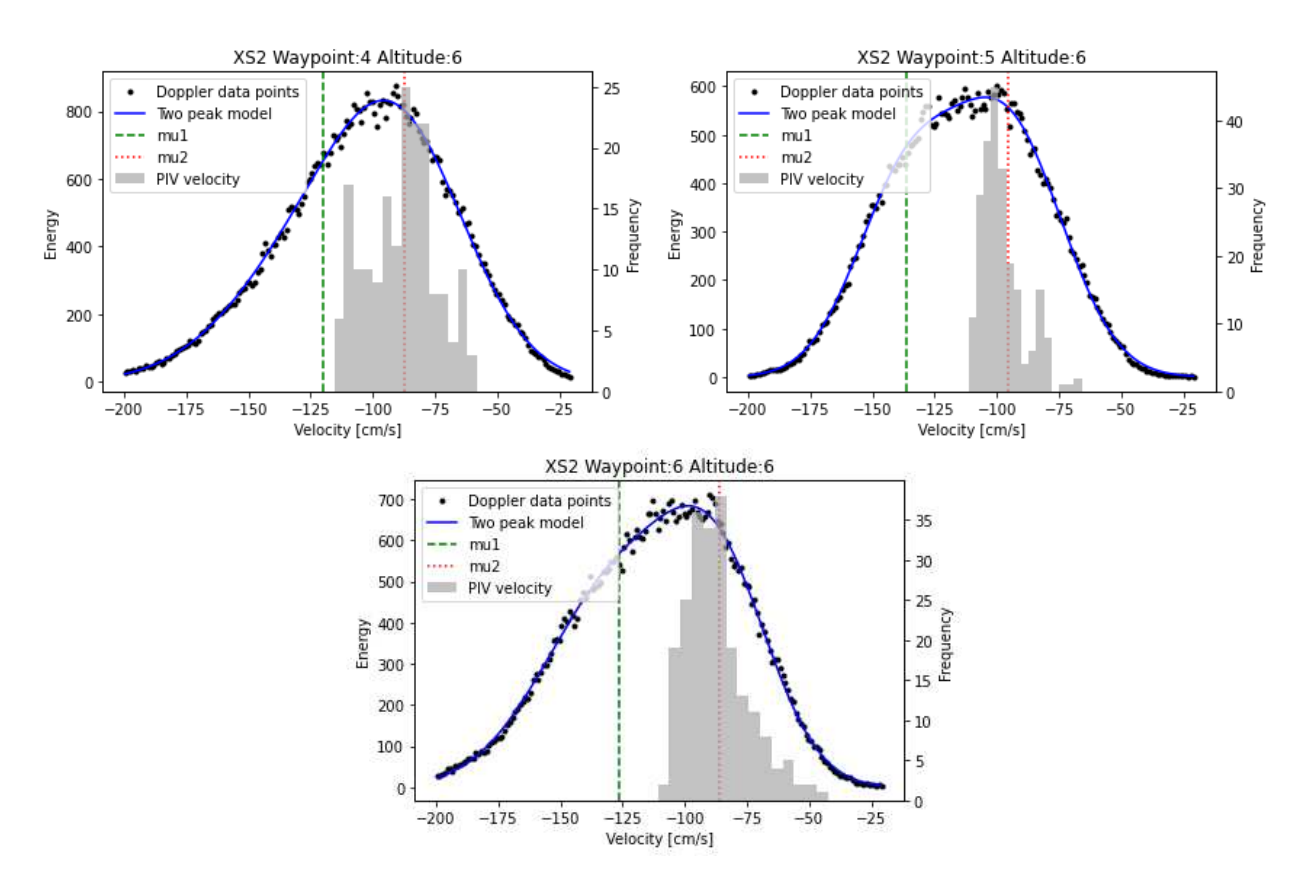


Figure 36: Histogram of PIV estimated velocities in the footprints of waypoints 4, 5 and 6 from altitude 6 m.

3.3.2 XS3

PIV results from XS3 were only present around the middle of the cross section, described in section 3.2.3. This makes it impossible to validate all footprints. Histograms are inspected only for the footprints with sufficient PIV data. For XS3, waypoint 4 and 5 from altitude 4, and waypoint 3 and 4 from altitude 6 m have sufficient PIV data. Extracting the velocities within these footprints, histograms of the velocities can be created. Figure 37 shows the histograms of the velocities estimated by PIV within the footprint of waypoint 4 and 5 altitude 4 m, in the same plot as the Doppler velocity spectrum of the same waypoint. The frequency axis of the histograms is on the right side of the plots.

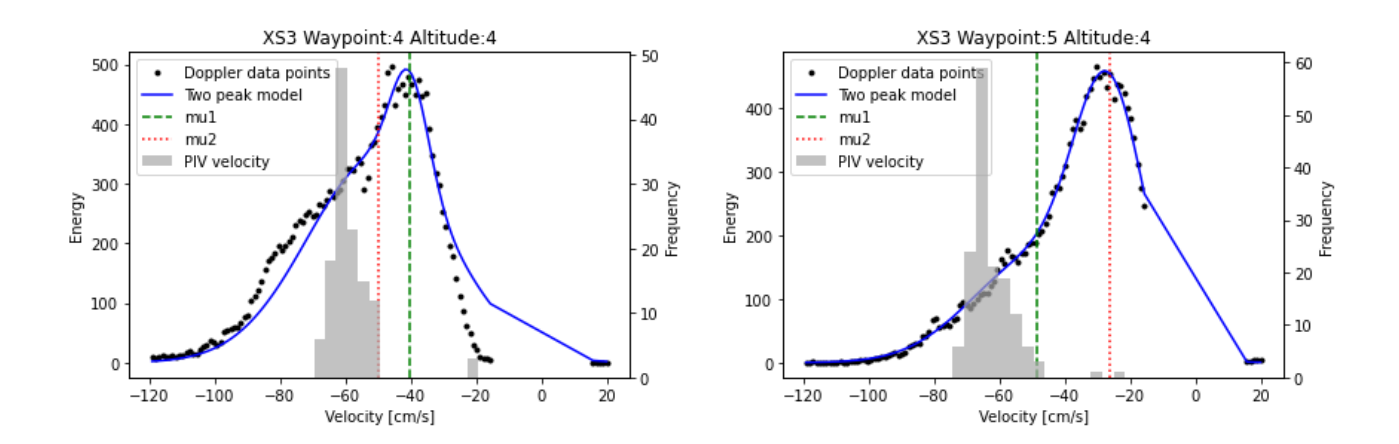


Figure 37: Left: Histogram of PIV estimated velocities in the footprint of waypoint 4, altitude 4m, XS3. Right: Histogram of PIV estimated velocities in the footprint of waypoint 5, altitude 4m, XS3.

In figure 37, the histograms of velocities found from the PIV analysis show one peak. The most frequent velocities are around 60 cm/s and 65 cm/s. The closest in-situ velocity to waypoint 4 is 63.24 cm/s, underestimated by the Doppler at around 48 cm/s, but it is clear from the spectrum the model should have picked a peak at around 60 cm/s, like the most frequent velocity from PIV. For waypoint 5 the second peak in the Doppler velocity spectrum is less prominent, and the true velocity is thus hard to estimate based on the data. PIV indicates the surface velocity should be found between 63 cm/s and 66 cm/s, where the double peak model estimates the surface velocity to be around 50 cm/s, which is however in line with in-situ measurements. The PIV estimated velocities are however also present in the Doppler spectrum. Most importantly, both histograms show just one peak, indicating that the right most peak in the Doppler spectrum is due to propwash.

From altitude 6 m, waypoint 4 and 3 are inspected. In figure 38, these waypoints are shown in the same format as above.

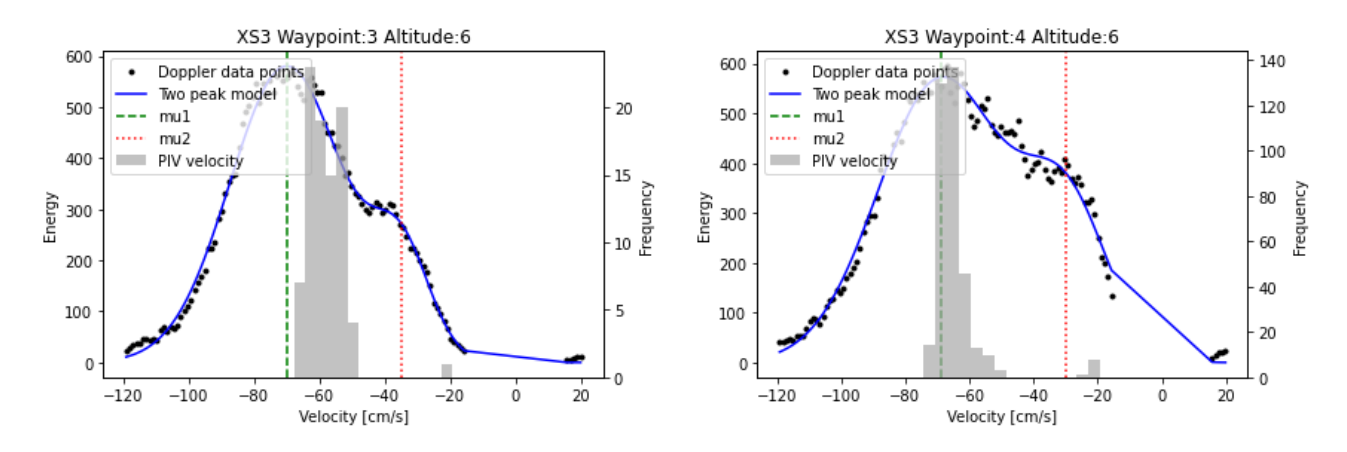


Figure 38: Left: Histogram of PIV estimated velocities in the footprint of waypoint 3, altitude 6 m, XS3. Right: Histogram of PIV estimated velocities in the footprint of waypoint 4, altitude 6 m, XS3.

In figure 38 above, the shape of the PIV velocities encountered in the footprint again resemble one peak. At

waypoint 4, Doppler estimate and PIV estimate are in very good agreement.

From the footprint analysis, it is thus clear that the PIV data mostly indicated one peak of surface velocity within the footprint of each waypoint. In more rapid and fluctuating flows, PIV supports that a broadened peak in the Doppler spectrum is due to a range of river surface velocities being present within the footprint. PIV indicates that the lower mean may have been a better pick for XS2, but as shown in section 3.1.3, that led to an underestimation of in-situ observations. PIV also underestimated in-situ observations, as shown in section 3.2.2. Therefore, one should be careful to conclude anything on the exact PIV velocities. The shape and width of the histogram can however be used to illustrate the presence of multiple surface velocities within the footprints, regardless of a systematic underestimation by PIV.

4 Discussion

4.1 Discarded flights from XS5

A lot of data was discarded from XS5 on the basis of UAS instability. Here the results of the discarded flights will be inspected, to quantify the importance of drone movements. During surveying of XS5 heavy rainfall started and disturbed the surveying. Figure 39 shows the altitude recorded during the altitude 2 m and 4 m. The 4 m altitude flight only had few waypoints, as the rest of the flight was discontinued. These flights were done manually, as TTF was disabled. The altitude was instead read from the altimeter. Flight 2023-08-31-11-18-27 from altitude 2 m and flight 2023-08-31-11-42-32 from altitude 4 m is discussed. The altitude plots are shown below.

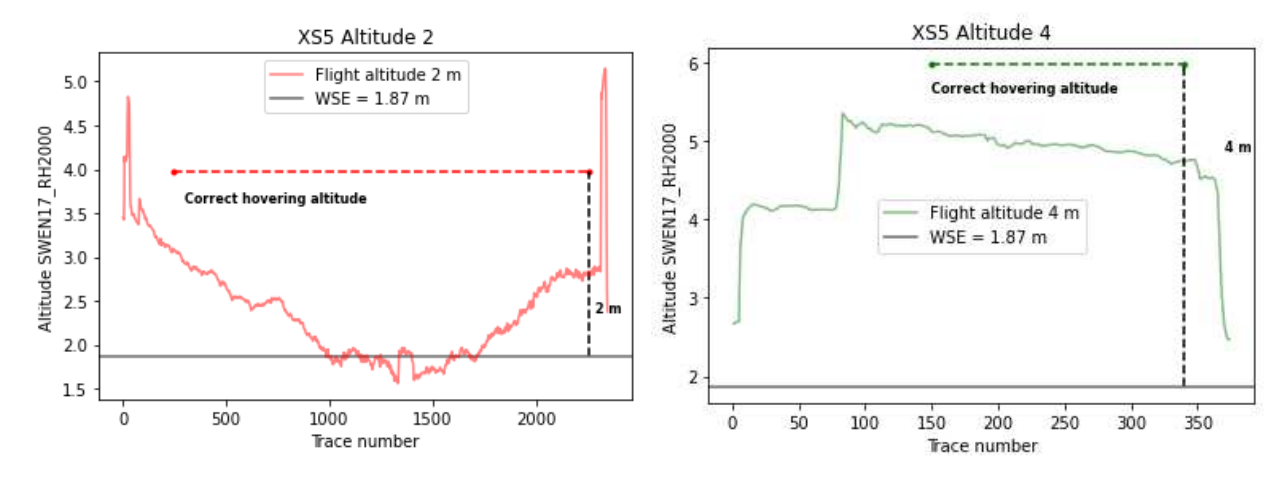


Figure 39: Left: Logged altitude for altitude 2 m from XS5. Right: Logged altitude for altitude 5 m from XS5. Both plots include a horizontal line for the WSE and a horizontal line for with the correct flight altitude for each flight.

Both of the altitude plots from the two flights indicate drone movements during hovering in the vertical direction. Especially for altitude 2 m, the altitude recorded seems to be incorrect, since the drone was not below the water surface (WSE) at any point. At altitude 4 m, the altitude recording shows a slight decrease in altitude during hovering, either due to an incorrectly logged altitude or due to the flight being done manually. When TTF is disconnected the true altitude could simply have been logged wrong or less likely the manual steering of the UAS could have been inaccurate. If the altitude was simply logged wrong, they might still have been relatively stable and could have been included originally.

Figure 40 shows the velocity estimates of these flights. The model was fitted with starting parameters rather than boundaries for altitude 2 m. The starting parameters used were (-30,30,20,20,100,3000). For altitude 4 m the flight was fitted with boundaries.

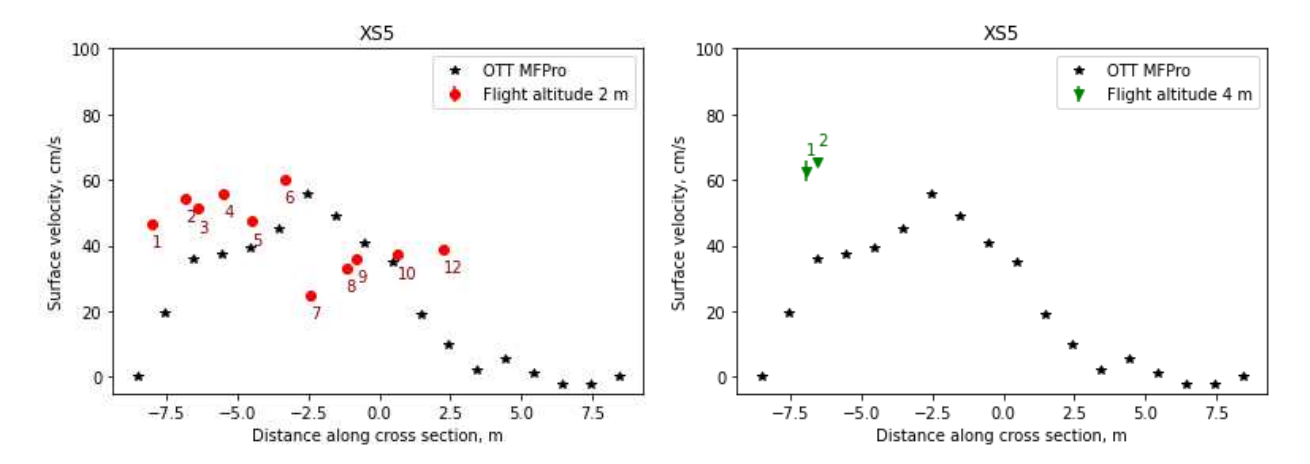


Figure 40: Results of XS5 from the originally discarded flights, altitude 2m and 4m

From figure 40, the velocities estimated by these flights do not seem to be worse than other flights at XS5. If the altitude was as unstable as the plots indicate, stability and the exact altitude does not seem have a big impact on the results. The UAS stability is shown to be less of an issue than previously thought to be. It was thought to be an issue due to the Doppler radar measuring relative velocity. In the paper by Bandini et al. (2022), it was recommended to account for UAS platform movements by inspecting the raw data. This was not done in this survey, as it seemed to not have an impact.

4.2 Decreasing hovering time

The surveying time of the Doppler radar was 1 min. at each hovering point. This makes the Doppler survey very time-consuming. It is here discussed, if the hovering time could be shortened to 30 seconds instead of 60 seconds. The data from each waypoint is decreased to half of the hovering period, by decreasing the total amount of traces included. Equation 11 shows how the new end trace is found.

New End Trace = Start Trace +
$$\frac{\text{End Trace} - \text{Start Trace}}{2}$$
 (11)

The start and end traces are thus found relative to the ones picked out as described in section 2.3.7. The velocities are determined from half and full waypoint and compared below. Each flight altitude is evaluated separately, shown for XS6 in figure 41. The results of the remaining cross-sections can be seen in Appendix G.

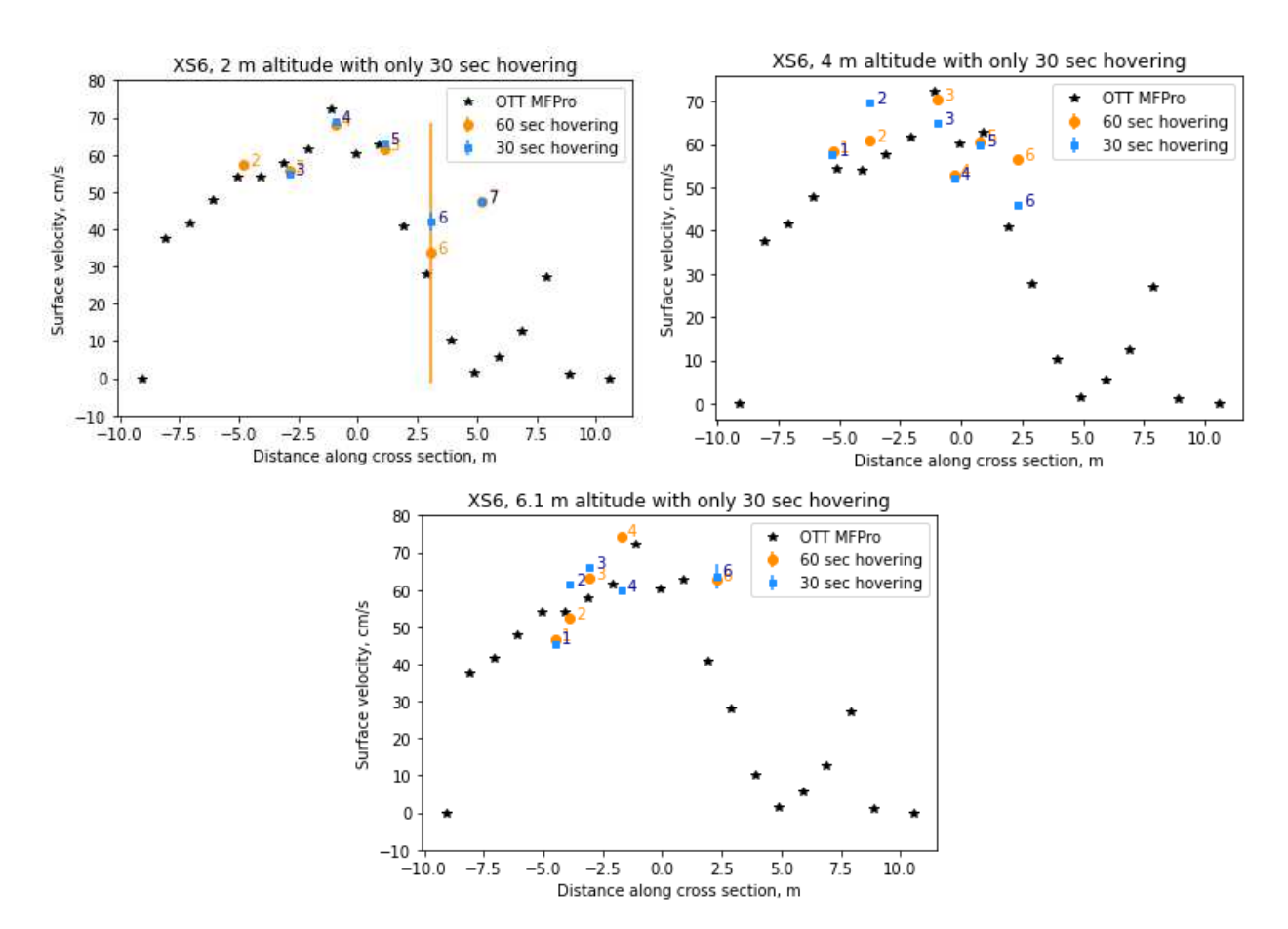


Figure 41: Comparing 30 sec. hovering and 60 sec. hovering velocity estimates for the three altitudes flown at XS6.

For altitude 2 m, the first waypoint model fit from the 30 seconds hovering period is not within the RMSE threshold of 50 and does not result in a final velocity. Altitude 4 m shows a slight increase in outliers, compared to the velocities found from the full hovering period. Waypoint 2, 3 and 6 at altitude 4 m show a clear variation. The velocity spectra of these waypoints are shown below.

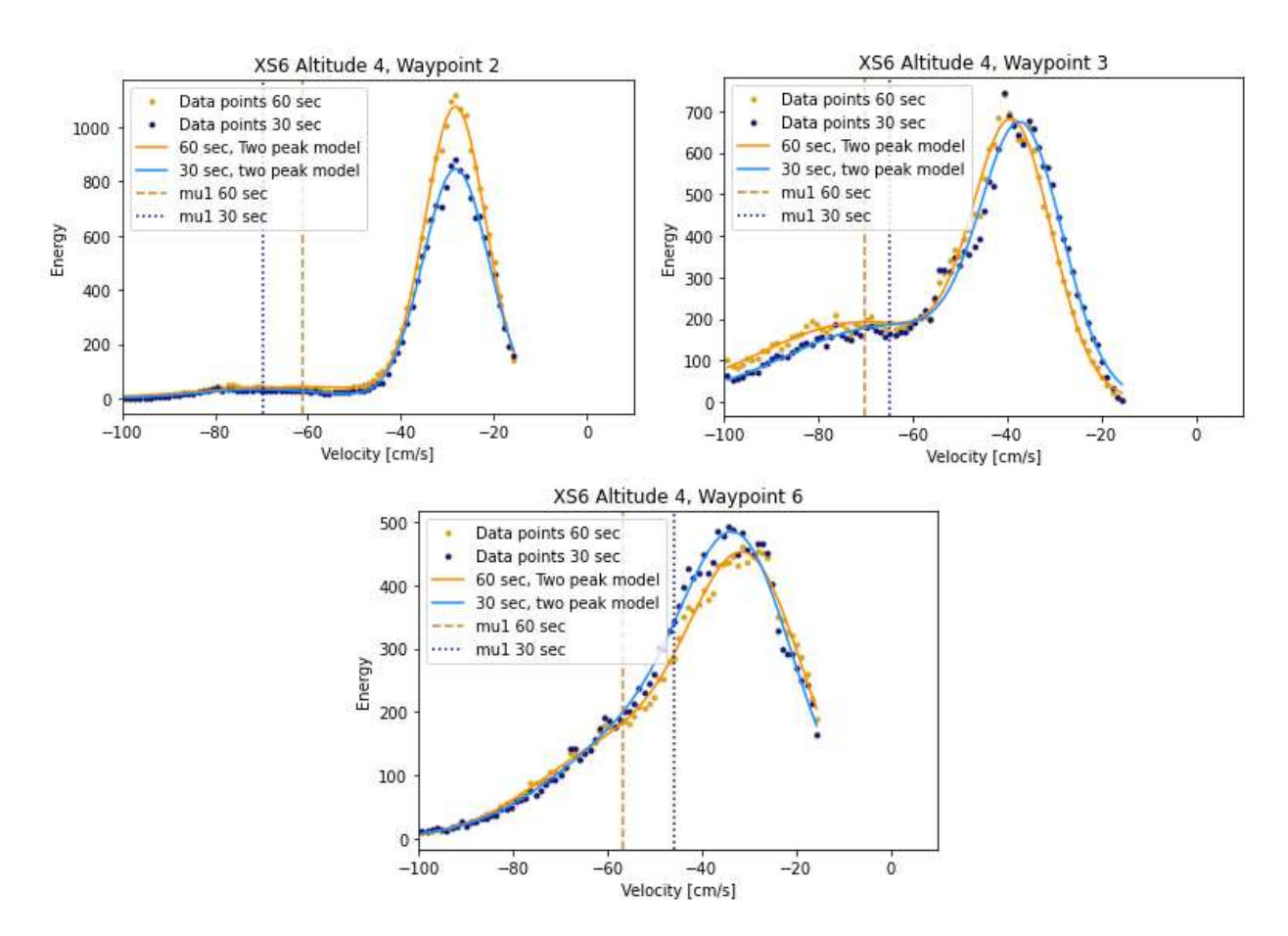


Figure 42: Doppler velocity spectra XS6 waypoints 2, 3 and 6. The plots show data from both a 60 sec. and 30 sec. hovering period.

At waypoint 2 both datasets seem to be picking up some background noise, that is registered as a peak. As a result, both overestimate the velocity, with a higher overestimation by 30 seconds data. For waypoint 3, the in-situ velocity is around 70 cm/s, where the 30 seconds velocity is found to be around 65 cm/s. This could be due to the slight variation in velocity found in the first peak, but also due to the peak being wide making it impossible to estimate the true velocity from the peak. In waypoint 6, the data only indicates one clear peak. The in-situ estimated velocity of 40 cm/s is not visible as a peak in this spectrum. The issues with estimating the correct velocity in these spectra seem to be the same, regardless of whether 30 second or 60 second data is fitted. It can therefore be concluded, that the wrong estimates are not due to the shorter hovering period, but other interpretation issues that were present at these waypoints already.

Inspecting a waypoint where the estimate is approximately the same, namely altitude 4 m waypoint 1. Here it is clear that the Doppler recognizes two velocities within the footprint, and the model thus creates a great fit for both datasets. The velocities chosen from the 60 seconds data set and the 30 seconds data set is the same, indicating that a decrease in hovering time would be possible.

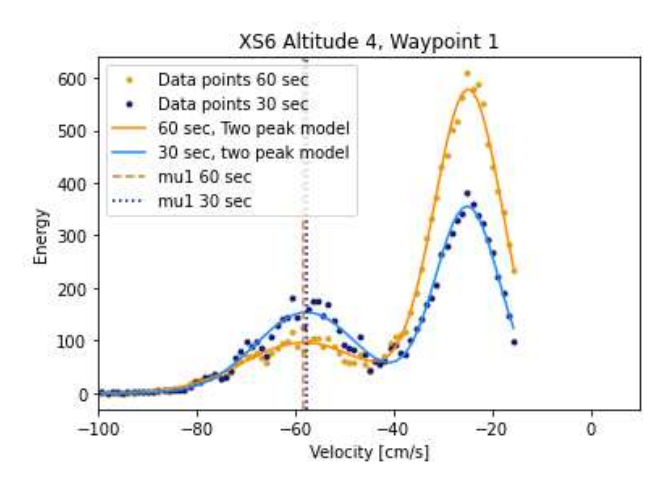


Figure 43: Doppler velocity spectra XS6 altitude 4 m waypoint 1 with 30 sec. and 60 sec. datasets. The estimated velocity is the same.

Since more waypoints seem to be the same or close to the same value, and those who differ seem to be difficult to interpret regardless of duration, 30 seconds hovering time can be recommended going forward to shorten surveying time.

4.3 Advantages and disadvantages of the three velocimetry methods

4.3.1 PIV

PIV showed some disadvantages in this study. Postprocessing including video selection and trimming, stabilizing, binarizing before running the analysis in PIVlab is very cumbersome currently but could be automated. The main problem is however with the lack of seeding. To improve it would require more operators applying woodchips. Seeding could be applied from another drone. However it is applied, it becomes an issue for wider rivers than the one surveyed in this study. The same can be said about the necessary GCPs in the frame which must also be placed by operators. While PIV may be faster in the field than both Doppler radar and OTT MF Pro, its postprocessing time is very long. It is obvious that the wider the cross-section, this becomes even more cumbersome if the full cross-section is not contained in one sequence. An advantage of PIV is its higher spatial resolution than the Doppler radar, as velocity can in theory be computed for every pixel of the image. Another advantage is that PIV can measure all directions of flow. This is an advantage as through a cross-section of a natural river, the flow will hardly ever be fully laminar. The heatmaps demonstrate that it is possible to get a very detailed image of the flow. PIV results show strictly the surface velocity, while OTT MF Pro is slightly submerged. The disadvantage to this is that wind for example may cause a surface velocity of seeding, that is not equal to the actual river flow velocity.

4.3.2 Doppler radar

Proposah had a major influence on the Doppler data. It was worked around by picking the other peak, but results showed that this algorithm did not always work, and sometimes only one peak was present. The Doppler radar flight time was quite long at 30-40 minutes per cross-section, however this will be notably shortened if hovering time is decreased to 30 seconds. Due to its large footprint, the Doppler radar has a low spatial resolution. This leads to larger errors, when flow fluctuates rapidly throughout the cross-section. It is not possible to get a full

velocity profile with the same shape as with OTT MF Pro, due to fringe measurements averaging over a larger area, leading to larger overestimations closer to the banks. It is therefore more suitable for large and wide rivers. The Doppler radar does not require seeding on the surface, which is an advantage, especially for surveying large rivers. The Doppler radar requires a minimum roughness of the water surface, this did not seem to be a problem in this survey, but may be a problem in smaller streams with low flow and slopes. The velocity measured by the Doppler radar is only in its line of sight, it cannot measure velocities in other directions. Postprocessing of the Doppler radar can be fully automatized, allowing for instantenous velocity measurements, which is a major advantage compared to PIV. However, more work is needed to fully understand how the velocity can be picked in its spectrum. The Doppler radar does not require daylight to operate, but results may like the PIV be influenced by wind or rain, as this can appear in the spectrum. Both UAS-borne methods are also currently sensitive to rain for operating, as equipment can be damaged in heavy rain.

4.3.3 OTT MF Pro

OTT MF Pro is still the most reliable velocimetry method in terms of repeatability of results. It is a point measurement, so precise point measurements can be done. It can only accurately measure velocities moving straight into the sensor, like with the Doppler radar, alignment is important. The major disadvantage of OTT MF Pro is how time consuming it is. It is not contactless, so it cannot be applied in hard-to-reach areas or during floods, where it may endanger operators. Unlike the UAS-borne Doppler radar and PIV, the OTT does not simultaneously measure position. Small errors in positioning may occur when having to manually read and note down tagline distance. Unlike the Doppler radar and PIV, OTT MF Pro can measure a full vertical velocity profile by submerging to several depths and automatically calculate discharge.

4.4 Results of PIV

Due to the low seeding density and lack of seeding across the full cross-section, PIV did not give comparable results for most of the cross-sections. The results of PIV could possibly be improved by piecing together several video sequences like a mosaic to get more accurate results in sections with low seeding. However, the little amount of seeding that was applied tends to congregate, and it is not necessarily possible to find sequences with dense seeding for the full cross-section. Due to time constraints it was not possible to improve PIV results with this method. For the few sections that were well-seeded in XS3 and XS6, PIV did give results within an acceptable range, like reported by Bandini et al. (2022) and Saso et al. (2020). Other studies report the same issues as this paper with low seeding density. It has previously been reported to cause systematic underestimation of flow velocities (Strelnikova et al., 2020). Detert and Weitbrecht (2015) also found that errors were due to "an insufficient seeding density or misleading standing waves at obstacles" (Detert and Weitbrecht, 2015), like the sunglints present at XS2. While Saso et al. (2020) demonstrated successful PIV methods, they also found PIV to be sensitive to seeding characteristics and challenging environmental conditions. As explained by Strelnikova et al. (2020), the reason is that with improper seeding density, no displacement is identified in many areas leading to a zero velocity estimate. When results are extracted from PIVlab, the temporal mean of all frames is calculated and the zero velocity estimates will decrease the mean.

4.5 Results of the Doppler radar

While the Doppler radar may have had higher accuracy in this study than previous studies such as the previous UAS-deployment by Bandini et al. (2022), it still has large errors. The velocity estimations by the three differ-

ent altitudes differed a lot from each other, a slight deviation is to be expected knowing how altitude influences footprint size, but ideally they should not be too far. XS6 had the closest to in-situ Doppler results. The velocity profile of XS6 is very stable, allowing for better results with the Doppler. Weather conditions had also changed slightly, which may have been more favorable conditions for the Doppler, as surface roughness increases when more wind is present. XS2 had the largest errors, indicating issues when velocities change rapidly. The Doppler radar was shown to have difficulty estimating very low surface velocities (below 20 cm/s) evident from fringe outliers at XS1, as these did not give a high energy return in the form of a peak. Generally, the radar is thought to estimate faster flows more reliably. This was not proven with XS2 having the fastest flow but large errors. The errors seem to be due to the large fluctuations in velocity.

There is a tendency for the Doppler radar to overestimate in-situ velocities. This could be explained by the fact that it is measuring a radial velocity, and the drone's own movement therefore has an impact. It will therefore be recommended to investigate the effect of this. The overestimation could also be due to the proposal disturbing the natural flow.

The specific velocity picking algorithm implemented in this paper has not been implemented on Doppler data before. The working hypothesis was that the two peaks, found in the Doppler spectra, represented the surface velocity and the surface velocity with the impact of propwash. The algorithm should therefore pick the higher velocity as the river surface velocity. The algorithm failed in too many cases where it either did not register the second peak, or the spectrum did not have the double peak shape at all. XS2 spectra were a special case often displaying just one (broadened) peak. The rapidly changing flow lead to the theory that the Doppler was simply picking up multiple river surface velocities in the footprint. Despite the large gaps and deviations in PIV results, it was possible to perform footprint analysis on some waypoints. So far, the working hypothesis seems to be true as demonstrated by footprint analysis of XS3. The PIV results show only one peak. Without the influence of propwash, there is only one dominant surface velocity within the footprint, solidifying the belief that the other peak must be caused by propwash. Footprint analysis of XS2 also helped to understand the Doppler spectra from this cross-section. The propwash did not seem to influence this higher velocity cross-section as much. The spectra from altitude 6 m especially had their broadened peak shape due to multiple velocities being contained in the large footprint.

4.6 Recommendations for future work

For the Doppler flights, not one altitude seems to work better than the others when looking at the error statistics. It could however be recommended to fly at 4 m altitude for the following reasons: signal decreases with altitude, therefore 6 m has a weaker signal. The larger footprint at 6 m decreases spatial resolution, and it was shown that many different surface velocities can be registered within one footprint of this size, making interpretation difficult. Propwash decreases with altitude, therefore 2 m is not ideal. Propwash was still not eliminated at altitude 4 m.

More work is necessary to establish the influence of proposah, which this survey showed was the major influence on results. The issues of proposah were previously reported by Fulton et al. (2020) to create a bias in results, as also shown here. It was worked around by picking the other velocity estimate, but results from XS2 show that this method may not work for higher flow velocities. To investigate the impact, the drone-induced velocity could be measured in stagnant water. It could also be attempted to measure the surface velocity from

both directions at each waypoint, both facing with and against the flow. Facing with the flow, rather than incoming as was done here, would result in a positive component from the river flow and a negative from the proposals. If the magnitude of the velocity generated by proposals could be quantified, the peak with the highest energy return could be chosen and the proposals subtracted. XS2 being the only cross-section with higher surface velocities, it would be interesting to conduct more surveys at higher velocity locations, to investigate the assumption that proposals has less of an impact in these cases. A different mount angle of the Doppler radar of e.g. 30 degrees rather than 45 would move the footprint further away from the UAS platform. This could minimize proposals contained in the footprint.

No filtering of background noise in the signal received by the Doppler radar was performed. Typically this would be done by calculating the power of the signal in a part of the spectrum where no peak is present. This baseline power can be subtracted from the signal to make actual peaks stand out more.

Other model fits can be attempted. The peaks do not always seem to be centered around a mean as is the case with a Gaussian distribution. The double peak model seemed to fit most spectra from this survey well, but there were cases where one peak looked more appropriate. One peak model was attempted on XS2 leading to seemingly closer to in-situ results, but with worse model fits especially for altitude 2 m.

4.7 Applications of the technologies

PIV will be an issue to apply in larger rivers due to the seeding requirements demonstrated, while the Doppler radar on the other hand will work better in larger rivers, seeing as the accuracy improves a few meter from the banks.

From surface velocities estimated by the Doppler radar or PIV, discharge can be calculated. Discharge data is currently delivered in real-time by streamgaging networks (Utah Water Science Center, 2018). Currently, streamgaging is limited by where the instruments for streamgaging can be placed in the water column (Fulton et al., 2020). By utilizing UAS-borne Doppler radar and PIV methods, data coverage can be improved. The paper by Fulton et al. (2020) elaborates on how discharge can be calculated from the maximum surface velocity measured from the UAS-borne Doppler radar. The paper by Bandini et al. (2021) elaborates on how discharge can be jointly estimated along with Manning's coefficient from PIV velocity estimates.

5 Conclusion

An UAS-borne Doppler radar was flown at five cross-sections within a 10 km stretch of Rönne Å to estimate river surface velocity. Three different altitudes were flown: 2 m, 4 m and 6 m above the water surface. The results were compared to OTT MF Pro in-situ velocimetry. Surveying time of the Doppler flights and in-situ measurements took almost equally long. Based on the 30 seconds vs. 60 seconds hovering period discussion, a 30 second hovering period can be attempted going forward, to bring down surveying time for the Doppler radar. Even though it gives different results for some waypoints, these are the waypoints where the model already with 60 second data had a hard time fitting to two peaks. Therefore the velocity becomes somewhat randomly picked in these cases, rather than clearly corresponding to a peak. Surveying time can also be brought down by only flying one altitude. It has not been possible to conclude that one flight altitude gave better results for all cross-sections, since for each cross-section it varies which altitude gave lower errors. The error statistics show low repeatability because cross-sections with similar conditions, e.g. XS5 and XS6 that were close to each other, have very varying errors. The fact that two different flights at 4 m altitude at XS6 gave different error statistics also show repeatability issues. Both flights were carried out right after each other. The repeatability of the results should therefore be inspected.

Generally it is evident from the MBEs that the Doppler radar overestimates surface velocities. RMSEs range from 4.84 to 32 cm/s across altitudes and cross-sections. Deviations are especially large nearing the banks of the cross-sections, when considering the cross-sectional velocity profiles. It can be explained by the Doppler radar measuring in a footprint rather than a point measurement as the OTT MF Pro. The footprint causes the spatial resolution to be lower than what is possible with PIV. It can be concluded from the error statistics that the Doppler radar performed best at XS6 and worst at XS2. The relative better performance of the Doppler radar at XS6 could be due to the following factors: (1) weather change with more wind increasing surface roughness, a necessary condition for the Doppler radar. (2) Stable velocities across the cross-section. The Doppler radar performs better when surface velocities do not fluctuate too much, due to the lower spatial resolution of the Doppler radar.

Overall the double peak model seemed to fit the data well in majority of waypoints. The relatively high errors and overestimations by the Doppler radar compared to in-situ measurements do not seem to be due to a wrong model assumption. The model and algorithm for surface velocity estimation from the Doppler spectra failed in some cases where either: the model did not find the peak of the data points corresponding to the river surface velocity, or no second peak was present. The model fit can be improved by improving starting parameters and boundaries. A one peak model was attempted on data from XS2, showing worse fits evaluated by the RMSE between the model and the data points. Generally, XS2 was a particularly difficult case, as the spectra were very broadened, making correct velocity estimation difficult. The rapidly varying flow field seems to be the issue.

Videos for PIV analysis were also taken at the survey sites. Statistics were not computed for PIV because the issues with low seeding density gave large gaps in results. The parts that were well-seeded yielded results in good agreement with OTT MF Pro, indicating that PIV as a method can come very close to in-situ observations, with proper execution with regards to seeding application and video frame selection. Histograms of PIV estimated velocities inside Doppler footprints from XS2 and XS3 were able to confirm the following assumptions: (1) for cross-sections other than XS2, one of the peaks in the Doppler spectrum is the sum of proposals induced

velocity and river surface velocity. (2) For XS2, a wider range of river surface velocities are captured within the footprint, due to the very varied velocity profile of this cross-section. The general interpretation of what is captured in the Doppler velocity spectra seem to be right. More surveys with higher surface velocities are needed to conclude whether proposals still has an influence.

References

Athanasiou, L. S., Fotiadis, D. I., and Michalis, L. K. (2017). Atherosclerotic Plaque Characterization Methods Based on Coronary Imaging, chapter 8 - Propagation of Segmentation and Imaging System Errors. Academic press.

- Bandini, F., Frias, M. C., Liu, J., Simkus, K., Karagkiolidou, S., and Bauer-Gottwein, P. (2022). Challenges with regard to unmanned aerial systems (uass) measurement of river surface velocity using doppler radar. *Remote Sensing*, 14.
- Bandini, F., Lüthi, B., Peña-Haro, S., Borst, C., Liu, J., Karagkiolidou, S., Hu, X., Lemaire, G. G., Bjerg, P., and Bauer-Gottwein, P. (2021). A drone-borne method to jointly estimate discharge and manning's roughness of natural streams. *Water Resources Research*, 57.
- Bauer-Gottwein, P. (2023). Personal communication.
- Detert, M. and Weitbrecht, V. (2015). A low-cost airborne velocimetry system: proof of concept. *Journal of Hydraulic Research*, 53.
- DJI Enterprise (N.D.). Dji matrice 300 aircraft specs. https://enterprise.dji.com/matrice-300/specs. Accessed 2023-10-26.
- Emlid (N.D.a). Canadian spatial reference system precise point positioning (csrs-ppp). https://docs.emlid.com/reachrs/tutorials/post-processing-workflow/nrcan-workflow. Accessed 2023-11-16.
- Emlid (N.Db). How PPK works. https://docs.emlid.com/reach/tutorials/basics/ppk-introduction/. Accessed 2023-09-27.
- Emlid~(N.D.c).~How~ppp~works.~https://docs.emlid.com/reachrs/tutorials/post-processing-workflow/ppp-introduction.~Accessed~2023-11-16.
- Emlid (N.D.d). Multi-band rtk gnss receiver with centimeter precision. https://emlid.com/reachrs2plus/. Accessed 2023-11-23.
- Emlid (N.De). Post-process data from GNSS receivers and RTK drones. https://emlid.com/emlid-studio/. Accessed 2023-11-23.
- Fulford, J., Thibodeaux, K., and Kaehrle, W. (N.D.). Comparison of current meters used for stream gaging. Technical report, United States Geological Survey.
- Fulton, J., Anderson, I., Chiu, C.-L., Sommer, W., Adams, J., Moramarco, T., Bjerklie, D., Fulford, J., Sloan, J., Best, H., Conaway, J., Kang, M., Kohn, M., Nicotra, M., and Pulli, J. (2020). Qcam: suas-based doppler radar for measuring river discharge. Remote Sensing, 12.
- Fulton, J. and Ostrowski, J. (2008). Measuring real-time streamflow using emerging technologies: Radar, hydroacoustics, and the probability concept. *Journal of Hydrology*, 357.
- Geolux (N.D). RSS-2-300W Surface Velocity Radar. https://www.geolux-radars.com/rss2300w. Accessed 2023-09-27.

Kempe, C., Jivall, L., Lidberg, M., and Lilje, M. (2016). On the management of reference frames in sweden. https://www.fig.net/resources/proceedings/fig_proceedings/fig2016/papers/ts02b/TS02B_kempe_jivall_et_al_8179.pdf. Accessed 2023-10-26.

- Lantmäteriet (N.D.a). Swedish geoid models. https://www.lantmateriet.se/en/geodata/gps-geodesi-och-swepos/reference-systems/the-geoid/swedish-geoid-models/. Accessed 2023-10-26.
- Lantmäteriet (N.D.b). Sweref 99. https://www.lantmateriet.se/en/geodata/gps-geodesi-och-swepos/reference-systems/three-dimensional-systems/SWEREF-99/#anchor-0. Accessed 2023-10-26.
- Lantmäteriet (N.D.c). Wgs 84. https://www.lantmateriet.se/en/geodata/gps-geodesi-och-swepos/reference-systems/three-dimensional-systems/wgs-84/. Accessed 2023-10-26.
- Lindenhoff, C. (2023). Workflow for measuring surface flow velocity with airborne doppler radar.
- M. Padhma (2023). A comprehensive introduction to evaluating regression models. https://www.analyticsvidhya.com/blog/2021/10/evaluation-metric-for-regression-models/. Accessed 2023-11-16.
- Martin, J. (2017). Dji phantom 4 advanced review. https://www.techadvisor.com/article/717953/dji-phantom-4-advanced-review.html. Accessed 2023-11-13.
- MATLAB (2022). FMCW Radar for Autonomous Vehicles Understanding Radar Principles. https://www.youtube.com/watch?v=-N7A5CIiOsg&list=RDCMUCgdHSFcXvkN6O3NXvifO-pA&index=1. Accessed 2023-09-28
- Nanoradar (N.D.). 24ghz alimeter radar nra24. http://en.nanoradar.cn/Article/detail/id/372.html. Accessed 2023-11-07.
- Nielsen, S. (2023). Personal communication.
- Odonohue, D. (2023). What is gnss rtk. https://mapscaping.com/what-is-gnss-rtk/#:~:text=So%2C% 20the%20main%20difference%20between,provides%20less%20accurate%20positioning%20information. Accessed 2023-11-21.
- OTT HydroMet (2015). Flow and discharge measurement with the ott mf pro. Technical report, OTT Hydromet.
- OTT HydroMet (N.D.). Ott mf pro water flow meter. https://www.ott.com/products/water-flow-3/ott-mf-pro-water-flow-meter-968/. Accessed 2023-09-19.
- Plant, W., W.C.Keller, and Hayes, K. (2005). Measurement of river surface currents with coherent microwave systems. *IEEE TRANSACTIONS ON GEOSCIENCE AND REMOTE SENSING*, 43.
- Saso, S. D., Pizzaro, A., and Manfreda, S. (2020). Metrics for the quantification of seeding characteristics to enhance image velocimetry performance in rivers. *Remote Sensing*, 12.
- Siegel, A. F. and Wagner, M. R. (2022). *Practical Business Statistics*, chapter Chapter 3 Histograms: Looking at the Distribution of Data. Academic press.

SPHEngineering (2021).enable Altimeter for precise terrain following to flight constant agl. https://www.sphengineering.com/news/ drone at low and altimeter-for-precise-terrain-following-to-enable-drone-flight-at-low-and-constant-agl. Accessed 2023-10-26.

- SPH Engineering (2023). Skyhub 3 datasheet. https://integrated.ugcs.com/dl/docs/skyhub-v3-datasheet-r3.pdf. Accessed 2023-10-26.
- SPH Engineering (N.D.). Ugcs professional drone mission planning software. https://www.sphengineering.com/flight-planning/ugcs. Accessed 2023-11-07.
- Strelnikova, D., Paulus, G., Käfer, S., Anders, K., Mayr, P., Mader, H., Scherling, U., and Schneeberger, R. (2020). Drone-based optical measurements of heterogeneous surface velocity fields around fish passages at hydropower dams. *Remote Sensing*, 12.
- The scipy community (N.D.). scipy.optimize.curvefit. https://docs.scipy.org/doc/scipy/reference/generated/scipy.optimize.curve_fit.html. Accessed 2023-10-20.
- Thielicke, W. (N.D.). Pivlab tutorial. https://pivlab.blogspot.com/p/blog-page_19.html. Accessed 2023-11-07.
- Utah Water Science Center (2018). What is a streamgage? https://www.usgs.gov/centers/utah-water-science-center/science/what-streamgage. Accessed 2023-11-24.

A Cross-sections from above

Cross-sections as seen from above. Flow direction is from top to bottom. Right bank is therefore left side of the images, as right and left bank are determined when looking in the direction of the flow.

XS1



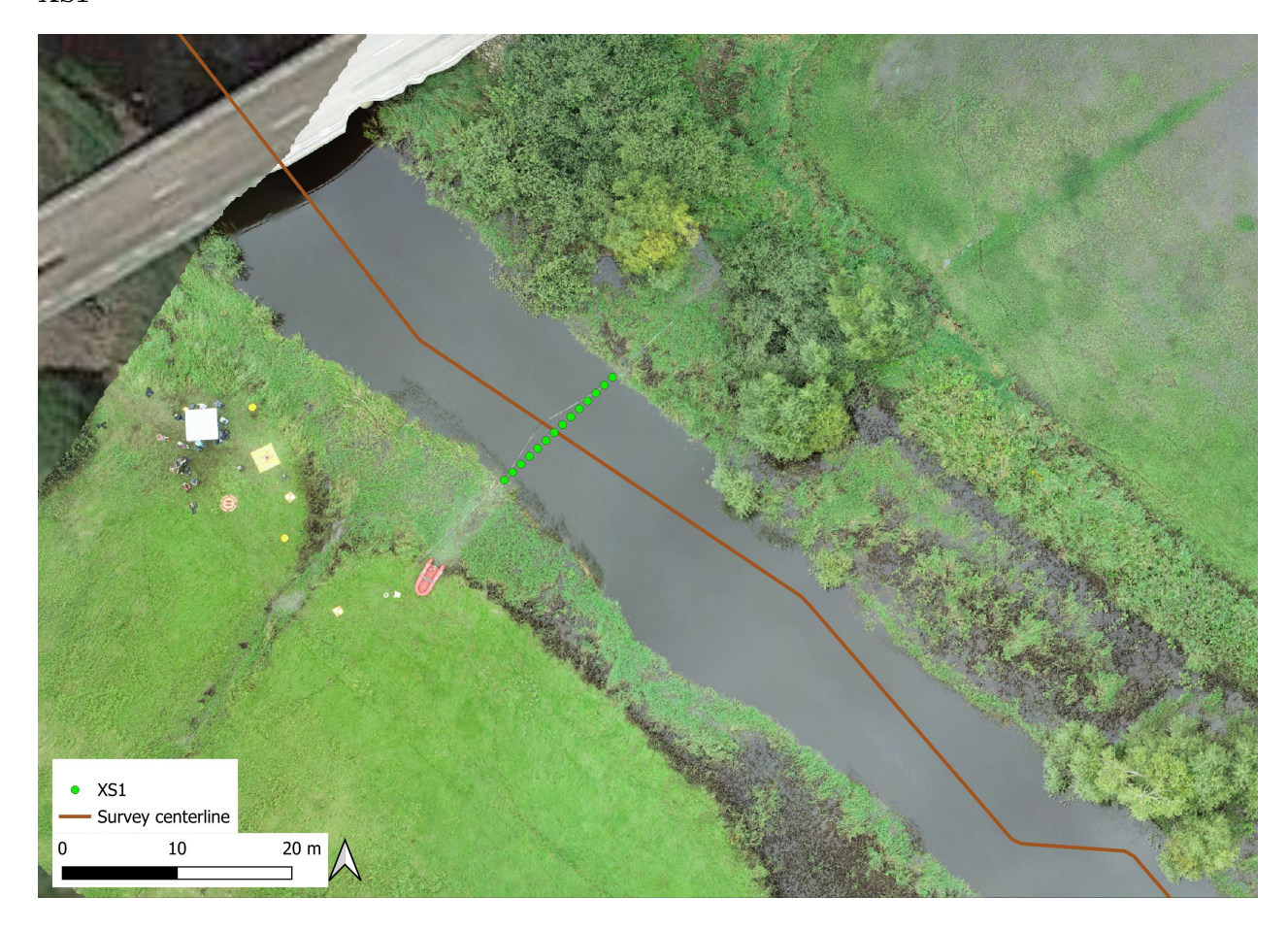


XS3

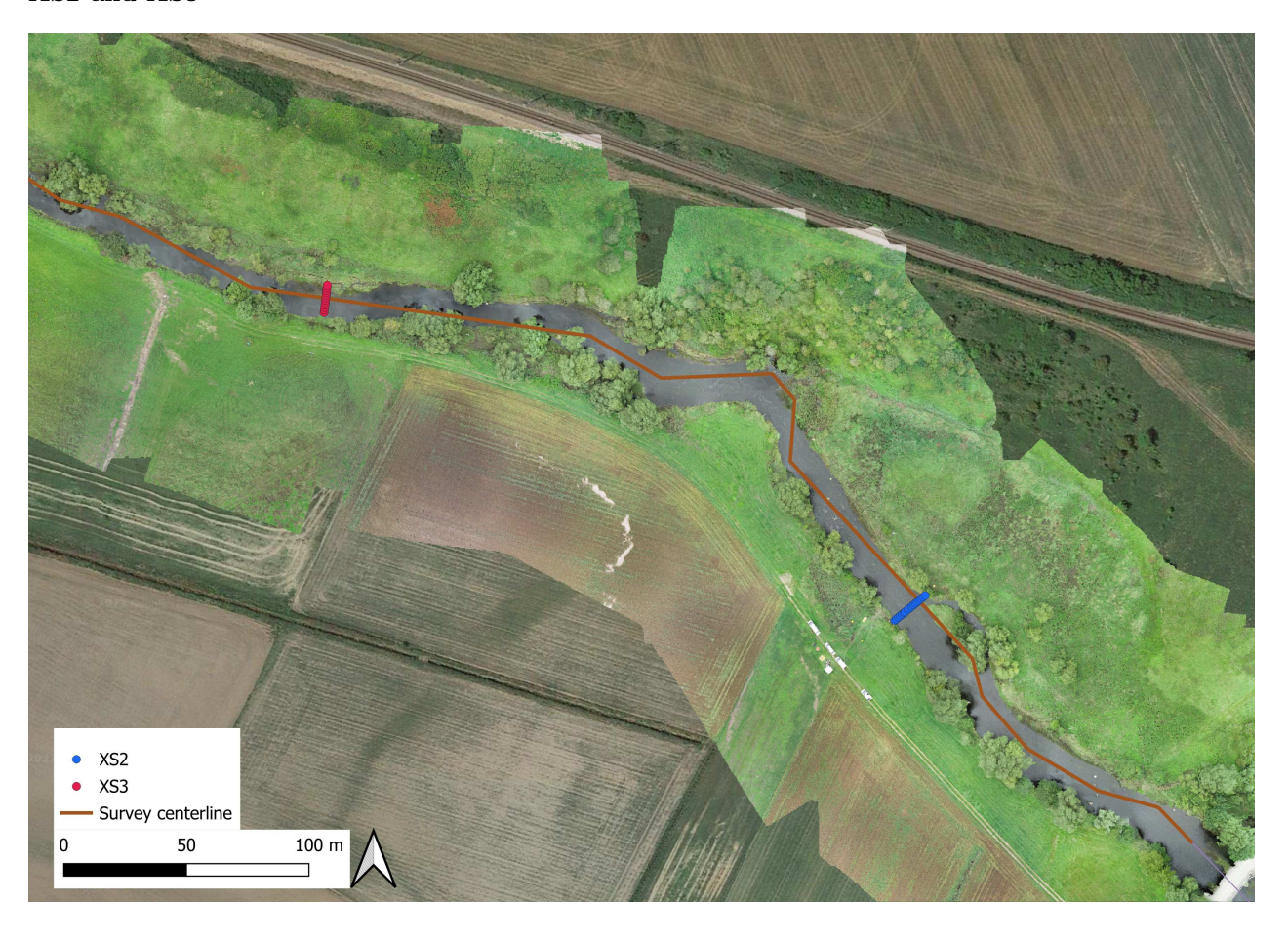








XS2 and XS3



XS5 and XS6



B Boundaries and starting parameters for each flight

$\mathbf{X}\mathbf{S}$	Altitudo [m]	Method	Bounds			p	0		
AS	Altitude [m]	Method	Bounds	mu1	mu2	sd1	sd2	f1	f2
1	2	p0		-40	20	40	20	2000	3000
1	5	ро		-40	20	40	20	2000	3000
	2								
2	4	p0		-110	-90	20	20	3000	2500
	6								
	2		((-150,-50,5,5,100,100),						
3	4	Bounds	(-20,20,50,50,5000,5000)						
	6		(-20,20,30,30,3000,3000))						
5	2	Bounds	((-150, -50, 5, 5, 100, 100),						
9	4	Dounds	(-20,20,50,50,5000,5000))						
	2			-70	-50	20	20	200	3000
6	4 (1)	200		-50	-30	20	20	200	3000
O	4(2)	p0		-50	-30	20	20	200	3000
	6			-60	-20	10	40	100	3000

C Hovering positions

XS1

XS	Altitude	Waypoint	Easting [m]	SD easting [m]	Northing [m]	SD northing [m]
		1	377189.725	0.03	6227699.920	0.08
		2	377190.633	0.07	6227700.669	0.03
		3	377191.156	0.02	6227701.272	0.02
	2	4	377191.932	0.03	6227701.907	0.02
1		5	377192.822	0.04	6227702.806	0.03
1		6	377193.378	0.03	6227703.509	0.02
		7	377194.339	0.03	6227704.231	0.02
		8	377194.969	0.05	6227705.863	0.04
		9	377195.794	0.05	6227705.525	0.05
		10	377196.927	0.02	6227706.569	0.03

XS	Altitude	Waypoint	Easting [m]	SD easting [m]	Northing [m]	SD northing [m]
		2	377189.341	0.02	6227703.651	0.04
1	5	3	377190.514	0.02	6227704.676	0.02
		4	377192.400	0.03	6227705.843	0.06

XS	Altitude	Waypoint	Easting [m]	SD easting [m]	Northing [m]	SD northing [m]
		1	381437.156	0.04	6222658.640	0.07
		2	381437.775	0.11	6222658.850	0.04
		3	381438.500	0.02	6222659.419	0.02
		4	381439.252	0.03	6222659.992	0.04
		5	381440.116	0.04	6222660.280	0.03
		6	381441.105	0.02	6222660.761	0.02
$\frac{1}{2}$	2	7	381441.921	0.02	6222661.393	0.02
2	2	8	381443.0234	0.01	6222662.235	0.03
		9	381443.005	0.02	6222662.533	0.02
		10	381443.854	0.02	6222663.618	0.04
		11	381444.401	0.04	6222663.295	0.06
		12	381444.608	0.02	6222663.865	0.02
		13	381445.606	0.02	6222664.464	0.02
		14	381445.652	0.02	6222665.040	0.01

XS	Altitude	Waypoint	Easting [m]	SD easting [m]	Northing [m]	SD northing [m]
		1	381435.290	0.04	6222659.751	0.04
		2	381436.392	0.02	6222660.617	0.02
		3	381437.561	0.02	6222661.565	0.02
2	4	4	381438.741	0.02	6222662.423	0.01
-	4	5	381439.850	0.03	6222663.350	0.01
		6	381441.035	0.01	6222664.301	0.02
		7	381442.182	0.01	6222665.153	0.01
		8	381443.047	0.02	6222666.251	0.03

XS	Altitude	Waypoint	Easting [m]	SD easting [m]	Northing [m]	SD northing [m]
		1	381435.227	0.05	6222662.407	0.05
		2	381436.639	0.03	6222663.526	0.03
9	6	3	381438.033	0.03	6222664.694	0.02
-	0	4	381439.566	0.03	6222665.945	0.02
		5	381441.138	0.02	6222667.207	0.02
		6	381442.090	0.03	6222667.981	0.05

XS3

XS	Altitude	Waypoint	Easting [m]	SD easting [m]	Northing [m]	SD northing [m]
3	9	1	381202.915	0.05	6222783.707	0.06
'		2	381202.992	0.01	6222784.849	0.02

XS	Altitude	Waypoint	Easting [m]	SD easting [m]	Northing [m]	SD northing [m]
		1	381200.264	0.03	6222781.677	0.02
		3	381200.855	0.02	6222783.754	0.01
3	4	4	381200.451	0.03	6222784.005	0.03
"	4	5	381201.143	0.01	6222786.124	0.02
		6	381201.019	0.01	6222787.196	0.02
		7	381201.052	0.01	6222787.633	0.02

XS	Altitude	Waypoint	Easting [m]	SD easting [m]	Northing [m]	SD northing [m]
		2	381198.381	0.07	6222781.773	0.05
3	6	3	381198.540	0.01	6222783.601	0.07
		4	381198.588	0.03	6222785.519	0.13

XS	Altitude	Waypoint	Easting [m]	SD easting [m]	Northing [m]	SD northing [m]
		1	379625.444	0.02	6226246.977	0.03
		2	379625.161	0.03	6226247.819	0.03
		3	379624.947	0.02	6226248.820	0.03
		4	379624.547	0.03	6226249.983	0.03
		5	379624.135	0.06	6226251.040	0.12
		6	379623.795	0.01	6226251.889	0.03
		7	379623.431	0.02	6226252.736	0.02
5	2	8	379623.012	0.05	6226253.853	0.02
		9	379622.775	0.02	6226254.561	0.02
		10	379622.462	0.02	6226255.591	0.04
		11	379622.119	0.01	6226256.550	0.02
		12	379621.796	0.02	6226257.456	0.01
		13	379621.413	0.02	6226258.357	0.01
		14	379621.019	0.01	6226259.281	0.02
		15	379620.729	0.02	6226260.282	0.02

XS	Altitude	Waypoint	Easting [m]	SD easting [m]	Northing [m]	SD northing [m]
5	5 4	1	379623.340	0.02	6226246.815	0.02
	4	2	379622.856	0.02	6226248.180	0.02

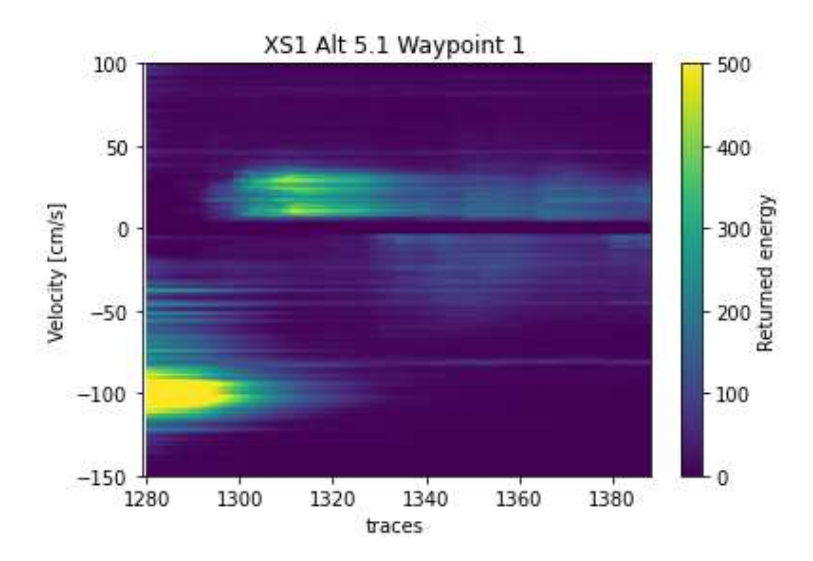
XS	Altitude	Waypoint	Easting [m]	SD easting [m]	Northing [m]	SD northing [m]
		2	379396.419	0.02	6226230.986	0.02
		3	379395.841	0.02	6226232.783	0.03
6	2	4	379395.244	0.02	6226234.631	0.03
		5	379394.625	0.02	6226236.602	0.03
		6	379394.024	0.02	6226238.459	0.03
		7	379393.252	0.03	6226240.443	0.04

XS	Altitude	Waypoint	Easting [m]	SD easting [m]	Northing [m]	SD northing [m]
6	4, (1)	1	379394.527	0.02	6226229.843	0.03
		2	379394.028	0.03	6226231.278	0.03
		3	379393.184	0.02	6226233.952	0.03
	4, (2)	4	379393.054	0.02	6226234.595	0.02
		5	379392.591	0.02	6226235.581	0.02
		6	379392.155	0.02	6226237.059	0.02

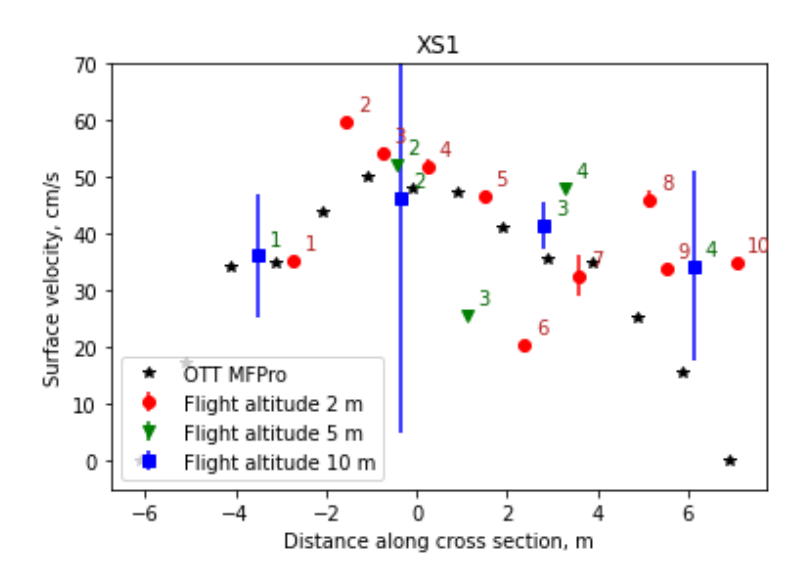
XS	Altitude	Waypoint	Easting [m]	SD easting [m]	Northing [m]	SD northing [m]
6	6	2	379392.194	0.03	6226229.879	0.02
		3	379391.756	0.02	6226230.354	0.02
		4	379391.656	0.01	6226231.203	0.01
		5	379391.237	0.01	6226232.502	0.01
		6	379390.626	0.02	6226234.351	0.02
		7	379390.061	0.01	6226236.317	0.02

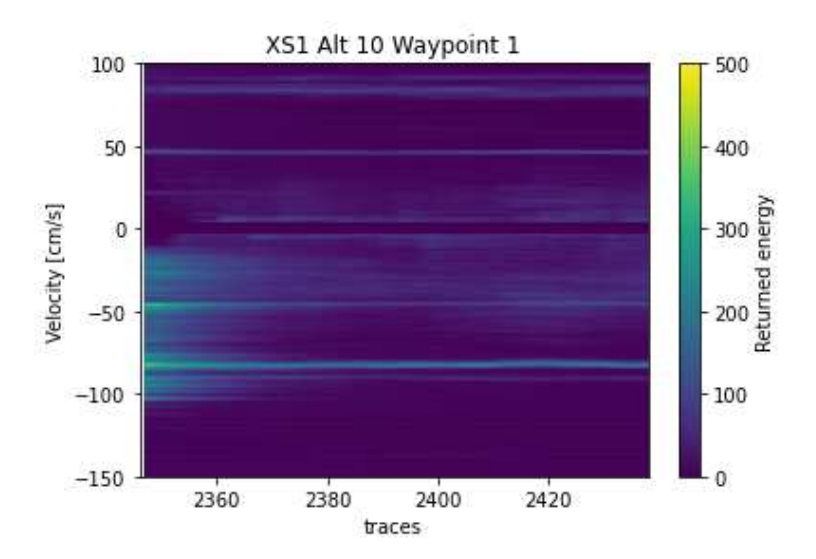
D Argumentation for discarded waypoints

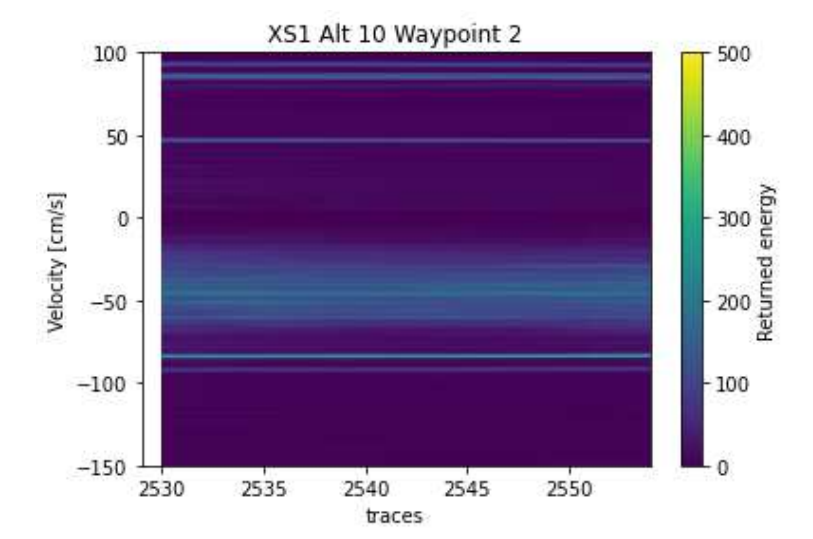
XS1, flight 2023-08-29-14-27-35, altitude 5.1

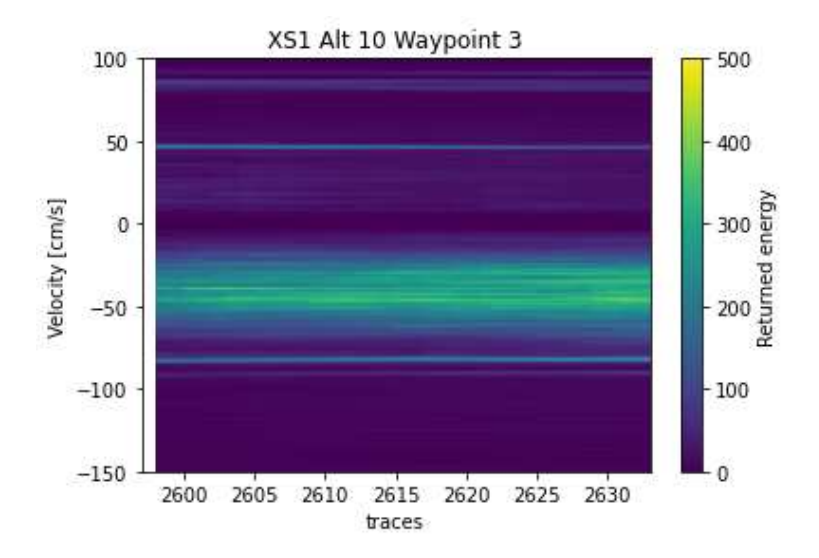


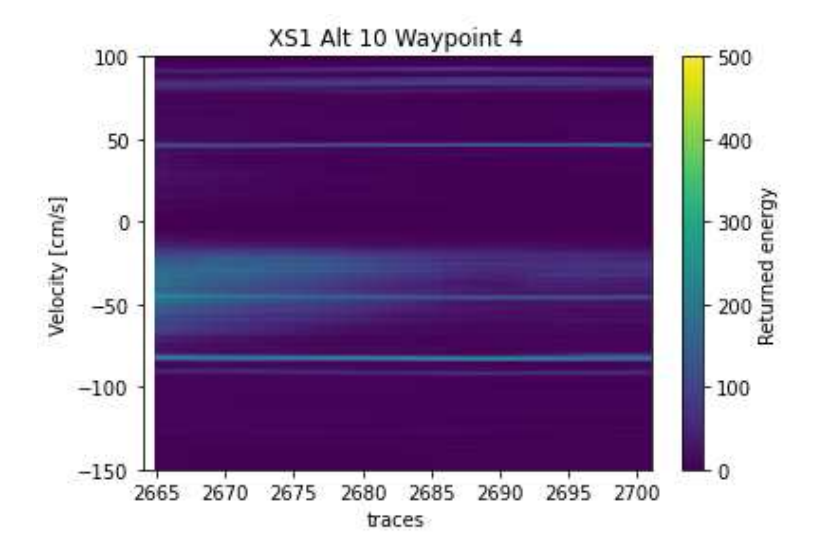
XS1, flight 2023-08-29-14-27-35, altitude 10.1



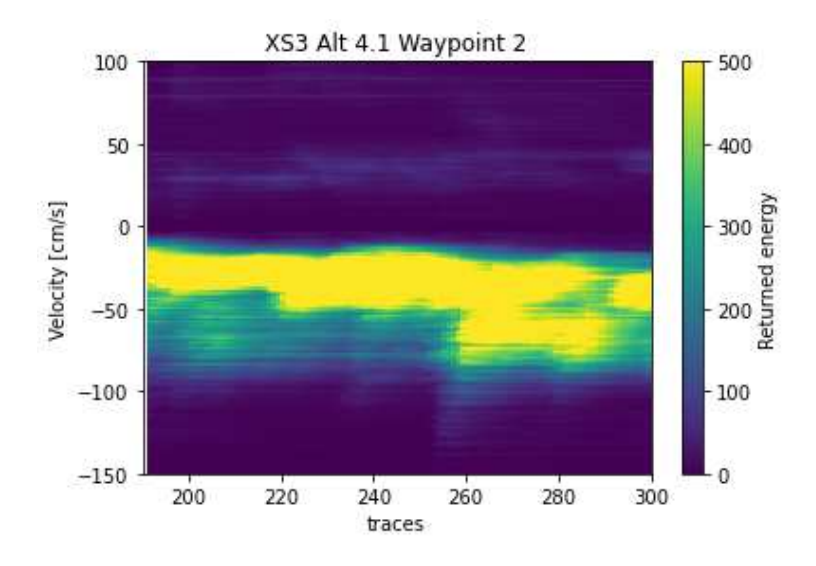




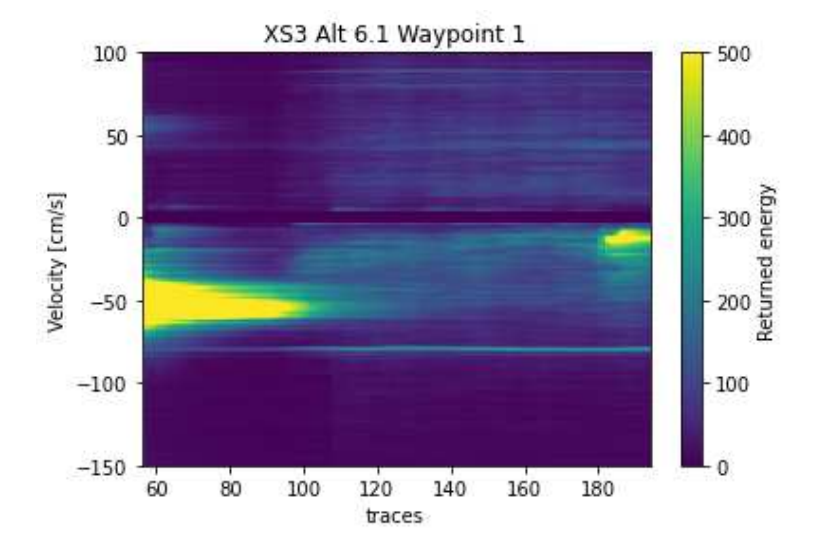


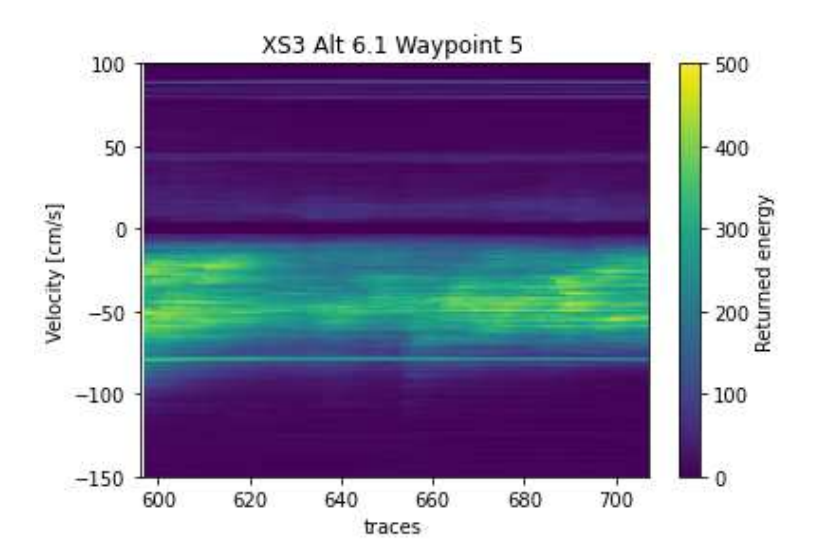


XS3, flight 2023-08-30-19-16-02, altitude 4.1

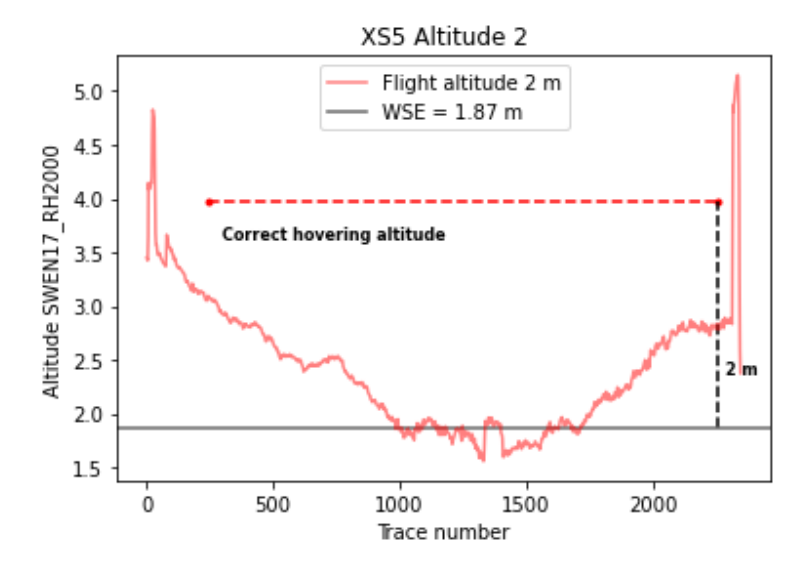


XS3, flight 2023-08-30-19-27-42, altitude 6.1

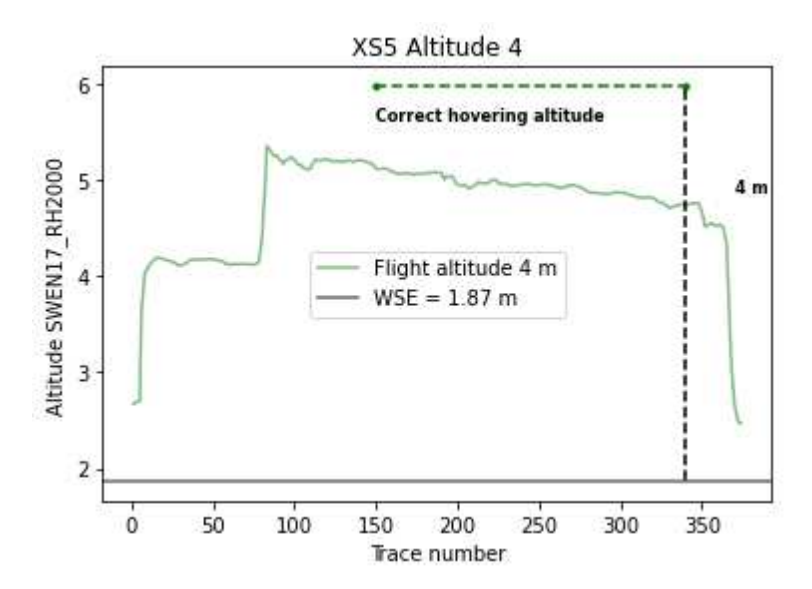




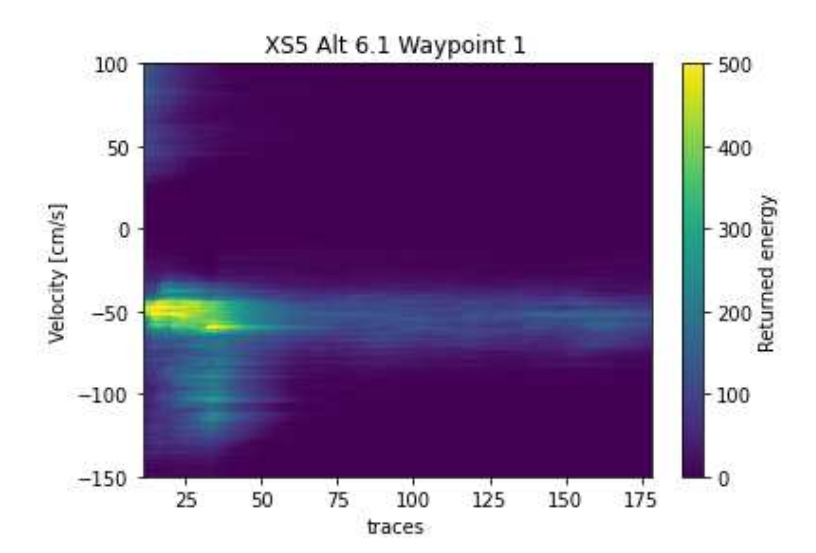
XS5, flight 2023-08-31-11-18-27, altitude 2.1

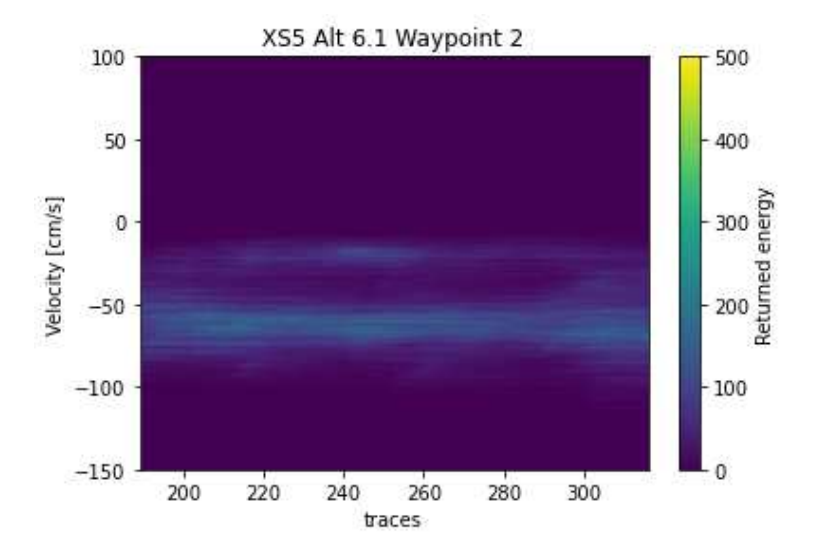


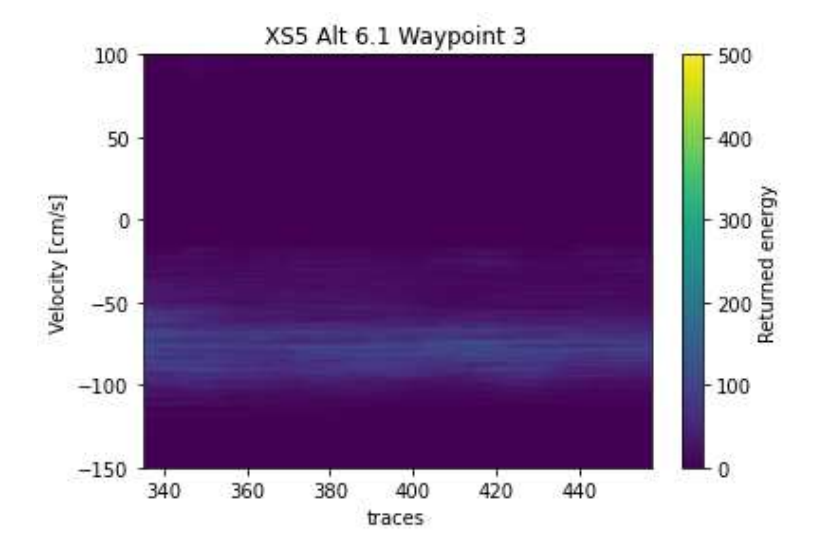
XS5, flight 2023-08-31-11-42-32, altitude 4.1

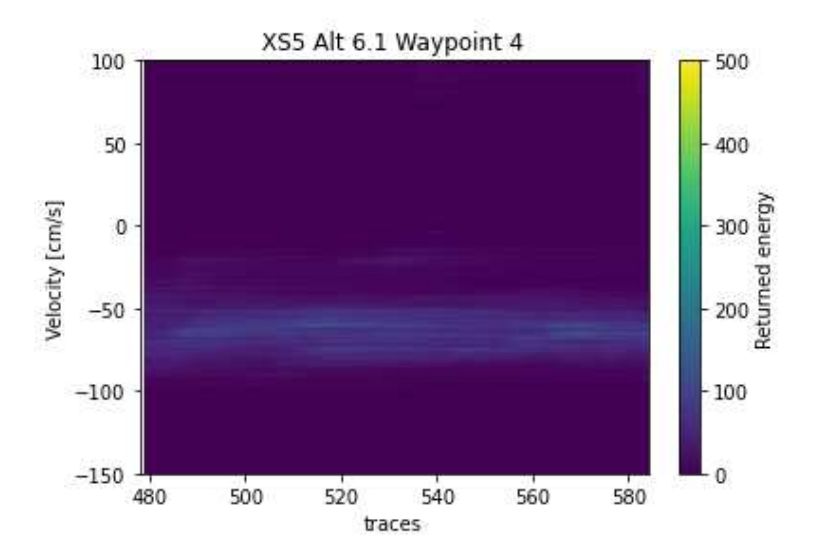


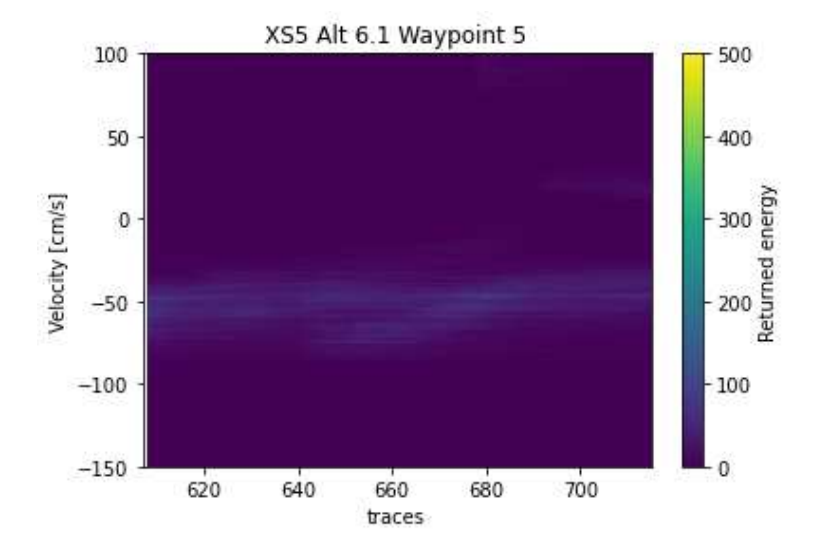
XS5, flight 2023-08-31-17-15-37, altitude 6.1



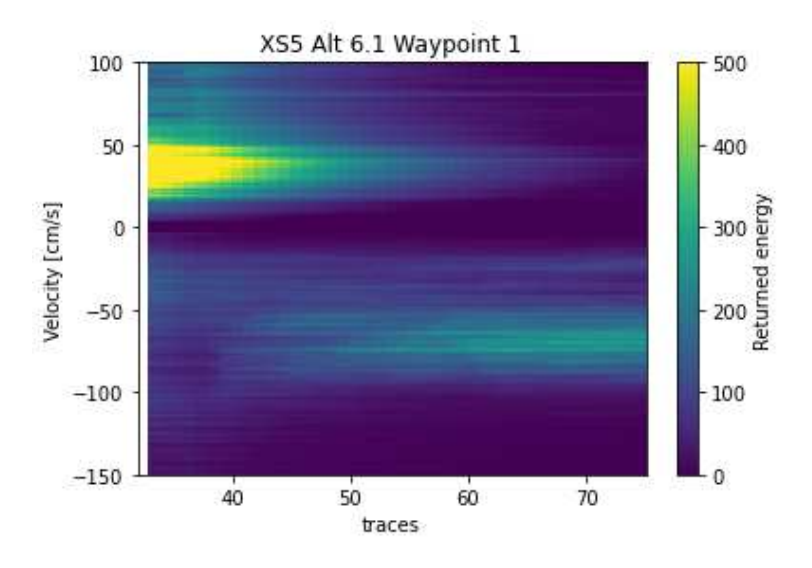


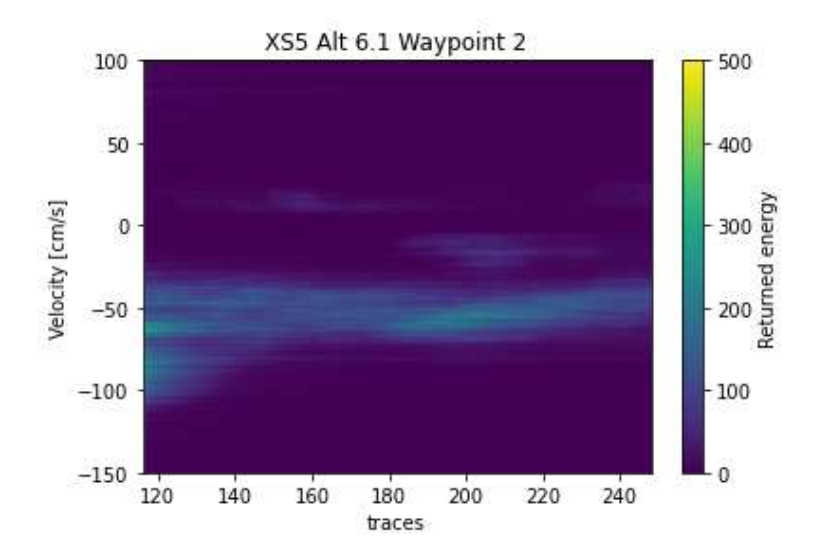


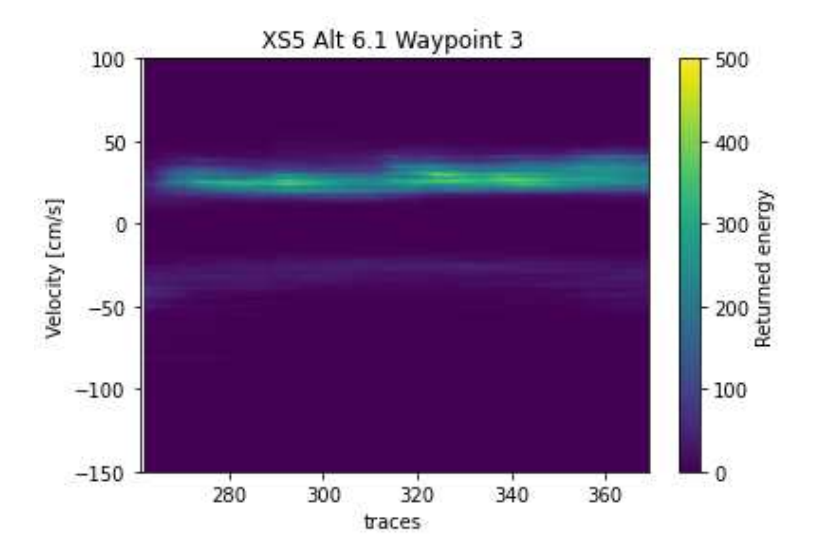


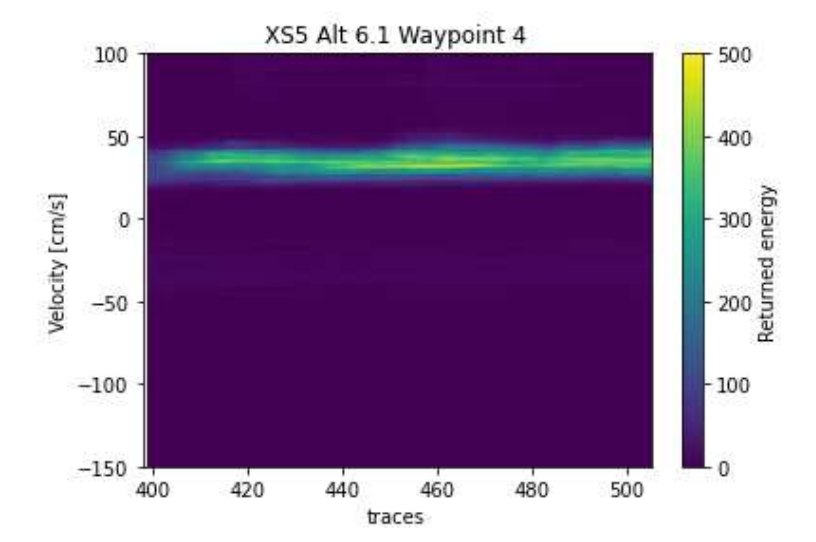


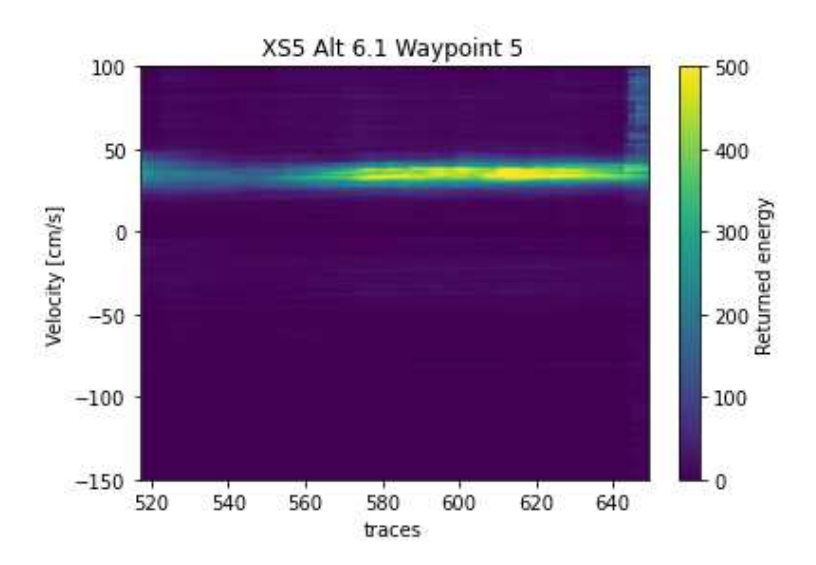
XS5, flight 2023-08-31-17-25-53, altitude 6.1



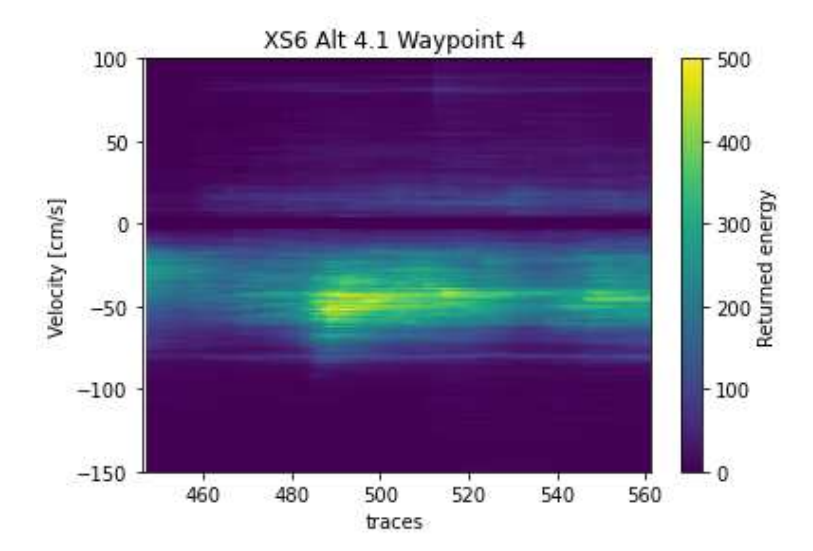


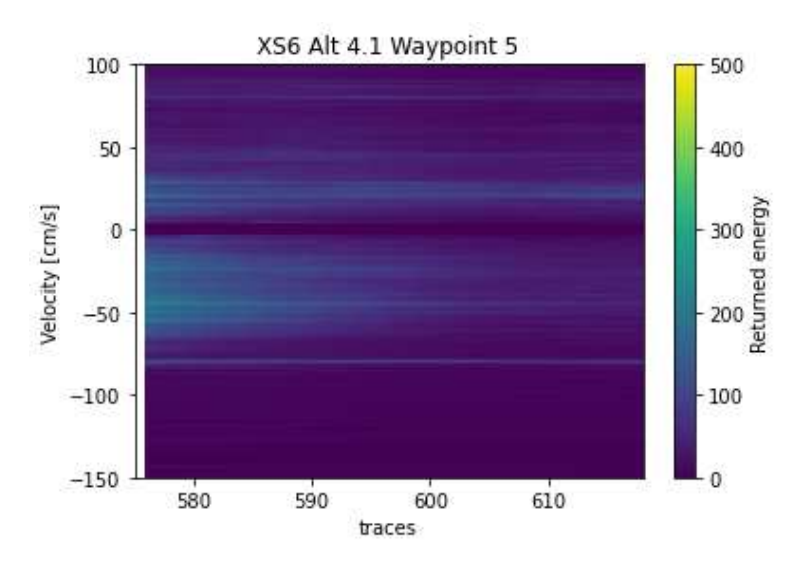




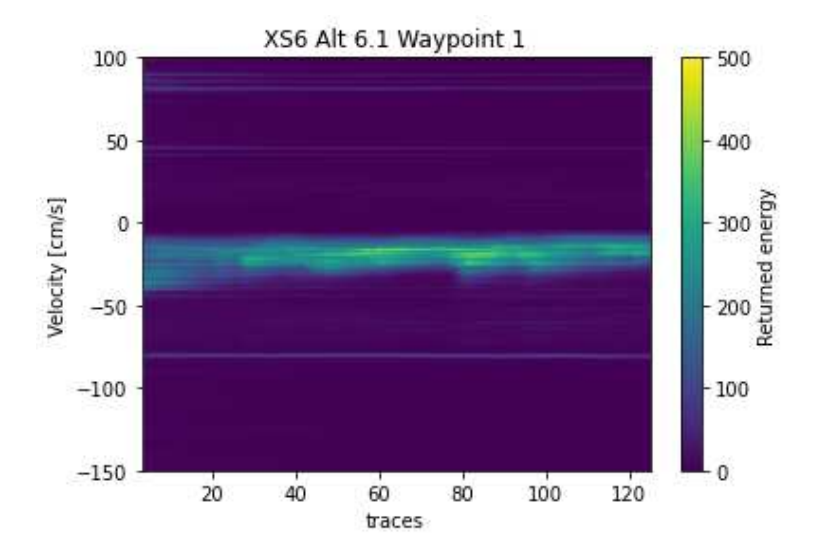


XS6, flight 2023-08-31-18-00-19, altitude 4.1



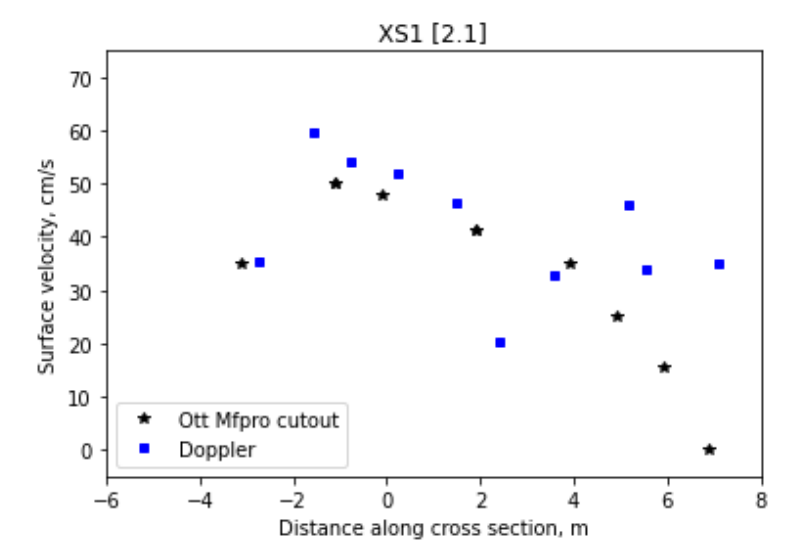


XS6, flight 2023-08-31-18-08-21, altitude 6.1

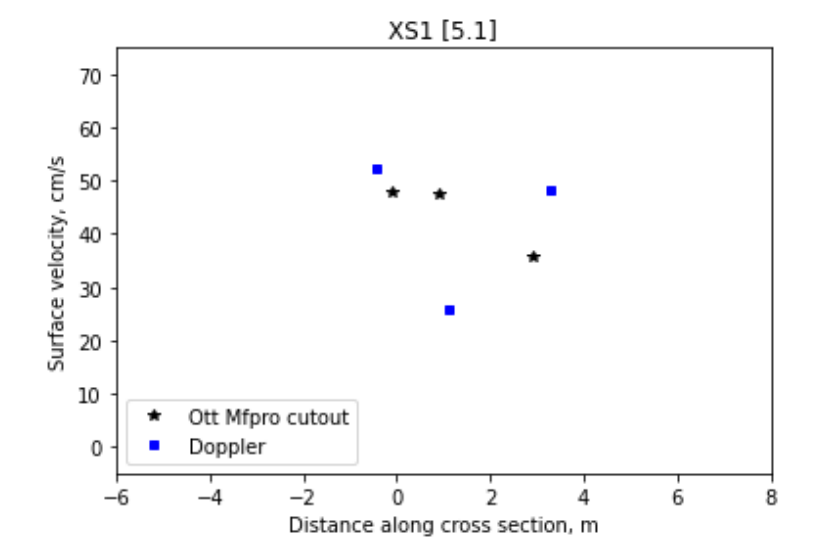


E Basis for error statistics

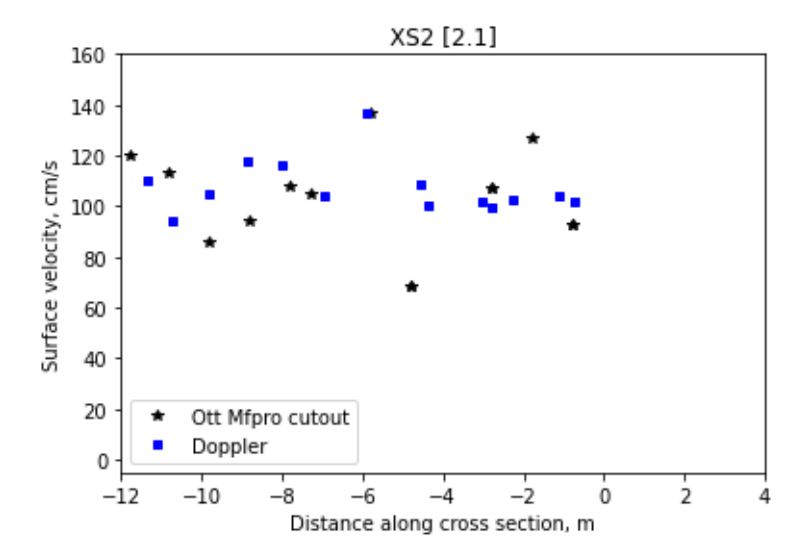
XS1, alt. 2



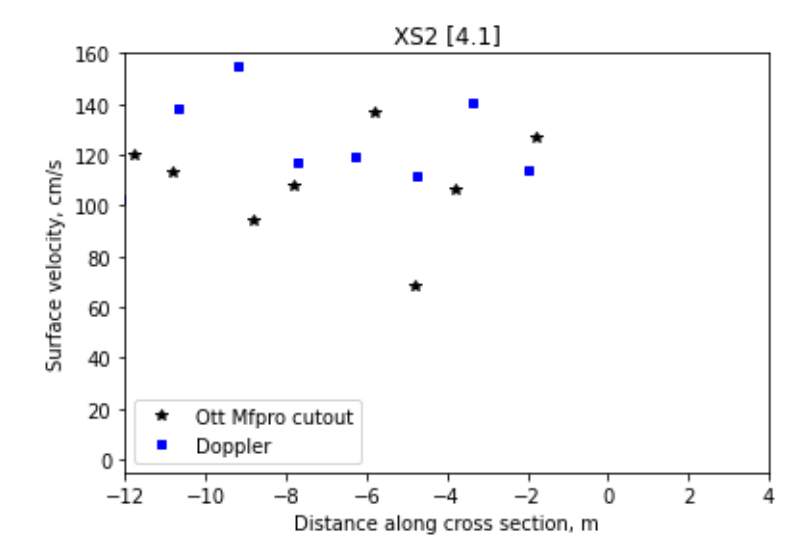
XS1, alt. 5



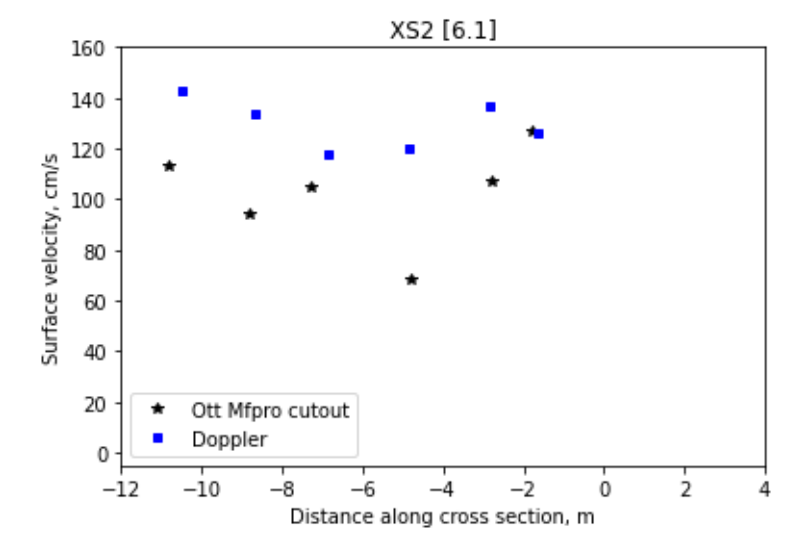
XS2, alt. 2



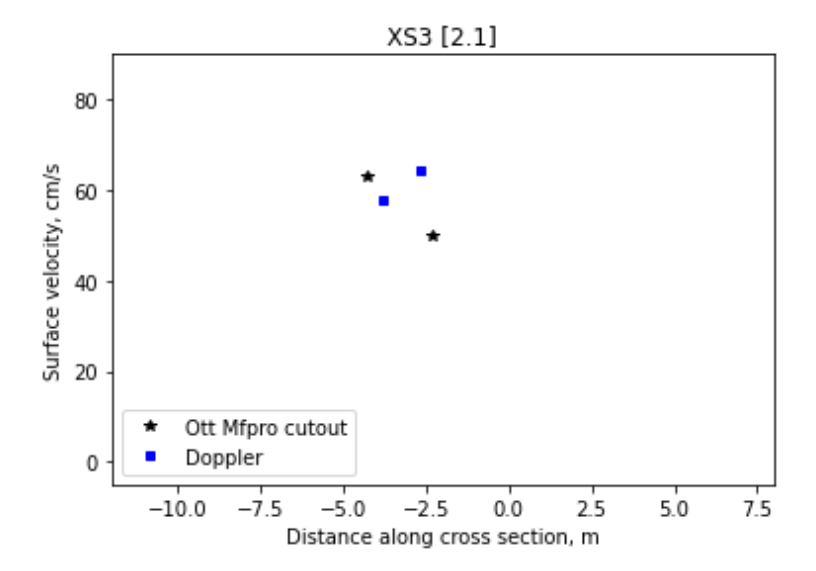
XS2, alt. 4



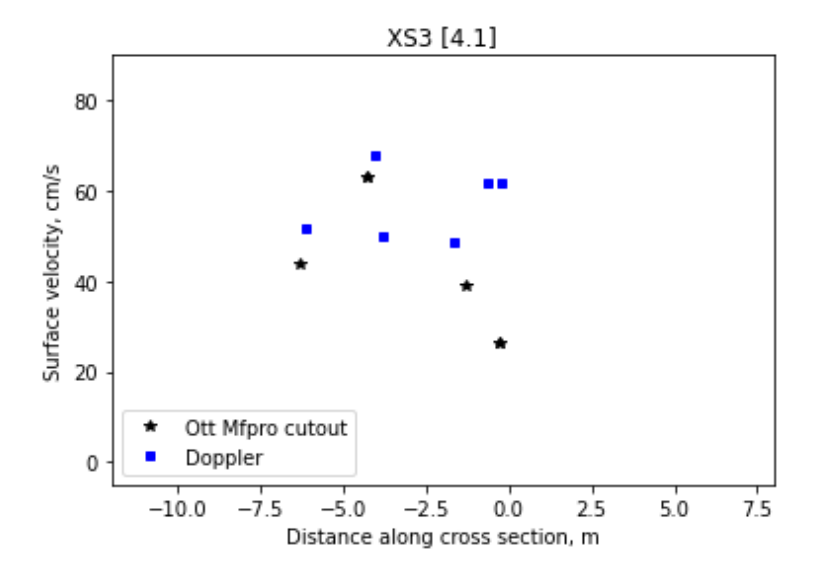
XS2, alt. 6



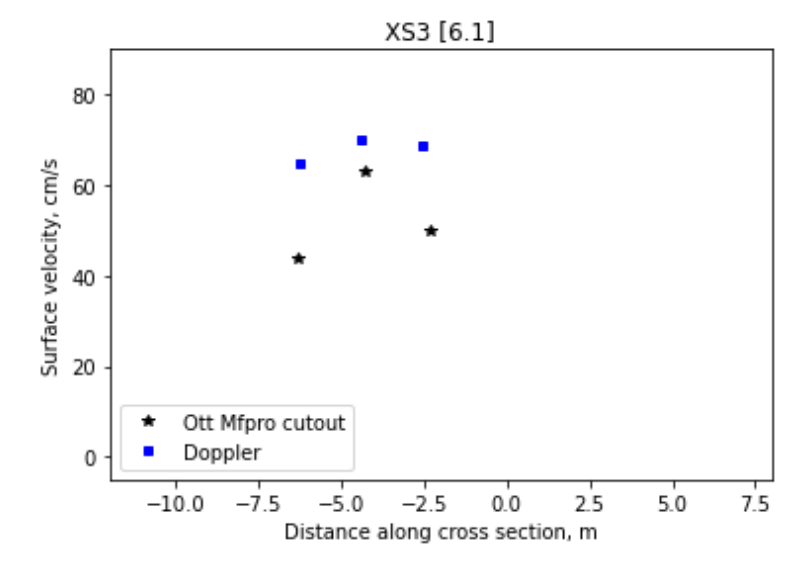
XS3, alt. 2



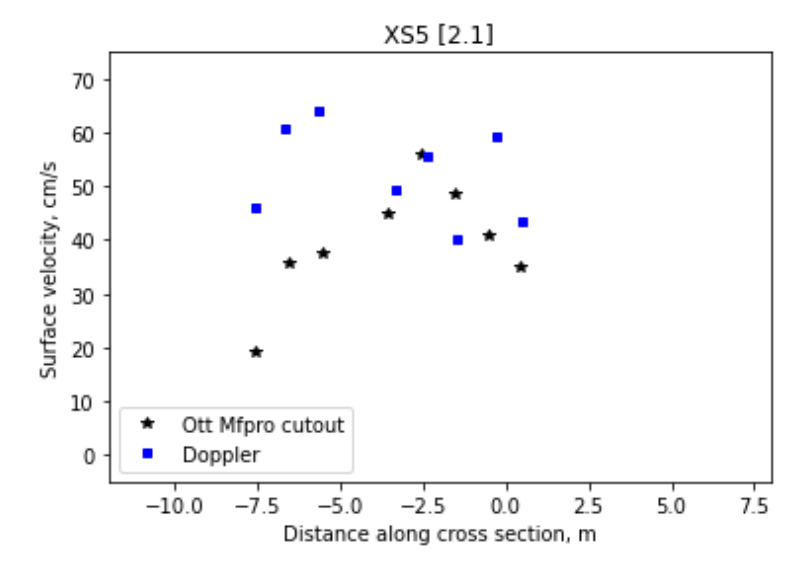
XS3, alt. 4



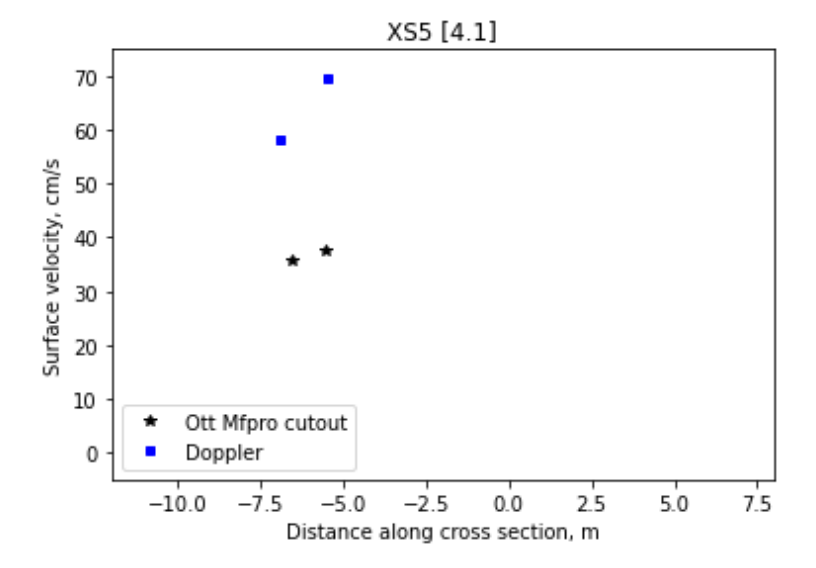
XS3, alt. 6



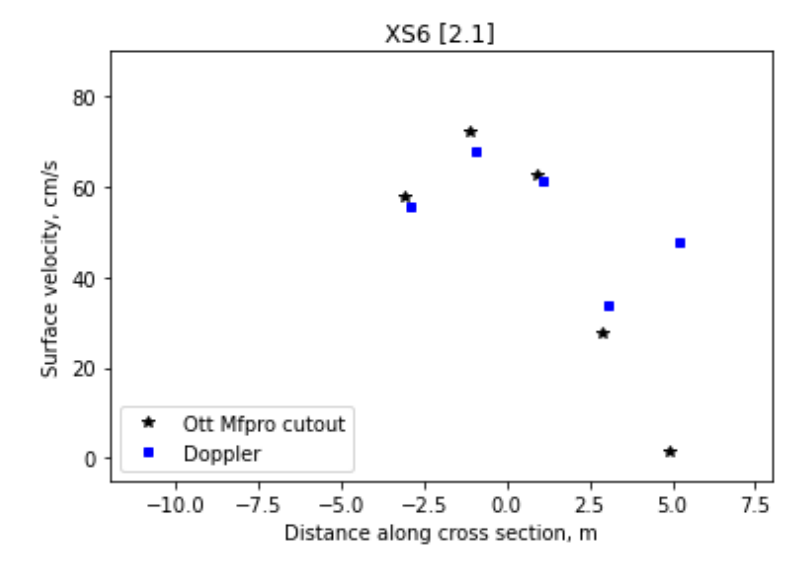
XS5, alt. 2



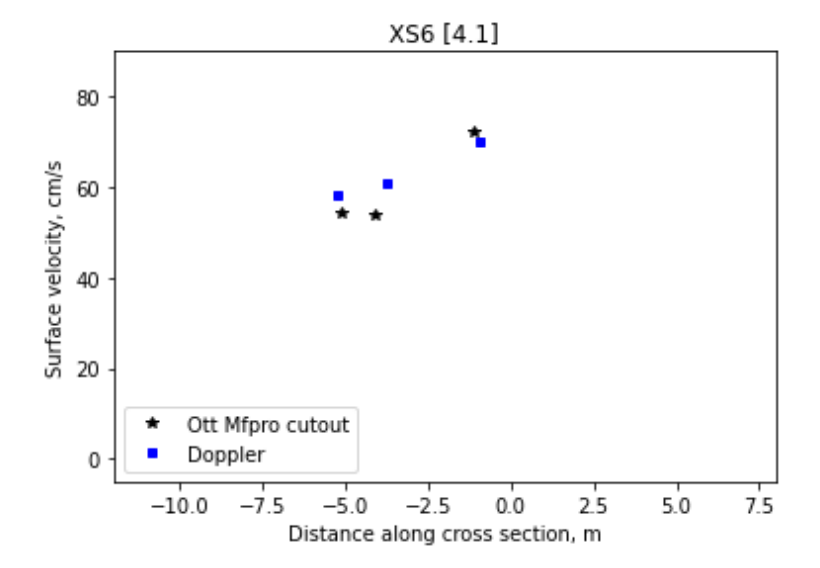
XS5, alt. 4



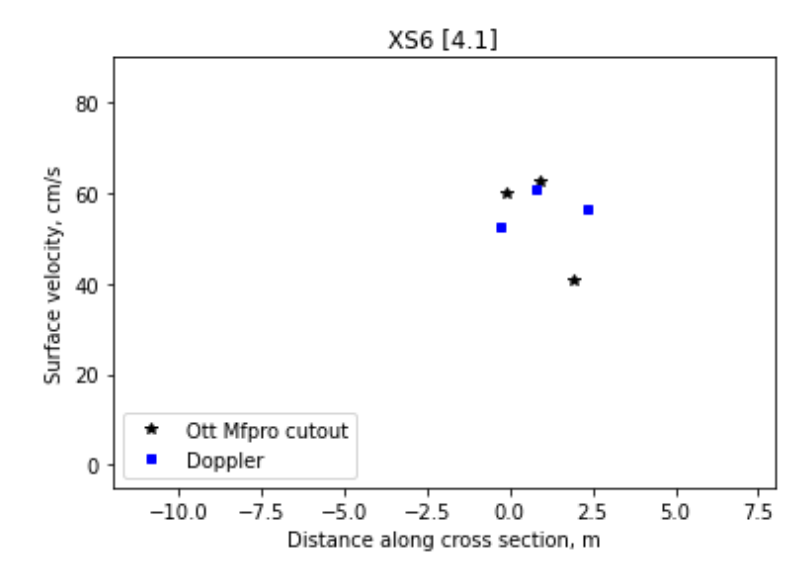
XS6, alt. 2



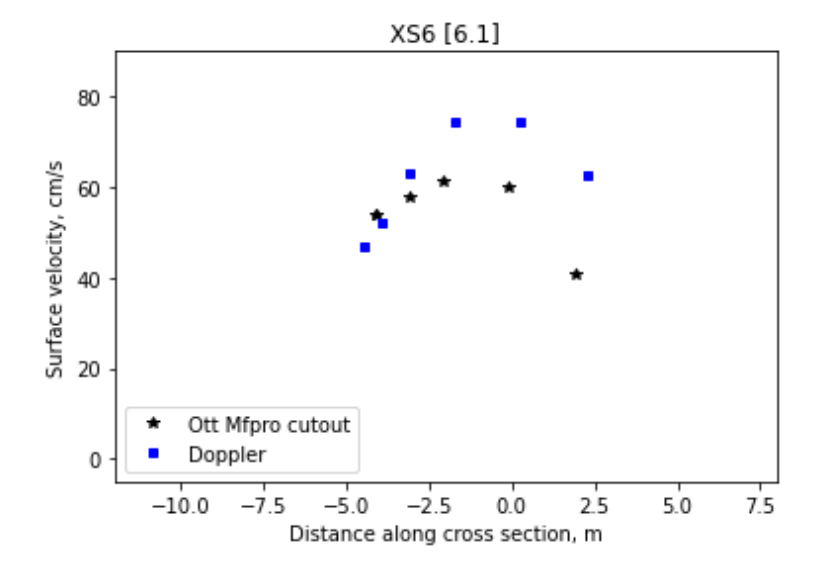
XS6, alt. 4 (1)



XS6, alt. 4 (2)



XS6, alt. 6



F Footprint analysis

XS2

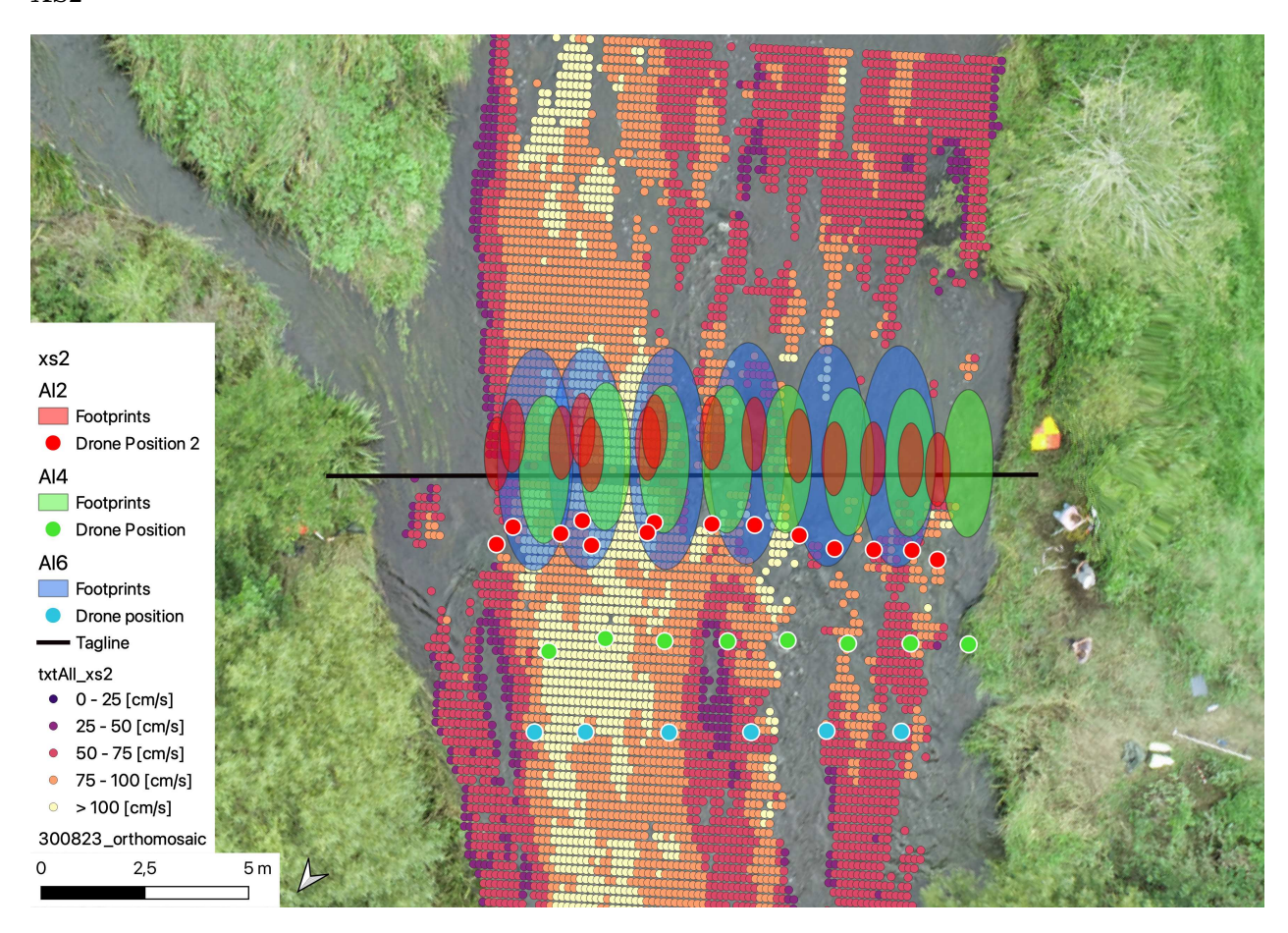


Figure 44: Heatmap and footprints for the three altitudes flown at XS2.

G 30 sec hovering results

